Pontifícia Universidade Católica
do Rio de Janeiro

Gustavo Brattstroem Wagner

An excursion in the dynamics of flexible beams: from modal analysis to nonlinear modes

Tese de Doutorado

Thesis presented to the Programa de Pós–graduação em Engenharia Mecânica, do Departamento de Engenharia Mecânica da PUC-Rio in partial fulfillment of the requirements for the degree of Doutor em Engenharia Mecânica.

Advisor : Prof. Rubens Sampaio Filho
Co-advisor: Profa. Roberta de Queiroz Lima

Rio de Janeiro
February 2022

Pontifícia Universidade Católica
do Rio de Janeiro

Gustavo Brattstroem Wagner

An excursion in the dynamics of flexible beams: from modal analysis to nonlinear modes

Thesis presented to the Programa de Pós–graduação em Engenharia Mecânica da PUC-Rio in partial fulfillment of the requirements for the degree of Doutor em Engenharia Mecânica. Approved by the Examination Committee:

Prof. Rubens Sampaio Filho
Advisor
Departamento de Engenharia Mecânica – PUC-Rio

Profa. Roberta de Queiroz Lima
Co-advisor
Pontifícia Universidade Católica do Rio de Janeiro – PUC-Rio

Prof. Domingos Alves Rade
ITA

Profa. Aline Souza de Paula
UnB

Prof. Marcelo Amorim Savi
UFRJ

Prof. Rafael Holdorf Lopez
UFSC

Rio de Janeiro, February the 7th, 2022

Gustavo Brattstroem Wagner

Bachelor and master's degree in mechanical engineering by the Pontifical Catholic University of Rio de Janeiro. Worked as project engineer in the oil and gas industry in Norway and as a vibration engineer at Electrolux.

Bibliographic data

Wagner, Gustavo Brattstroem

An excursion in the dynamics of flexible beams: from modal analysis to nonlinear modes / Gustavo Brattstroem Wagner; advisor: Rubens Sampaio Filho; co-advisor: Roberta de Queiroz Lima. – 2022.

148 f: il. color. ; 30 cm

Tese (doutorado) - Pontifícia Universidade Católica do Rio de Janeiro, Departamento de Engenharia Mecânica, 2022.

Inclui bibliografia

1. Engenharia Mecânica – Teses. 2. Engenharia Mecânica – Teses. 3. Modos normais não lineares. 4. Análise modal. 5. Elementos finitos co-rotacionais. 6. Balanço harmônico. 7. Método do tiro. I. Sampaio Filho, Rubens. II. de Queiroz Lima, Roberta. III. Pontifícia Universidade Católica do Rio de Janeiro. Departamento de Engenharia Mecânica. IV. Título.

CDD: 621

This thesis is dedicated to my parents.

Acknowledgments

I would like to thank my family for its unconditional support while I pursued this doctor's degree. The love, strength and principles transmitted to me during my entire life allowed me to have this opportunity.

To my advisor Rubens, I would like to thank for all the dedicated time spent with me during this research. The vast knowledge transferred to me during the years as graduate student was impressive and inspirational. I would also like to thank my co-advisor Roberta for being an example of a successful and awarded young researcher and professor. Her dedication in expanding the knowledges of students is admirable. To Wagner, the laboratory technician, I would like to thank for all the prompt help given to me during all those years of friendship.

To my former managers at Electrolux, Marcio Miranda and João Nascimento, I would like to thank for their great support offered to me during the years within the company. Without the flexibility and comprehension, this thesis would not be completed.

I would like the thank CNPq for the financial support during this post-graduate program.

This study was financed in part by the Coordenação de Aperfeiçoamento de Pessoal de Nível Superior - Brasil (CAPES) - Finance Code 001.

Abstract

Wagner, Gustavo Brattstroem; Sampaio Filho, Rubens (Advisor); de Queiroz Lima, Roberta (Co-Advisor). **An excursion in the dynamics of flexible beams: from modal analysis to nonlinear modes**. Rio de Janeiro, 2022. 148p. Tese de Doutorado – Departamento de Engenharia Mecânica, Pontifícia Universidade Católica do Rio de Janeiro.

Flexible beams are becoming ubiquitous in several industrial applications, as new projects often aim for lighter and longer structures. This fact is directly related to the new challenging demands on structural performances, or it is a simple consequence of the engagement of industries in cost reduction programs (usage of less material). Flexible beams are usually modeled under the assumption of large displacements, finite rotations, but with small strains. Such hypotheses allow the equation of motion to be built using co-rotational finite elements. The co-rotational formulation decomposes the total motion of a flexible structure into two parts: a rigid body displacement and an elastic (small) deformation. This way, the geometric nonlinearity caused by the large displacements and rotations of the beam's cross sections can be efficiently computed. One of the novelties of this thesis is the direct usage of the equation of motion generated by a co-rotational finite element formulation in the computation of nonlinear normal modes (NNM). So far, most of the dynamic analyses with co-rotation finite element models were restricted to numerical integrations of the equation of motion. The knowledge of NNMs can be beneficial in the analysis of any nonlinear structure since it allows a thoroughly understanding of the vibratory response in the nonlinear regime. They can be used, for example, to predict a hardening/softening behavior, a localization of the responses, the interactions between modes, the existence of isolas, etc. The Rosenberg's definition of NNM as periodic solutions (non-necessarily synchronous motion) is adopted here. The Harmonic Balance method and the Shooting methods are presented and used to compute periodic solutions of nonlinear systems. A numerical path continuation scheme is implemented to efficiently compute NNMs at different energy levels. Numerical examples show the capability of the proposed method when applied to co-rotational beam elements.

Keywords

Nonlinear normal modes; Modal analysis; Co-rotational finite element; Periodic solutions; Harmonic balance; Shooting method.

Resumo

Wagner, Gustavo Brattstroem; Sampaio Filho, Rubens; de Queiroz Lima, Roberta. **Uma excursão na dinâmica de vigas flexíveis: de análise modal a modos não lineares**. Rio de Janeiro, 2022. 148p. Tese de Doutorado – Departamento de Engenharia Mecânica, Pontifícia Universidade Católica do Rio de Janeiro.

Vigas flexíveis são encontradas com cada vez mais frequência em diferentes indústrias, uma vez que novos projetos têm buscado por estruturas mais longas e leves. Isso pode ser uma consequência direta das novas demandas estruturais nos projetos, ou uma simples consequência do engajamento das indústrias em programas de redução de custo (utilização de menos materiais). Em geral, vigas flexíveis são modeladas sob hipóteses de grandes deslocamentos, grandes rotações, mas com pequenas deformações. Essas hipóteses permitem que o equacionamento da dinâmica de vigas flexíveis seja feito através de elementos finitos co-rotacionais. A formulação co-rotacional decompõe o movimento das estruturas flexíveis em duas partes: uma contendo o movimento de corpo rígido e outra com uma (pequena) deformação elástica. Dessa forma, a não-linearidade geométrica causada pelos grandes deslocamentos e rotações das seções transversais das vigas podem ser computadas de forma eficiente. Uma das inovações dessa tese é o uso direto das equações de movimentos geradas pelos elementos finitos co-rotacionais no cálculo dos modos normais não-lineares (MNNs). Até agora, a maioria das análises dinâmicas com elementos finitos co-rotacionais foram restritas à integração das equações de movimento. O conhecimento de MNNs é útil na análise de sistemas não-lineares pois permitem um detalhado entendimento das vibrações nos regimes não-lineares. Com eles, pode-se, por exemplo, prever comportamentos de enrijecimento/relaxamento, localização de respostas, interação entre modos, existência de *isolas*, etc. A definição de Rosenberg sobre MNNs como sendo soluções periódicas (não necessariamente síncronas) do sistema é adotado na tese. Os métodos do Balanço Harmônico e do Tiro são apresentados e utilizados no cálculo de soluções periódicas de sistemas não-lineares. Um procedimento de continuação numérica é implementado para computar os MNN eficientemente para diferentes níveis de energia. Exemplos numéricos mostram a capacidade do método proposto quando aplicado aos elementos finitos co-rotacionais.

Palavras-chave

Modos normais não lineares; Análise modal; Elementos finitos co-rotacionais; Balanço harmônico; Método do tiro.

Table of contents

List of figures

List of tables

List of Abreviations

AFT – Alternating Frequency-Time

DOF – Degrees of freedom

EMA – Experimental modal analysis

FEM – Finite element method

FFT – Fast Fourier transform

FRF – Frequency response function

FS – Fourier series

HBM – Harmonic Balance Method

HOT – Higher order terms

NFRC – Nonlinear frequency response curve

NNM – Nonlinear normal modes

RMS – Root mean square

And the seasons, they go round and round
And the painted ponies go up and down
We're captive on the carousel of time
We can't return, we can only look
Behind, from where we came
And go round and round and round, in the
circle game.

Joni Mitchell, *Ladies of the Canyon.*

1
Introduction

For several industries, the dimensions of some structures are being extended to new limits in order to satisfy new challenging needs. Those new dimensions led many structures to exhibit significant nonlinearities in their dynamics. A typical example of those structures is the offshore pipelines that are being used in the exploration of oil at deep see levels [1, 2]. The extended length of the pipes turn them into extremely slim beams, and therefore, with significant flexibility. A geometric nonlinearity is then generated from the large displacements and rotations of the cross sections. Other similar examples of slim beams with high flexibility (and therefore exhibiting geometric nonlinearities) are wind turbine blades, helicopter blades, drill-strings, and large suspended bridges.

Many other types of nonlinearities are commonly found in structural dynamics besides the geometric one. For some types of material, the constitutive law relating stresses and strains can be considered as nonlinear. This is often the case of foams [3, 4, 5] and rubber isolators [6]. Also, the dissipation mechanisms of many structures are usually modeled as linear viscous damping because of their mathematical benefits. But, in reality, the dissipation can be essentially nonlinear, as in the case of dry friction and hysteretic damping [7, 8, 9, 10]. Nonlinearity can also be generated from the boundary conditions of the system. For example, discontinuity in the model occurs when dealing with clearances or vibro-impact systems [11]. The non-smooth force-deflection characteristic requires additional attention when compared with other types of nonlinearities. External body forces such as magnetoelastic, electrodynamic, and hydrodynamic forces can also be considered as source of nonlinearity in many systems.

Practical examples of nonlinearity in structures are found in different industries. In the automotive, the friction variation between the breaking pads and rotors is responsible for self-excitation of the rotor, resulting in an irritating and undesirable noise [12]. Also, many automobiles have viscoelastic engine mounts that present indications of nonlinearity, including a dependence on amplitude, frequency and preload. For the aerospace industry, the nonlinearities in airplanes emerge from the fluid-structure interaction, the backlash

and friction in control surfaces, joints hardening in the engine-to-pylon connection and the saturation effects in the hydraulic actuators [13]. A non-smooth nonlinearity was also reported in a small satellite conceived by Airbus Defence and Space [14]. A so-called wheel elastomer mounting system was designed as a mechanical filter that mitigates the in-orbit micro vibration induced by the inertia of the wheel. To support the loads during launch, the axial and lateral motion of the mounting systems were limited by two mechanical stops, creating the non-smooth nonlinearity in the system.

The dynamics of nonlinear systems can be rich and complex. It can exhibit phenomena that have no counterpart in linear systems. This includes: jumps, bifurcations, saturation, subharmonic, superharmonic, internal resonances, resonance captures, limit cycles, modal interactions and chaos [13]. The major difficulty when analyzing the response of nonlinear system is the lack of modal superposition, a property widely used in most of the analysis tools for linear systems. Without the modal superposition, those analysis tool must be somehow modified due to the nonlinearities. Two common tools widely used in linear systems are the frequency response function (FRF) and modal analysis. The former predicts the amplitude of the response (at steady state condition) when excited by a harmonic function. The latter on the other hand consists in extracting the modal parameters of a model through an eigenvalue problem. Those parameters are then used to characterize the structure uniquely. This analysis tool can be applied for many purposes: system identification, system modification, model updating, troubleshooting, response prediction and health monitoring. In this thesis, both tools will be modified for nonlinear system, but with greater emphasis on the modifications of modal analysis.

1.1 Boundary value problem

When analyzing nonlinear vibration problems, an important task is to find periodic solutions that describe the motion of the system. This allows one to construct analysis tools to interpret the nonlinear systems, e.g. when computing the nonlinear frequency response curves (NFRCs), which are nonlinear extension of the FRF, and the nonlinear normal modes (NNM), which are nonlinear extensions of the linear normal modes. In this thesis, all the analyzed systems, some after discretization, will have their dynamics modeled by a generic differential equation in the form of

$$\mathbf{r}\left(\mathbf{y}, \dot{\mathbf{y}}, t\right) = \mathbf{0}, \tag{1-1}$$

where t is the only independent variable, $\mathbf{y} \in \mathbb{R}^m$ is the state of the system and $\dot{\mathbf{y}}$ is its time differentiation. In structural dynamics, this generic differential equation depends only on the geometry of the system, the material properties and the boundary conditions. Characteristics of Eq. (1-1) can be further used to categorize the system: if $\mathbf{r}(\mathbf{y}, \dot{\mathbf{y}}, t)$ is not explicitly time-depended, the system is referred to as autonomous, otherwise, it is called non-autonomous. Only the non-autonomous systems with periodic time dependency are considered in this thesis, i.e., one must have $\mathbf{r}(\mathbf{y}, \dot{\mathbf{y}}, t) = \mathbf{r}(\mathbf{y}, \dot{\mathbf{y}}, t + T)$ where T is the period. This condition restricts the analysis to non-autonomous systems that can have periodic solutions. Furthermore, if the matrix $\partial\mathbf{r}/\partial\dot{\mathbf{y}}$ is regular, the system is simplified and described by ordinary differential equations.

In order to find a periodic solution of the differential equation, a periodic boundary value problem needs to be created. This is accomplished by adding periodic restrictions to the solution. It establishes that a given state at a particular time (usually at $t = 0$ for convenience) must be repeated after some value of time $T \neq 0$, which represents the fundamental period of the solution. Mathematically, the periodic boundary value problems can be stated as follows:

$$\begin{cases} \mathbf{r}(\mathbf{y}, \dot{\mathbf{y}}, t) = \mathbf{0}, \quad t \in [0, T] \\ \mathbf{y}(t) = \mathbf{y}(t + T) \end{cases} . \tag{1-2}$$

Such problem can have no solutions, one solution or many solutions. It all depends on the type of system represented by $\mathbf{r}(\mathbf{y}, \dot{\mathbf{y}}, t)$. Next, examples illustrate each of those three possibilities.

Linear non-conservative autonomous system: Let's consider the case of a free response of a non-conservative oscillator with the following equation of motion:

$$\ddot{q}(t) + 2\zeta\omega_n\dot{q}(t) + \omega_n q(t) = 0, \tag{1-3}$$

where ζ, ω_n and $q(t)$ represents the damping ratio, natural frequency and displacement of the system, respectively. By defining $\mathbf{y} = \begin{bmatrix} q(t) & \dot{q}(t) \end{bmatrix}^T$ as the state of the system, this second order differential equation can be first recast as a first order, and later replace $\mathbf{r}(\mathbf{y}, \dot{\mathbf{y}}, t)$ by it in Eq. (1-2). Such periodic boundary value problem have no solution since the damping dissipates energy at all times so that the energy required for the initial state is never recovered.

Linear conservative autonomous system: By removing the viscous damping term in Eq. (1-3), the system becomes conservative and the motion is governed by

$$\ddot{q}(t) + \omega_n q(t) = 0. \tag{1-4}$$

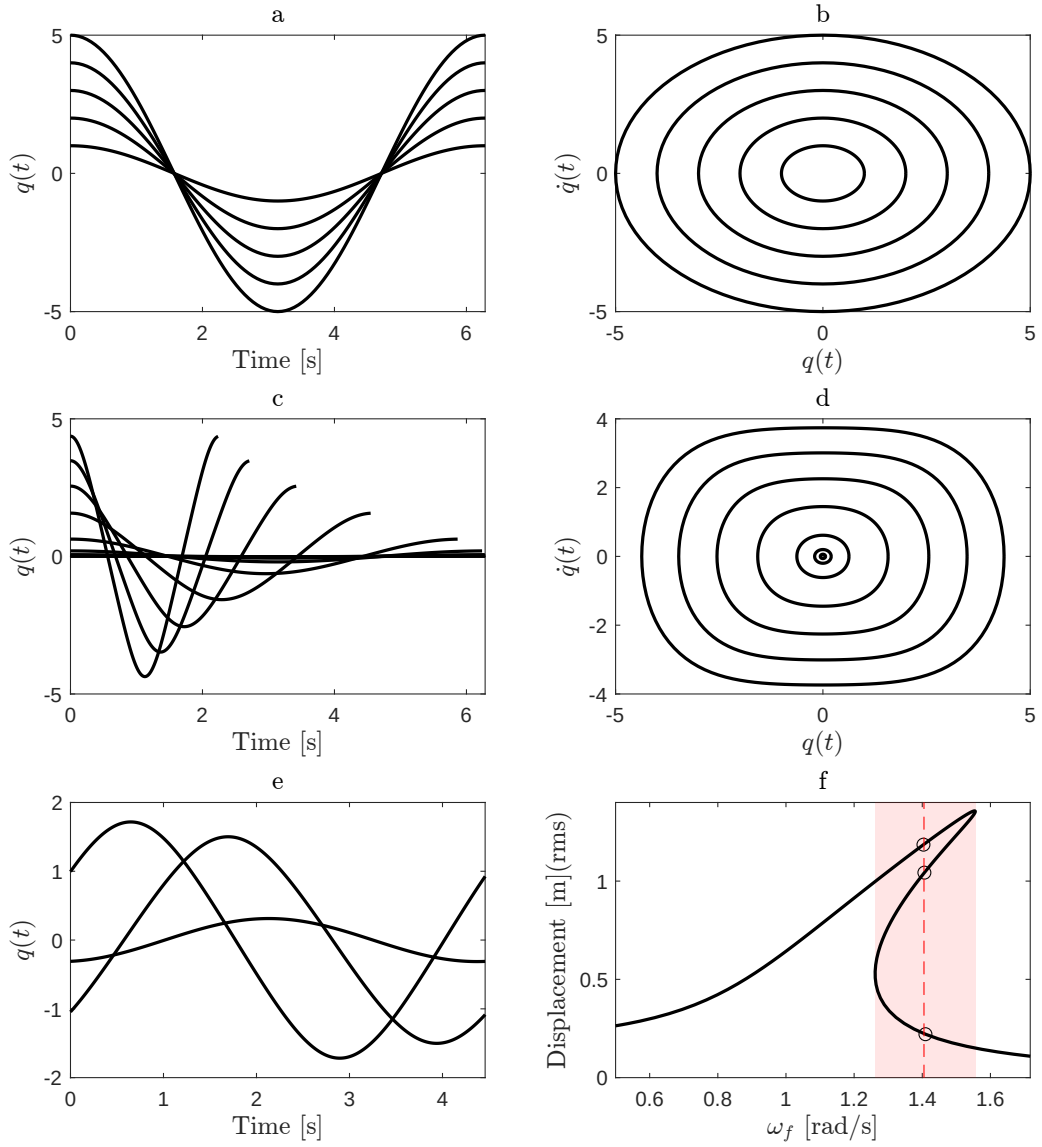

Figure 1.1: Responses of periodic boundary value problems considering different types of systems.

Rewriting this equation as a fist order differential equation, and replacing $\mathbf{r}(\mathbf{y}, \dot{\mathbf{y}}, t)$ by it in Eq. (1-2), a periodic boundary value problem with infinite solutions is created. Some of those solutions are presented in Fig. 1.1a for $\omega_n = 1$. Notice that the periodicity of the solutions are all the same, i.e., the period is independent of the energy in the system. Also, the trajectories in the phase plane are all ellipses, as showed in Fig. 1.1b. This is a characteristic of linear systems.

Nonlinear conservative autonomous system: A Duffing conservative oscillator can be built by adding a cubic restoring force in Eq. (1-4), i.e.,

$$\ddot{q}(t) + \omega_n q(t) + k_3 q^3(t) = 0. \tag{1-5}$$

This differential equation can be used to build a periodic boundary value problem that also has infinity solutions. Some of them are shown in Fig. 1.1c for $\omega_n = 1$ and $k_3 = 0.5$. Notice that, for this nonlinear system, the period of each solution depends on the energy of the system. Also, the trajectories in the phase plane are no longer ellipses, as showed in Fig. 1.1d.

Nonlinear non-autonomous system: Let's now consider the case of a Duffing oscillator with equation of motion defined by

$$\ddot{q}(t) + 2\zeta\omega_n\dot{q}(t) + \omega_n q(t) + k_3 q^3(t) = F_{\mathrm{D}}\cos(\omega_f t). \tag{1-6}$$

This differential equation builds periodic boundary value problems that can have one or more solutions depending on the values of F_{D} and ω_f. For the case where $\omega_n = 1$, $\zeta = 0.05$, $F_{\mathrm{D}} = 0.3$ and $\omega_f = 1.4\mathrm{rad/s}$, the problem has three solutions. They are presented in Fig. 1.1e. Each solution has a different energy level, but the period is the same and was defined by ω_f in Eq. (1-6), i.e., it was known before the problem is solved. If this particular magnitude of the harmonic force is maintained, the periodic boundary value problem admits three solution for $1.26 < \omega_f < 1.55$, the region marked by light red in Fig. 1.1. Outside this interval, the problem admits only one solution.

There are several methods already established in the literature that search for the periodic solutions of those kind of problems. Two of the most popular ones will be widely used in this thesis. Both are numerical methods that search for approximations of the periodic solution. Their methodologies are summarized as following:

1. Find the Fourier coefficients (and sometimes the fundamental frequency) of a guessed solution (an *Ansatz*) that is written as a truncated Fourier series and that approximates to the periodic solution $\mathbf{y}(t, \epsilon)$ as the truncation order increases. This approach is known as Harmonic Balance Method (HBM) and is covered in chapter 2.

2. Numerically integrate $\mathbf{y}(t, \mathbf{y}_0)$ from an unknown initial conditions $\mathbf{y}_0$ at $t = 0$ until $t = T$, where the period is sometimes also an unknown of the problem. A system of residual equations, $\mathbf{y}(T) - \mathbf{y}(0, \mathbf{y}_0) = \mathbf{0}$, is then built and solved with respect to the unknown initial conditions, and possibly with respect to the period as well. This approach is known as Shooting method and it is covered in chapter 3.

Each of those methods have their advantages and limitations. The Shooting method requires a numerical integration scheme which can increase the computational cost for large dimensional systems and might lead to numerical instabilities, but its concept is simple and allows one to characterize the stability of the responses without further computation (asymptotic stability through the monodromy matrix). On the other hand, the HBM is computationally fast and robust, but the stability analysis of the responses requires further computation (e.i. implementing the Hill's method as in [15, 16] or as in [17, 18, 19]).

1.2 Nonlinear normal modes

Nonlinear normal modes (NNM) extends, in some aspects, the concept of linear normal modes (LNM) to nonlinear systems. Modes are intrinsic characteristics of the system, being them linear or nonlinear, so that they do not depend on the applied excitation. The main difference between linear and nonlinear modes relies in the energy dependency of the NNM, which is not true for LNM. Around equilibrium points and with low energy levels, a nonlinear system behaves as a linear system, so that the NNMs tends to the LNMs of the underlying linearized system. Then, as the energy in the system increases, the NNMs gradually change their motion.

When searching for synchronous motions of linear systems, guessed solutions with separated space and time terms are used. When substituting those trial solutions (*Ansatz*) into the equation of motion, an eigenvalue problem is created. Such problem is independent of the energy in the system, so that the respective eigensolution pairs (the natural frequencies squared and LNMs) are also independent of energy. The natural frequency defines the period of the synchronous motion, so that it is a parameter that is related to the time terms of the *Ansatz*. The LNMs are real valued vectors that define a relationship between the displacements of all degrees of freedom of the system. Such relationship is constant along the synchronous motions, so that the LNMs contain only spacial information. They also have important mathematical properties that allow the system to be uncoupled. With this properties each modal response can be evaluated separated and added later to construct the response of the coupled system, a process known as modal superposition.

If the same process of finding synchronous motion with separated space and time solutions is applied to nonlinear system, no eigenvalue problem can be created. Hence, no basis can be found that uncouples the system, and

the modal superposition does not exist. A question regarding why the NNMs should then be computed could arise at this point. The knowledge of the NNMs is extremely useful because it allows a thoroughly understanding of the vibratory responses in the nonlinear regime. For example, it can be used to understand and explain complex dynamic interactions such as nonlinear localization of energy in space and an irreversible energy transfer between subsystems that compose a nonlinear system, a phenomenon known as energy pumping. It can also be used to predict a hardening or softening behavior of the solution. New publications [20] also show that NNM can be used in the prediction and computation of isolated forced response functions (isolas), which is also shown in the appendix C of this thesis.

Two definitions of NNMs are commonly found in the literature, the Rosenberg's definition [21, 21, 22] and the invariant manifold definition [23, 24, 25]. This thesis will focus on the former, which initially defined a NNM as a synchronous motion of the system, similar to the linear case. Such definition was later extended to periodic motion of a system (non-necessarily synchronous) to account for internal resonances (defined in chapter 5). Therefore, the process of finding NNMs includes the process of solving periodic boundary value problems. Since the modes are independent of the excitation, only conservative systems can be used when computing Rosenberg's NNMs. For this particular type of systems, as showed in the examples in section 1.1, the periodic boundary value problem admits an infinite number of solutions, each one of them related to a certain energy level. Therefore, to solve the periodic boundary value problem that characterize the NNM, a energy level must be defined. This is done by defining an amplitude restriction to the responses. But, the knowledge of a NNM at just one energy level does not allow a thoroughly understanding of the system's dynamics. Therefore an efficient way to compute periodic solutions for a predetermined interval of energy should be implemented, which can be done using numerical continuation schemes (discussed in chapter 4).

1.3 Co-rotational finite element models

In this thesis, the target structure corresponds to flexible beams. This type of structure is usually analyzed under the assumptions of large displacements, large rotations, but with small strains. Those hypotheses allow the structure to be accurately modeled using co-rotational finite elements, which is a simpler alternative to the inertial and floating frame approaches [26, 27]. The main idea of the co-rotational formulation is to decompose the motion

of each element as a small elastic deformation added to a rigid body motion. A local coordinate system is then incorporated to each element and forced to move with it according to its rigid body part of the motion. Then, the small deformation is written with respect to this local coordinate system (using typical linear beam elements), and latter transformed to an inertial frame. This transformation between frames considers the rigid body motion and therefore generates the geometric nonlinear terms in the model that are associated with the large displacements and rotations of the beam's cross sections. The equation of motion is then formulated in the inertial coordinate system using the Lagrangian equations. The nonlinear elastic forces generated by those co-rotational finite elements are usually nonzero at all entries, which means the nonlinearity is distributed along all structure and not just a local point. The equation of motion (represented earlier by the generic differential equation $\mathbf{r}(\mathbf{y}, \dot{\mathbf{y}}, t)$) is then used to build the periodic boundary value problem used to compute the NNMs. The process of finding the periodic solution with numerical methods becomes computationally expensive due to the fact that the nonlinearity depends on all DOFs, and not just a few ones as in the case of local nonlinearity.

1.4 Development of this thesis

The research topic of this thesis emanated from earlier studies in modal analysis and some industrial experiences. The research started with a review in the modal identification of structures using experimental modal analysis (EMA). This classical approach is already well established in the literature and it is used in most of the structural characterization cases in the industry. It requires input signals (from impact hammers or electromagnetic shakers) and output signals (from accelerometers, lasers, etc.) to estimate frequency response functions (FRF) or impulse response function (IRF). The identification methods are then applied in either of those two functions to extract the modal parameters. Therefore, a deep knowledge in signal processing and identification techniques was required. As main result, a stand alone application for modal testing and identification was developed. It allows the recordings of data from accelerometers, displacement sensors, strain gauges, impact hammers, force sensors, etc. The visualization of the data is updated in real time. The acquisition frequency and the amount of data acquired is adjustable. For the impact test, a trigger for automatic detection of the impact was implemented. For the shaker test, several input signals are possible: random noises, sine sweeps, multisines and sine waves. Also, the frequency content of the input signal is

adjustable. The application emphasizes the estimation of the impulse response function using the Observer/Kalman Filter Identification (OKID) and uses the eigensystem realization algorithm (ERA) for the modal identification, although other estimation and identification methods are also available in the software. The emphasis on OKID was justified because it presents a better estimation of the impulse response functions when only a few noisy samples are available, which leads to better modal identification of a system [28].

Later, the research topic proceed to operational modal analysis (OMA). Such technique consists in finding the dynamic characteristics of a structure through its modal parameters using output-only measurements and ambient excitation [29]. Differently from EMA, where the excitation in the structure is controlled and measured, OMA only uses hypothesis of the stochastic nature of the inputs. This fact allows the identification of systems under circumstances where EMA is limited. To apply OMA, the knowledge of stochastic modeling and random vibration was necessary. The main drawback of OMA is the fact that the excitation quality of the signal can no longer be guaranteed. The excitation level at some frequencies can become particularly low, reducing the signal-to-noise ratio significantly. Therefore, a study of the influence of measurement noise on statistical functions was conducted in [30], and improvements on the robustness of new identification methods were proposed in [31]. Most of the identification methods for OMA relies on the hypothesis of white noise excitation. This is not the case for real life applications. In general the excitation corresponds to a colored noise that can not be measured. When assuming a white noise excitation in the identification process, the identified modal parameters are actually related to two subsystems: an excitation filter that transforms the ideal white noise into a colored noise and the actual physical structure. To distinguish which modal parameters belong to each subsystem, the analyst usually assess the modal parameters values (e.g. high damping ratios are usually related to the excitation filter) or compare the results with a numerical model.

Primary examples of OMA applications are focused on large and heavy structures (usually civil structures), where a controlled input is hard to apply and expensive, or systems under operational conditions, where a laboratory condition can not be obtained (interference from the ambient can not be eliminated). In this context, OMA is used as an analysis tool to validate numerical models of new structures or to continuously assess the integrity of them along the time. The latter is referred to in the literature as structural health monitoring, and corresponds to a periodic identification of the modal (an possibly others) parameters. Any deviation from the baseline parameters

can trigger alerts and point out the possible source of defect, which should be inspected to confirmed. As an innovation on this research topic, another case where OMA becomes necessary was demonstrated experimentally by the author in [32], and corresponds to structures that are too small and have a high flexibility simultaneously. The small size does not allow the use of an electromagnetic shaker because it adds significant mass to the system. On the other hand, the high flexibility restricts the use of a modal hammer since a clean single impact becomes hard to apply. The alternative is an unmeasurable ambient excitation even though it might be artificially generated in the laboratory. Examples are strong wind flows that generate a turbulent fluid-structure interaction and amplified acoustic waves. The former can excite the structure with high magnitudes but without any control of its frequency content [33]. The later, in the other hand, can be controlled in terms of its frequency content but usually have low magnitudes.

Along the years as graduate student, the author of this thesis worked as vibration engineer for more than three years at Electrolux, where several modal testing (EMA and OMA) were conducted in different household appliances. Because of the competitive market around this type of industry, the development of new products is always somehow connected to cost reduction. This usually reflects in material reduction, which frequently leads to nonlinear dynamics in the structures. An example is the reduction of the steel sheet wall used in the construction of a washing machine cabinet (through a stamping process). The thin wall of the sheet creates a flexible plates. By performing EMA on new prototypes, the peaks in the FRF became dependent on the force magnitude, which characterize nonlinearity [34]. Another particular case of nonlinearity is the poor adjustment of the washing machine feet, which leads to gaps in the boundary conditions (between the feet of the machine and the floor). Depending on the magnitude of the unbalance inside the machine (caused by an unevenly distribution of clothes), the first natural frequency of the cabinet can have its value drastically reduced, potentially causing the washing machine to "walk". Those examples are the main reason for the choice of nonlinear normal modes as main topic of this thesis. The theory covered in modal analysis was not able to explain phenomena such as hardening/softening effect and subharmonic resonances experimented during test campaigns.

To limit the scope of this thesis, the geometric nonlinearities that appear in flexible structures was chosen as the main topic of the research, although local nonlinearity was also discussed throughout many examples in this thesis. The study of nonlinear normal modes of flexible structures was restricted to beams spatially discretized by co-rotational finite elements [35], even though

the proposed procedure could be extended to other types of structures (e.g. flexible plates). A potential sector that could benefit from the results of this thesis is the oil and gas industry since flexible beams are found ubiquitous. Examples are flexible risers [1, 36, 2], long drill-strings [105, 37, 38, 39] and umbilical cables.

1.5 Contributions of this thesis

The first contribution of this thesis is in the generation of a single reference that covers, in detail, two of the most popular method for computing periodic solutions of periodic boundary value problems: the Harmonic Balance Method (HBM) and the Shooting method. Those two different approaches play an important role in the numerical computation of Rosenberg's NNMs, each having their unique advantages and drawbacks, as already mentioned. The references related to NNMs usually covers only one of those methods, generating a lack of a single reference written in an unified framework.

Also, the theory of NNMs is not yet well developed. In the literature, there are only a few references to NNMs of slender structures whose nonlinearity is due to the slenderness of the structure (geometric nonlinearities). Examples are drill strings, flexible risers, umbilical cables and wind turbine blades. The main contribution of this thesis is to propose a methodology for computing the NNM of flexible (slender) beams. Most of the publications on the dynamic analysis of flexible beams with co-rotational finite element models are restricted to numerical integration of the resulting nonlinear equations of motion. Such analysis provides information about the system for a specific initial condition and excitation history, but fails to supply an overall picture about the dynamics of the structure. For example, it can not prescribe if the system presents a hardening or a softening behavior with changes in the energy, or if the motion can present a localization in its motion with changes in the energy. The author believes that the computation of the NNMs (and also the NFRCs) fills this lack of information. Several numerical examples with different complexity and different nonlinearities are provided here to validate the methodology.

One recent application of NNMs is in the detection and computation of isolated force response curves (isolas). In this thesis, the computation of isolas was presented in the appendix C since it departs from the main topic of this thesis (flexible beams). Although it follows the same procedure already proposed in [20], the appendix presents an example with a different type of nonlinearity. Instead of local cubic spring attached to the beam, an unilateral

spring is used, generating a discontinuity in the model. Therefore, the method proposed in [20] is also validated in this thesis for a stronger nonlinear and for a non-smooth system.

1.6 Outline of the thesis

Chapter 2 is dedicated to the HBM. It starts with a review of Fourier series [40], discussing its properties and the possible estimation error generated from the finite sampling frequency of an analog signal (aliasing). The HBM is then presented as a particular weighted residual method (of Galerkin type) with focus on solving a periodic boundary value problem. The Harmonic Balance equations are then further developed in more detail for mechanical systems. A procedure known as Alternating Frequency-Time is then presented at the end of the chapter to deal with the Fourier coefficients of different nonlinear forces.

Chapter 3 deals with the Shooting method as an alternative to the HBM in the computation of periodic solutions. Since it requires a numerical integration of the equation of motion, a modified version of the Newmark method (able to deal with nonlinear mechanical systems) is first presented. The residual equation of the Shooting method is then developed. A method to evaluate the stability of the periodic solutions is also presented based on the Floquet theory.

Chapter 4 addresses the numerical continuation of the periodic solution. The prediction-correction approach is demonstrated using different predictors and parameterization restrictions. The implemented algorithm is then explained and illustrated with the computation of NFRCs. Different types of nonlinearities are considered through several numerical examples.

Chapter 5 focuses in the definition and properties of the NNMs. The Rosenberg's definition is discussed and the NNMs are compared with the LNMs. The additional amplitude and phase restrictions required to compute the NNMs as periodic solutions are presented. The continuation algorithm is then used to compute the NNMs for different energy levels. The computation of several examples of systems with local nonlinearities is presented.

Chapter 6 covers the modeling and analysis of flexible beams. It starts with the co-rotational finite element formulation. The equation of motion is then constructed taking into consideration the geometric nonlinearity created by the large displacements and finite rotations. Such model is then incorporated into the periodic boundary value problem used to compute the NNMs. Numerical examples of NNMs of flexible beams are used to validade the pro-

posed method.

Chapter 7 states the main conclusions regarding the conducted reseach and principal results. Future works are also discussed.

In appendix A, a review on linear modes is performed to assists in the extension of LNMs to NNMs. It is considered as the starting point of this thesis. In appendix B, an alternative definition of NNMs as invariant manifolds is given. In appendix C, an procedure to compute isolas is presented and validated for a system with non-smooth nonlinearity.

2
Harmonic balance

The Harmonic Balance is a method that searches for an accurate approximation of the periodic solutions of a periodic boundary value problem using a truncated Fourier series (FS). In many practical cases, periodic functions can be accurately approximated with only a few number of terms of the series, i.e., with a truncated Fourier series. The truncation order usually depends on the smoothness of the periodic response. Systems that present some type of discontinuity usually require a higher number of harmonics (up to infinity) to well represent the periodic solution when compared to the smooth ones. Nevertheless, a good approximation is still within reach in many of those non-smooth cases. This enables the HBM to deal with mechanical systems that present discontinuity phenomena such as stick-slip, friction and impacts (gaps). Throughout this chapter, the guessed truncated approximation of the system's responses will be addressed the *Ansatz* of the solution.

When the *Ansatz* is substituted into the governing differential equations, a residual is usually expected since it is just an approximation. Because the governing equation and the *Ansatz* are periodic, the residual term must also be periodic. This allows one to expand it also as a FS. In summary, the HBM requires that the residue must be orthogonal to the subspace generated by the basis of the *Ansatz*. This consists in having the Fourier coefficients of the residual vanished up to the truncation order of the *Ansatz*. To achieve this requirement, a nonlinear system of algebraic equation must be solved with respect to the unknown Fourier coefficients of the *Ansatz*, and possibly the fundamental period of the FS. The construction of those algebraic equation are based in a weighted residual approach and this is the backbone of the HBM. When high dimension and/or complex nonlinearities are considered, the solution of the nonlinear algebraic equations can only be obtained numerically. The periodic solution that is found using the HBM only satisfies a weak formulation of the problem and therefore it is an approximation (of Galerkin type). Nevertheless, once the truncation order of the *Ansatz* is increased, the convergence of the approximation to the actual solution is expected. This statement is based on the Fourier theorem [40].

2.1 Fourier series

Let $\mathbf{x}(t)$, $\mathbf{x} : \mathbb{R} \to \mathbb{R}^n$, be a periodic function such that $\mathbf{x}(t) = \mathbf{x}(t+T)$ for all $t \in \mathbb{R}$ and $T > 0$. During this entire thesis, t represents time. T is the fundamental period and represents the smallest time value different from zero in which the function $\mathbf{x}(t)$ repeats itself. According to the Fourier theorem, any periodic function can be expanded by a infinite sum of sines and cosines such as

$$\mathbf{x}(t) = \tilde{\mathbf{x}}_0^{(c)} + \sum_{k=1}^{\infty} \tilde{\mathbf{x}}_k^{(c)} \cos(k\Omega t) + \tilde{\mathbf{x}}_k^{(s)} \sin(k\Omega t), \tag{2-1}$$

where $\Omega = \frac{2\pi}{T}$ is the fundamental frequency and $k = 1, \ldots, \infty$ is the harmonic index. The set of vectors $\left\{\tilde{\mathbf{x}}_0^{(c)}; \tilde{\mathbf{x}}_k^{(c)}; \tilde{\mathbf{x}}_k^{(s)}\right\}_{k=1}^{\infty}$ represents the Fourier coefficients while $\{1; \cos(k\Omega t); \sin(k\Omega t)\}_{k=1}^{\infty}$ are the Fourier base functions, here written in the trigonometric representation. In Eq. (2-1), the zero harmonic coefficient $\tilde{\mathbf{x}}_0^{(c)}$ represents the signal offset, $\tilde{\mathbf{x}}_1^{(c)}$ and $\tilde{\mathbf{x}}_1^{(s)}$ are the coefficients of the fundamental harmonic, while $\tilde{\mathbf{x}}_k^{(c)}$ and $\tilde{\mathbf{x}}_k^{(s)}$ with $k > 1$ are the coefficients of higher harmonics. In this expression, both the Fourier coefficients and the set of base functions are real-valued.

This FS representation of $\mathbf{x}(t)$ is not unique and can be written in a more compact form using complex exponential functions to create an equivalent base. Using Euler's formula, it is possible to rewrite Eq. (2-1) as

$$\begin{aligned}
\mathbf{x}(t) &= \tilde{\mathbf{x}}_0^{(c)} + \sum_{k=1}^{\infty} \tilde{\mathbf{x}}_k^{(c)} \cos(k\Omega t) + \sum_{k=1}^{\infty} \tilde{\mathbf{x}}_k^{(s)} \sin(k\Omega t) \\
&= \tilde{\mathbf{x}}_0^{(c)} + \sum_{k=1}^{\infty} \frac{\tilde{\mathbf{x}}_k^{(c)}}{2} \left(e^{\mathbf{i}k\Omega t} + e^{-\mathbf{i}k\Omega t}\right) - \sum_{k=1}^{\infty} \frac{\tilde{\mathbf{x}}_k^{(s)}\mathbf{i}}{2} \left(e^{\mathbf{i}k\Omega t} - e^{-\mathbf{i}k\Omega t}\right) \\
&= \tilde{\mathbf{x}}_0^{(c)} + \sum_{k=1}^{\infty} \frac{\tilde{\mathbf{x}}_k^{(c)} - \tilde{\mathbf{x}}_k^{(s)}\mathbf{i}}{2} e^{\mathbf{i}k\Omega t} + \sum_{k=1}^{\infty} \frac{\tilde{\mathbf{x}}_k^{(c)} + \tilde{\mathbf{x}}_k^{(s)}\mathbf{i}}{2} e^{-\mathbf{i}k\Omega t} \\
&= \sum_{k=-\infty}^{\infty} \tilde{\mathbf{x}}_k^{(e)} e^{\mathbf{i}k\Omega t}.
\end{aligned} \tag{2-2}$$

In the last line of Eq. (2-2), the values of k were extended to negative integers values to allows the FS to be written in its compact form. The relationship between the trigonometric ($\tilde{\mathbf{x}}_k^{(c)}$ and $\tilde{\mathbf{x}}_k^{(s)}$) and exponential ($\tilde{\mathbf{x}}_k^{(e)}$) FS coefficients are then given by

$$\begin{cases}
\tilde{\mathbf{x}}_0^{(e)} = \tilde{\mathbf{x}}_0^{(c)}, \\
\tilde{\mathbf{x}}_k^{(e)} = \frac{1}{2}\left(\tilde{\mathbf{x}}_k^{(c)} - \tilde{\mathbf{x}}_k^{(s)}\mathbf{i}\right), & \text{for } k > 0 \,. \\
\tilde{\mathbf{x}}_k^{(e)} = \frac{1}{2}\left(\tilde{\mathbf{x}}_k^{(c)} + \tilde{\mathbf{x}}_k^{(s)}\mathbf{i}\right), & \text{for } k < 0
\end{cases} \tag{2-3}$$

Analyzing the coefficient $\tilde{\mathbf{x}}_k^{(e)}$, one can easily note that they have the conjugate

mirror property, i.e.,

$$\tilde{\mathbf{x}}_{-k}^{(e)} = \tilde{\mathbf{x}}_{k}^{(e)^*}, \tag{2-4}$$

where $\square^*$ denotes complex conjugate. This property adds a redundancy to the exponential Fourier coefficients, which can be eliminated by defining a third equivalent FS representation:

$$\mathbf{x}(t) = \Re\left\{\sum_{k=0}^{\infty} \tilde{\mathbf{x}}_{k}^{(r)} e^{\mathbf{i}k\Omega t}\right\}, \tag{2-5}$$

where

$$\begin{cases} \tilde{\mathbf{x}}_{0}^{(r)} = \tilde{\mathbf{x}}_{0}^{(e)}, \\ \tilde{\mathbf{x}}_{k}^{(r)} = 2\tilde{\mathbf{x}}_{k}^{(e)}, \quad \text{for } k > 0 \end{cases} \tag{2-6}$$

Orthogonality: An important properties of the Fourier base functions is the orthogonality between the vectors. For the trigonometric representation, the orthogonality between the vectors in the base can be summarized using the following inner products:

$$\frac{1}{T}\int_0^T \cos(j\Omega t)\cos(k\Omega t)dt = \begin{cases} 0, & \text{for } j \neq k \\ 1/2, & \text{for } j = k \end{cases} \tag{2-7}$$

$$\frac{1}{T}\int_0^T \sin(j\Omega t)\sin(k\Omega t)dt = \begin{cases} 0, & \text{for } j \neq k \\ 1/2, & \text{for } j = k \end{cases} \tag{2-8}$$

$$\frac{1}{T}\int_0^T \cos(j\Omega t)\sin(k\Omega t)dt = 0 \quad \text{for any } j, k \tag{2-9}$$

The Fourier coefficients can then be easily calculated using this properties. By taking the inner product between $\mathbf{x}(t)$ and the elements of the base $\{1; \cos(k\Omega t); \sin(k\Omega t)\}_{k=1}^{\infty}$, one at a time, and using the results of Eq. (2-7) to (2-9), the Fourier coefficients can be written as:

$$\langle \mathbf{x}(t), 1 \rangle = \frac{1}{T}\int_0^T \mathbf{x}(t)dt = \tilde{\mathbf{x}}_{0}^{(c)} \tag{2-10}$$

$$\langle \mathbf{x}(t), \cos(k\Omega t) \rangle = \frac{1}{T}\int_0^T \mathbf{x}(t)\cos(k\Omega t)dt = \frac{\tilde{\mathbf{x}}_{k}^{(c)}}{2}; \quad k = 1, \ldots, \infty \tag{2-11}$$

$$\langle \mathbf{x}(t), \sin(k\Omega t) \rangle = \frac{1}{T}\int_0^T \mathbf{x}(t)\sin(k\Omega t)dt = \frac{\tilde{\mathbf{x}}_{k}^{(s)}}{2}; \quad k = 1, \ldots, \infty \tag{2-12}$$

The orthogonality can also be shown when using the exponential base $\left\{e^{\mathbf{i}k\Omega t}\right\}_{k=-\infty}^{\infty}$. First, let us show that the integral over the interval $[0, T]$ of any element in this base results in

$$\int_0^T e^{\mathbf{i}k\Omega t}dt = \left.\frac{e^{\mathbf{i}k\frac{2\pi}{T}t}}{\mathbf{i}k\frac{2\pi}{T}}\right|_0^T = \begin{cases} T & \text{for } k = 0 \\ 0 & \text{for } |k| > 0 \end{cases} \tag{2-13}$$

Although the expression in the middle is indeterminate for $k = 0$, its limit is well defined for $k \to 0$. The above result can then be used to define the following inner product between any two vectors of the base:

$$\begin{aligned} \langle e^{\mathbf{i}k\Omega t}, e^{\mathbf{i}m\Omega t} \rangle &= \frac{1}{T}\int_0^T e^{\mathbf{i}k\Omega t} e^{-\mathbf{i}m\Omega t} dt \\ &= \frac{1}{T}\int_0^T e^{\mathbf{i}(k-m)\Omega t} dt = \begin{cases} 1 & \text{for } k = m \\ 0 & \text{for } k \neq m \end{cases} \end{aligned} \tag{2-14}$$

Equation (2-14) shows that the vectors in the exponential Fourier base are orthogonal. This properties is again used to define the Fourier coefficients in Eq. (2-2). Multiplying both sides of the equation by $e^{-\mathbf{i}k\Omega t}/T$ and integrating over the interval $[0, T]$, it leads to

$$\begin{aligned} \frac{1}{T}\int_0^T \mathbf{x}(t) e^{-\mathbf{i}k\Omega t} dt &= \frac{1}{T}\int_0^T \sum_{m=-\infty}^{\infty} \tilde{\mathbf{x}}_m^{(e)} e^{\mathbf{i}m\Omega t} e^{-\mathbf{i}k\Omega t} dt \\ &= \tilde{\mathbf{x}}_k^{(e)} + \underbrace{\frac{1}{T}\int_0^T \sum_{\substack{m=-\infty \\ m\neq k}}^{\infty} \tilde{\mathbf{x}}_m^{(e)} e^{\mathbf{i}(m-k)\Omega t} dt}_{=0}, \end{aligned} \tag{2-15}$$

so that

$$\tilde{\mathbf{x}}_k^{(e)} = \frac{1}{T}\int_0^T \mathbf{x}(t) e^{-\mathbf{i}k\Omega t} dt. \tag{2-16}$$

Once the Fourier coefficients $\left\{\tilde{\mathbf{x}}_0; \tilde{\mathbf{x}}_k^{(c)}; \tilde{\mathbf{x}}_k^{(s)}\right\}_{k=1}^{\infty}$ or $\left\{\tilde{\mathbf{x}}_k^{(e)}\right\}_{k=-\infty}^{\infty}$ have been computed, $\left\{\tilde{\mathbf{x}}_k^{(r)}\right\}_{k=0}^{\infty}$ can also be obtained using the relationships defined in Eq. (2-3) and Eq. (2-6).

Discrete approximation: For some periodic functions, the integral in Eq. (2-16) may not have a closed-form expression. Also, when dealing with experimental data, only some finite samples of $\mathbf{x}(t)$ are available. In many cases those restrictions can be overcome using numerical integration to approximate the Fourier coefficients. An efficient way to do that is by using the discrete Fourier transform (DFT), but with the cost of two possible distortions in this approximation: aliasing and leakage [41]. Only the former is discussed here since it is assumed that the samples are perfectly acquired during one exact period, which automatically eliminates the leakage.

Let $\{\mathbf{x}_j = \mathbf{x}(j\Delta t)\}_{j=0}^{N-1}$ be N equally spaced samples acquired with a time increment $\Delta t = T/N$ over the time interval $[0, T[$. A discrete-time approximation of the FS coefficients defined in Eq. (2-16) can be constructed using the Riemann sum

$$\hat{\tilde{\mathbf{x}}}_k^{(e)} = \frac{1}{N}\sum_{j=0}^{N-1} \mathbf{x}_j e^{-\mathbf{i}k\bar{\Omega}j\Delta t}, \tag{2-17}$$

where $\bar{\Omega} = \frac{2\pi}{N\Delta t}$.

To evaluate the quality of this approximation and the potential distortions, it is possible to relate each of the estimated coefficients $\hat{\tilde{\mathbf{x}}}_k^{(e)}$ with the theoretical ones, $\left\{\tilde{\mathbf{x}}_k^{(e)}\right\}_{k=-\infty}^{\infty}$. Substituting Eq. (2-2) in its discrete form ($\mathbf{x}_j = \sum_{r=-\infty}^{\infty} \tilde{\mathbf{x}}_r^{(e)} e^{\mathbf{i}r\Omega j\Delta t}$) into Eq. (2-17), one has

$$\hat{\tilde{\mathbf{x}}}_k^{(e)} = \frac{1}{N}\sum_{j=0}^{N-1} \underbrace{\sum_{r=-\infty}^{\infty} \tilde{\mathbf{x}}_r^{(e)} e^{\mathbf{i}r\Omega j\Delta t}}_{\mathbf{x}_j} e^{-\mathbf{i}k\bar{\Omega}j\Delta t} = \sum_{r=-\infty}^{\infty} \tilde{\mathbf{x}}_r^{(e)} \underbrace{\frac{1}{N}\sum_{j=0}^{N-1} e^{-\mathbf{i}(k\bar{\Omega}-r\Omega)j\Delta t}}_{K_1(k\bar{\Omega}-r\Omega)}. \tag{2-18}$$

Equation (2-18) shows that each estimated coefficient $\hat{\tilde{\mathbf{x}}}_k^{(e)}$ contains the contribution of all theoretical Fourier coefficients $\{\tilde{\mathbf{x}}_r^{(e)}\}_{r=-\infty}^{\infty}$ weighted by the kernel function $K_1(\Omega)$. It is important to keep in mind that both $\{\tilde{\mathbf{x}}_r^{(e)}\}_{r=-\infty}^{\infty}$ and $K_1(\omega)$ are complex-valued. With some algebraic manipulation it is possible to rewrite $K_1(\Omega)$ in a more convenient way, where the terms related to the magnitude and phase become explicit. Additionally, the kernel function can also be written using a dimensionless variable, defined as $u = \frac{\Omega\Delta t}{2\pi}$. The kernel function $K_1(u)$ can then be rewritten as

$$K_1(u) = \underbrace{\frac{\sin N\pi u}{N\sin \pi u}}_{D_N(u)} e^{-\mathbf{i}\pi(N-1)u}. \tag{2-19}$$

In Eq. (2-19), the magnitude of K_1 is expressed by $|D_N|$, known as the *Dirichlet kernel* function. To better understand its form, a schematic plot of $|D_N|$ with different values of N is presented in Fig. 2.1. The main observations are:

- $|D_N|$ is periodic with a symmetric basic branch within $u \in [-1/2, 1/2]$, i.e., limited by the *Nyquist frequency* (half of the sampling frequency).
- It has global maximums equal to 1 at integer values of u ($u = 0, \pm1, \pm2, \dots$).
- In the limit $N \to \infty$,

$$\lim_{N\to\infty} |D_N|(u) = \begin{cases} 1, & \text{for } u = 0, \pm1, \pm2, \dots \\ 0, & \text{elsewhere} \end{cases}$$

From those three characteristics, the *aliasing* is analyzed hereafter using examples of sine waves.

Aliasing: Aliasing is the distortion that occurs when the analyzed function contains contributions of harmonics in which the respective frequencies are

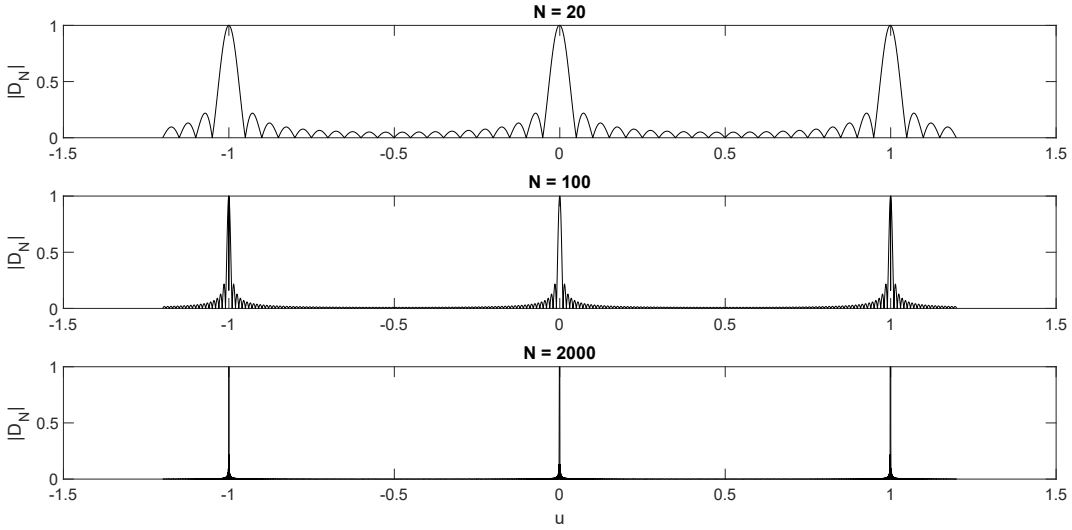

Figure 2.1: Schematic plot of the Dirichlet kernel function with $N = 20$, 100 and 2000 samples

above the Nyquist frequency. When this is the case, those harmonics appear wrong as lower frequencies. This distortion is explained mainly by the periodicity of the main peaks of $|D_N|$. Examples of sine waves with different frequencies are used here to exemplify aliasing.

Let $x(t)$ be a sine wave with unit amplitude and with some frequency f, sampled at a fixed rate of 10 Hz and during a total time of 2 seconds. The left column in Fig. 2.2 shows $x(t)$ (solid line) for three different frequencies ($f = 2$, 4 and 6 Hz) and the respective sampled signal $\{x_j\}_{j=0}^{19}$ (dots) . For the sampled signals, the total time is an exact multiple of their periods (4, 8 and 12, respectively) so leakage do not occurs.

For all three cases, the magnitude of all Fourier coefficients should have a zero value, except for $\left|\tilde{x}_{-1}^{(e)}\right| = \left|\tilde{x}_{1}^{(e)}\right| = 0.5$. Using Eq. (2-17), the discrete-time FS coefficient approximation is calculated and the results are presented in the middle plots in Fig. 2.2. The approximation is perfect for $f = 2$ and 4 Hz but wrong for $f = 6$ Hz since it should have zero value at 4 Hz. This error (aliasing) was expected since frequency of this the sine wave is higher than the Nyquist frequency ($6 > \frac{10}{2}$Hz). A graphical explanation is presented in the plots at the right column. They show the values of K_1 for all possible $(k\bar{\Omega} - \Omega)$. When the difference between the frequencies are higher than 5 Hz (the Nyquist frequency), the main peaks outside the fundamental branch $u \in [-1/2, 1/2]$ becomes reachable. This results in aliasing.

An important observation regarding aliasing and experimental data is that, once the signal has been digitalized, there is nothing to be done concerning this distortion. Therefore, the periodic functions that contains harmonics beyond the Nyquist frequency must first pass through an analog

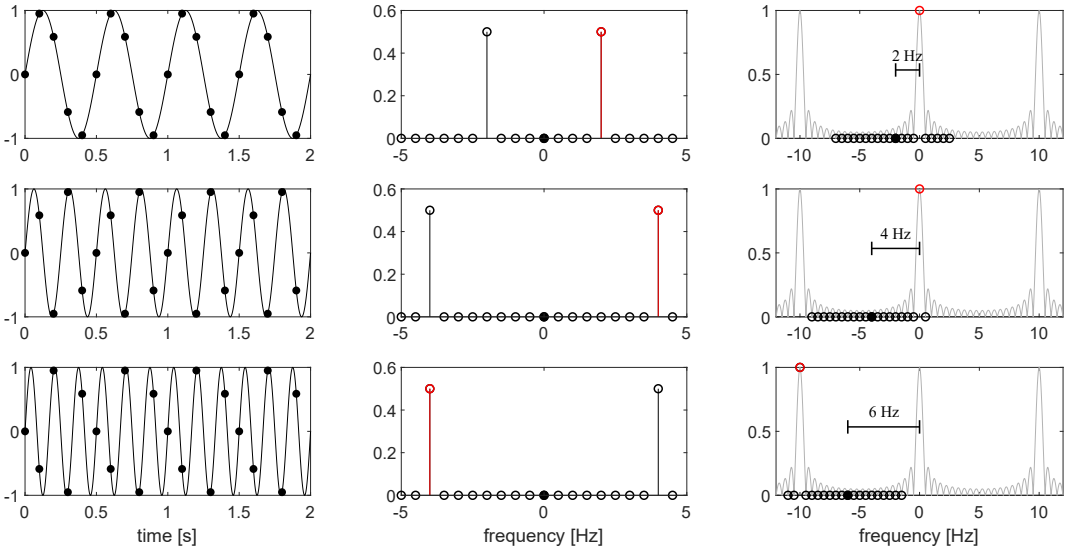

Figure 2.2: Example of aliasing using sine waves.

low pass filter that removes the contribution of such frequencies. Another alternative is to increase the sampling frequency until all frequencies are below the Nyquist frequency.

2.2 Weighted residual approach

Returning now to the boundary value problem described in Eq. (1-2), and repeated here for convenience:

$$\begin{cases} \mathbf{r}\left(\mathbf{y}, \dot{\mathbf{y}}, t\right) = \mathbf{0}, \quad t \in [0, T] \\ \mathbf{y}\left(t\right) = \mathbf{y}\left(t + T\right) \end{cases} \tag{2-20}$$

The goal of this chapter is to solve this periodic boundary value problem using the HBM. An analytic solution of Eq. (2-20) is impossible in many cases because of the complicated nonlinear terms in the differential equation. This motivates the search of an approximated solution that is governed by a less restricted formulation than the one given by Eq. (2-20). This alternative approach is accomplished using the a weighted residual methods, of which the HBM is a particular case. Let the approximated solution of Eq. (2-20), the *Ansatz*, be written in the form of a linear combination:

$$\mathbf{y}_H\left(t, \{\boldsymbol{\beta}_k\}\right) = \sum_{k=1}^{H} \boldsymbol{\beta}_k b_k(t), \tag{2-21}$$

where the set $\{b_k(t)\}_{k=1}^{H}$ is some chosen function basis and $\{\boldsymbol{\beta}_k\}_{k=1}^{H} \in \mathbb{R}^{2n}$ is a set of coefficients to be determined that approximates the $\mathbf{y}_H\left(t, \{\boldsymbol{\beta}_k\}\right)$ into $\mathbf{y}(t)$ for $t \in [0, T]$. When substituting Eq. (2-21) into the differential equation in

Method	***Ansatz* basis** $\{b_k\}$	**Weight functions** $\{\rho_j\}$
Harmonic Balance	Fourier basis functions	Fourier basis functions
Trigonometric Collocation	Fourier basis functions	Dirac delta distributions
Orthogonal Collocation	Lagrange polynomials	Dirac delta distributions

Table 2.1: Popular weighted residual methods

Eq. (2-20), a residual is expected since $\mathbf{y}_H\left(t, \{\boldsymbol{\beta}_k\}\right)$ is only an approximation. This residual function can then be defined as

$$\mathbf{r}_H\left(t, \{\boldsymbol{\beta}_k\}\right) = \mathbf{r}\left(\mathbf{y}_H\left(t, \{\boldsymbol{\beta}_k\}\right), \dot{\mathbf{y}}_H\left(t, \{\boldsymbol{\beta}_k\}\right), t\right). \tag{2-22}$$

If $\mathbf{r}_H\left(t, \{\boldsymbol{\beta}_k\}\right) = \mathbf{0}$ and the periodic boundary conditions are satisfied, the approximation is actually the periodic solution of the problem. Instead of requiring that $\mathbf{y}_H\left(t, \{\boldsymbol{\beta}_k\}\right)$ satisfies the differential equation in Eq. (2-20) for all $t \in [0, T]$ (the so call *strong* formulation), one can set a milder requirement of satisfying it only in a weighted average sense (the *weak* formulation):

$$\langle \rho_j, \mathbf{r}_H \rangle = \frac{1}{T}\int_0^T \rho_j(t)\mathbf{r}_H\left(t, \{\boldsymbol{\beta}_k\}\right) dt = \mathbf{0} \quad \text{for} \quad j = 1, \ldots, H \tag{2-23}$$

where $\{\rho_j(t)\}_{j=1}^H$ are weight functions. It states that the residual must be orthogonal to the weight functions. When the functions that compose the basis of the *Ansatz*, $\{b_k(t)\}_{k=1}^H$, and the weight functions, $\{\rho_j(t)\}_{j=1}^H$, are chosen, the integration in Eq. (2-23) removes the time dependency of the problem, leaving a system of algebraic equations to be solve with respect to the coefficients $\{\boldsymbol{\beta}_k\}_{k=1}^H$. Since the resulting algebraic equations are generally nonlinear, they are usually solved using numerical methods (e.g. using the Newton-Raphson method).

What distinguishes the various types of weighted residual methods is the choice of basis for the *Ansatz* and of the weight functions. The HBM uses the same functions for the basis and for the weight functions, which makes it a Galerkin method. It uses a Fourier basis, which is of great advantages for the periodic boundary value problems since it fulfills the periodicity restriction $\mathbf{y}_H\left(0, \{\boldsymbol{\beta}_k\}\right) = \mathbf{y}_H\left(T, \{\boldsymbol{\beta}_k\}\right)$ automatically. Also, the *Ansatzs* become efficient to compute and show quick convergence for many periodic functions. Other popular weighted residual methods are summarized in table 2.1 with their respective bases and weight functions.

Since the solution of Eq. (2-20) is real-valued, it seems natural first to require $\mathbf{y}_H\left(T, \{\boldsymbol{\beta}_k\}\right)$ to be also real-valued. This motivates the choice of the trigonometric representation here for the Fourier basis in Eq. (2-21) and not the complex exponential one, although both are equivalent. In the next section, the exponential representation will be adopted because of its algebraic

conveniences and computation efficiency.

Substituting the trigonometric Fourier basis functions in the *Ansatz*, the approximation becomes

$$\mathbf{y}_H\left(t, \{\boldsymbol{\beta}_k\}\right) = \boldsymbol{\beta}_1 + \sum_{k=1}^{H} \boldsymbol{\beta}_{2k} \cos(k\Omega t) + \boldsymbol{\beta}_{2k+1} \sin(k\Omega t). \tag{2-24}$$

which is a truncated FS up to the truncation order H. The total number of functions used in this linear combination is $B = 2H + 1$. Equation (2-24) shows that the coefficients $\{\boldsymbol{\beta}_k\}$ are nothing more than the Fourier coefficients of $\mathbf{y}_H\left(t, \{\boldsymbol{\beta}_k\}\right)$. Since the *Ansatz* and its time derivative are T-periodic, the residual $\mathbf{r}_H\left(t, \{\boldsymbol{\beta}_k\}\right)$ must be also T-periodic. Using the same Fourier basis function as the weight function (requirement of a Galerkin method), the weak formulation of Eq. (2-23) can be rewritten as

$$\frac{1}{T}\int_0^T 1 \;.\; \mathbf{r}_H\left(t, \{\boldsymbol{\beta}_k\}\right) dt = \mathbf{0} \tag{2-25}$$

$$\frac{1}{T}\int_0^T \cos(k\Omega t) \;.\; \mathbf{r}_H\left(t, \{\boldsymbol{\beta}_k\}\right) dt = \mathbf{0} \quad k = 1, \ldots, H \tag{2-26}$$

$$\frac{1}{T}\int_0^T \sin(k\Omega t) \;.\; \mathbf{r}_H\left(t, \{\boldsymbol{\beta}_k\}\right) dt = \mathbf{0} \quad k = 1, \ldots, H \tag{2-27}$$

Equations (2-25), (2-26) and (2-27) show the main concept of the HBM. It requires that the Fourier coefficients of the residual $\mathbf{r}_H\left(t, \{\boldsymbol{\beta}_k\}\right)$ vanish up to the truncation order H of the *Ansatz* $\mathbf{y}_H\left(t, \{\boldsymbol{\beta}_k\}\right)$. Equations (2-25), (2-26) and (2-27) results in $(2H + 1)2n$ algebraic equations to be solve for the $(2H + 1)$ Fourier coefficients $\{\boldsymbol{\beta}_k\} \in \mathbb{R}^{2n}$.

2.3 HBM for vibration problems in solid mechanics

In the previous section, the HBM was derived to solve a generic periodic boundary value problem using trigonometric Fourier basis to span the subspace of the *Ansatz*. Now, the problem is revisited, but for a more specific type of system and using the exponential Fourier basis. The equation of motion for vibration problems in solid mechanics corresponds to a second-order differential equation that can be written as

$$\underbrace{\mathbf{M}\ddot{\mathbf{q}}(t) + \mathbf{C}\dot{\mathbf{q}}(t) + \mathbf{K}\mathbf{q}(t)}_{\text{Linear forces}} + \underbrace{\mathbf{f}_{nl}\left(t, \mathbf{q}(t), \dot{\mathbf{q}}(t)\right)}_{\text{Nonlinear forces}} = \underbrace{\mathbf{f}_{ex}(t)}_{\text{External forces}} \quad , \tag{2-28}$$

where $\mathbf{q}$, $\mathbf{f}_{nl}$ and $\mathbf{f}_{ex} \in \mathbb{R}^n$ are vectors of the generalized coordinates, nonlinear internal forces and external forces, respectively. n is the number of degrees of freedom of the system. The matrices $\mathbf{M}$, $\mathbf{C}$ and $\mathbf{K} \in \mathbb{R}^{n \times n}$ are constant matrices responsible for the linear forces that are proportional to the acceleration,

velocity and displacement, respectively. No restriction in the nature of those matrices are made. They can be symmetric, anti-symmetric or even zero (no linear part in the system).

To compute periodic solutions of such equation of motion, a periodic boundary value problem must be first created. This is done by adding a periodic boundary restrictions to it, i.e.,

$$\begin{cases} \mathbf{M}\ddot{\mathbf{q}}(t) + \mathbf{C}\dot{\mathbf{q}}(t) + \mathbf{K}\mathbf{q}(t) + \mathbf{f}_{nl}\left(t, \mathbf{q}(t), \dot{\mathbf{q}}(t)\right) - \mathbf{f}_{ex}(t) = \mathbf{0}, \quad t \in [0, T] \\ \mathbf{q}(0) = \mathbf{q}(T) \\ \dot{\mathbf{q}}(0) = \dot{\mathbf{q}}(T). \end{cases} \tag{2-29}$$

A periodic solution of this periodic boundary value problem can only exist if the terms that dependent explicit on time (e.g. the nonlinear internal forces and the external forces) are also T-periodic.

Let an *Ansatz* of the periodic solution be a truncated FS of order H written now with an exponential Fourier basis:

$$\mathbf{q}_H\left(t, \Omega, \left\{\tilde{\mathbf{q}}_k^{(e)}\right\}\right) = \sum_{k=-H}^{H} \tilde{\mathbf{q}}_k^{(e)} e^{\mathbf{i}k\Omega t}. \tag{2-30}$$

The Fourier coefficients $\left\{\tilde{\mathbf{q}}_k^{(e)}\right\}_{k=-H}^{H} \in \mathbb{C}^n$, and possibly the fundamental period $\Omega \in \mathbb{R}$, are the unknowns of the problem and need to be found in order to approximate $\mathbf{q}_H(t)$ to the periodic solution $\mathbf{q}(t)$ of periodic boundary value problem. The *Ansatz* defined in Eq. (2-30) automatically satisfies the periodic boundary condition since the fundamental frequency is defined as $\Omega = 2\pi/T$, which forces the Fourier basis functions to be T-periodic. Taking the time derivative of the *Ansatz* and substituting the respective results in Eq. (2-28), a new definition for the residual function $\mathbf{r}_H\left(t, \Omega, \left\{\tilde{\mathbf{q}}_k^{(e)}\right\}\right)$ can be made:

$$\mathbf{r}_H\left(t, \Omega, \left\{\tilde{\mathbf{q}}_k^{(e)}\right\}\right) = \sum_{j=-H}^{H} \overbrace{\left[-(j\Omega)^2\mathbf{M} + \mathbf{i}j\Omega\mathbf{C} + \mathbf{K}\right]}^{\mathbf{S}_j(\Omega)} \tilde{\mathbf{q}}_j^{(e)} e^{\mathbf{i}j\Omega t} + \\ + \mathbf{f}_{nl}\left(t, \Omega, \left\{\tilde{\mathbf{q}}_k^{(e)}\right\}\right) - \mathbf{f}_{ex}(t, \Omega). \tag{2-31}$$

In Eq. (2-31), the matrix $\mathbf{S}_j(\Omega)$ is the dynamic stiffness matrix (widely applied in linear modal analysis) evaluated at the j-th harmonic frequency ($j\Omega$). The nonlinear and external forces can also be expanded as FS since they are assumed to be T-periodic. As result, the residual can be written as

$$\mathbf{r}_H\left(t, \Omega, \left\{\tilde{\mathbf{q}}_k^{(e)}\right\}\right) = \sum_{j=-\infty}^{\infty} \tilde{\mathbf{r}}_j^{(e)}\left(\Omega, \left\{\tilde{\mathbf{q}}_k^{(e)}\right\}\right) e^{\mathbf{i}j\Omega t} \tag{2-32}$$

where

$$\tilde{\mathbf{r}}_j^{(e)} = \begin{cases} \tilde{\mathbf{f}}_{nl,j}^{(e)}\left(\Omega, \left\{\tilde{\mathbf{q}}_k^{(e)}\right\}\right) & \text{for} \quad |j| > H \\ \mathbf{S}_j(\Omega)\tilde{\mathbf{q}}_j^{(e)} + \tilde{\mathbf{f}}_{nl,j}^{(e)}\left(\Omega, \left\{\tilde{\mathbf{q}}_k^{(e)}\right\}\right) - \tilde{\mathbf{f}}_{ex,j}^{(e)}(\Omega) & \text{for} \quad |j| \leq H \end{cases} \tag{2-33}$$

$\tilde{\mathbf{r}}_j^{(e)}$, $\tilde{\mathbf{f}}_{nl,j}^{(e)}$ and $\tilde{\mathbf{f}}_{ex,j}^{(e)}$ represent the j-th Fourier coefficients of the residual, nonlinear force and external force, respectively. An important observation is necessary regarding the limits of the summation in Eq. (2-32). It had to be extended to $\pm\infty$ to account for the possible higher harmonic terms created by the nonlinear forces.

When projecting the residual into the Fourier basis of the *Ansatz* (performing a Fourier-Galerkin projection), the time dependency of Eq. (2-32) is removed. Also, using the orthogonality of the Fourier basis and imposing that the residual must be orthogonal to the subspace of the *Ansatz* (i.e., balanced up to the H-th harmonic), a system of nonlinear algebraic equation is constructed. This is mathematically shown as

$$\int_0^T \mathbf{r}_H(t) e^{-\mathbf{i}m\Omega t} dt = \mathbf{0} \quad \text{for} \quad m = -H, \ldots, H \tag{2-34}$$

which leads to

$$\begin{aligned} \int_0^T \left[\sum_{j=-\infty}^{\infty} \tilde{\mathbf{r}}_j^{(e)}\left(\Omega, \left\{\tilde{\mathbf{q}}_k^{(e)}\right\}\right) e^{\mathbf{i}j\Omega t} \right] e^{-\mathbf{i}m\Omega t} dt &= \mathbf{0} \\ \sum_{j=-\infty}^{\infty} \int_0^{2\pi} \tilde{\mathbf{r}}_j^{(e)}\left(\Omega, \left\{\tilde{\mathbf{q}}_k^{(e)}\right\}\right) e^{\mathbf{i}(j-m)\tau} d\tau &= \mathbf{0} \\ \tilde{\mathbf{r}}_m^{(e)}\left(\Omega, \left\{\tilde{\mathbf{q}}_k^{(e)}\right\}\right) &= \mathbf{0} \quad \text{for} \quad m = -H, \ldots, H. \end{aligned} \tag{2-35}$$

Equation (2-34) is analogous to Eq. (2-25), (2-26) and (2-27), but this time in the exponential form. It imposes that the Fourier coefficients of the residual must be zero up to the truncation order H, as showed by the Harmonic Balance equations defined in Eq. (2-35). Since the complex exponential representation of the FS was used this time, those equations present some redundancies that must be eliminated. The Fourier coefficients of the residual have the conjugate mirror property, so that $\Re\left\{\tilde{\mathbf{r}}_m^{(e)}\right\} = \Re\left\{\tilde{\mathbf{r}}_{-m}^{(e)}\right\}$ and $\Im\left\{\tilde{\mathbf{r}}_m^{(e)}\right\} = -\Im\left\{\tilde{\mathbf{r}}_{-m}^{(e)}\right\}$. Therefore, it is sufficient to solve Eq. (2-35) only for $m \geq 0$. The Harmonic Balance equations form a system of nonlinear algebraic equations that can be written in a compact form as

$$\mathbf{R}_{HB}(\mathbf{u}) = \begin{bmatrix} \tilde{\mathbf{r}}_0^{(e)}(\mathbf{u}) \\ \Re\left\{\tilde{\mathbf{r}}_1^{(e)}(\mathbf{u})\right\} \\ \Im\left\{\tilde{\mathbf{r}}_1^{(e)}(\mathbf{u})\right\} \\ \vdots \\ \Re\left\{\tilde{\mathbf{r}}_H^{(e)}(\mathbf{u})\right\} \\ \Im\left\{\tilde{\mathbf{r}}_H^{(e)}(\mathbf{u})\right\} \end{bmatrix} = \mathbf{0}, \tag{2-36}$$

where $\mathbf{u} = \left[\tilde{\mathbf{q}}_{-H}^{(e)}, \ldots, \tilde{\mathbf{q}}_0^{(e)}, \ldots, \tilde{\mathbf{q}}_H^{(e)}, \Omega\right]$ represents the vector of unknowns. In total, there are $(2H+1)n$ nonlinear algebraic equations to be solve with respect to the $(2H+1)$ Fourier coefficients $\tilde{\mathbf{q}}_k^{(e)} \in \mathbb{C}^n$ and with respect to the fundamental frequency $\Omega \in \mathbb{R}$. Since the Fourier coefficients $\tilde{\mathbf{q}}_k^{(e)}$ share the conjugate mirror property, only $(2H+1)n$ independent parameter must be found to define them. Only the real and imaginary parts of $\tilde{\mathbf{q}}_k^{(e)}$ for $k \geq 0$ must be found. Therefore, the vector of unknowns can be reduced to $\mathbf{u} = \left[\tilde{\mathbf{q}}_0^{(e)}, \Re\left\{\tilde{\mathbf{q}}_1^{(e)}\right\}, \Im\left\{\tilde{\mathbf{q}}_1^{(e)}\right\}, \ldots, \Re\left\{\tilde{\mathbf{q}}_H^{(e)}\right\}, \Im\left\{\tilde{\mathbf{q}}_H^{(e)}\right\}, \Omega\right]$, where the redundancy of the negative Fourier coefficients are eliminated. By looking the relationship between the exponential and trigonometric representation of the Fourier coefficients defined in Eq. (2-3), it is equivalent to write the vector of unknowns as $\mathbf{u} = \left[\tilde{\mathbf{q}}_0^{(c)}, \tilde{\mathbf{q}}_1^{(c)}/2, -\tilde{\mathbf{q}}_1^{(s)}/2, \ldots, \tilde{\mathbf{q}}_H^{(c)}/2, -\tilde{\mathbf{q}}_H^{(s)}/2, \Omega\right]$.

There are many cases where the fundamental frequency is not an unknown, for example, when the external force is not zero. In those cases, the fundamental frequency is assumed to be equal to the fundamental frequency of the periodic excitation, or integer divisor of it (to account for possible subharmonics in the responses). When this is the case, Eq. (2-36) is already balanced and leads to a unique solution. For the case where the fundamental frequency is in fact an unknown, the periodic boundary value problem can have infinite solutions, as in the case of computation of NNMs. Therefore, additional equations must be added to Eq. (2-36) to generate a unique solution. A discussion about those additional equations are postponed to the following chapters.

2.4 Solution of Harmonic Balance equations

For now, let's assume that the fundamental frequency of the periodic solution is given, so that Ω can be removed from $\mathbf{u}$. Therefore, the system of nonlinear algebraic equations defined in Eq. (2-36) is already balanced. The

problem can then be summarized as:

$$\begin{aligned} \text{Solve:} \quad & \mathbf{R}_{HB}(\mathbf{u}) = \mathbf{0} \\ \text{With respect to:} \quad & \mathbf{u} \\ \text{Where:} \quad & \mathbf{u} \in \mathbb{R}^{(2H+1)n},\ \mathbf{R}_{HB} : \mathbb{R}^{(2H+1)n} \rightarrow \mathbb{R}^{(2H+1)n} \end{aligned} \tag{2-37}$$

Analytical solutions of such problem is limited to systems with simple nonlinearities and small dimensions (only a few DOF). A standard example is the Duffing oscillator covered in many textbooks [42]. For most of the other cases, numerical approaches are the only possibility. The Newton-type methods are the most popular ones.

The rest of this section addresses how to solve Eq. (2-36) numerically. The chosen method is the Newton-Raphson. It corresponds to a local method that updates an initial guess for the solution in a recursive way until it converges to the actual solution (within some tolerance margin). It is a method with fast convergence if good initial guesses are provided, otherwise the convergence is not guaranteed. This makes the initial guess an important input in the search of the periodic solutions. In general, the solution of the underlying linear system is a good starting point. If the energy in the system is too high (so that the actual solution is to far away from the linear regime), one may look for several solutions with an increasing energy level and update the new initial guess with predecessor results each time.

The Newton method corrects a guessed solution by expanding $\mathbf{R}_{HB}$ in a Taylor series around the solution $\left(\mathbf{u}^{(i)} + \Delta\mathbf{u}^{(i)}\right)$, where $\mathbf{u}^{(i)}$ is the current guessed solution and $\Delta\mathbf{u}^{(i)}$ is the correction needed. This leads to the following expression:

$$\mathbf{R}_{HB}\left(\mathbf{u}^{(i)} + \Delta\mathbf{u}^{(i)}\right) = \mathbf{R}_{HB}\left(\mathbf{u}^{(i)}\right) + \left.\frac{\partial \mathbf{R}_{HB}}{\partial \mathbf{u}}\right|_{\mathbf{u}^{(i)}} \Delta\mathbf{u}^{(i)} + \text{HOT} = \mathbf{0}, \tag{2-38}$$

where HOT stands for higher-order terms. Assuming that the guessed solution $\mathbf{u}^{(i)}$ is close to the actual solution, the correction term $\Delta\mathbf{u}^{(i)}$ becomes small and the HOT can be neglected. As a result, an estimation of the correction can be found solving the following system of linear algebraic equations:

$$\Delta\hat{\mathbf{u}}^{(i)} = -\left(\left.\frac{\partial \mathbf{R}_{HB}}{\partial \mathbf{u}}\right|_{\mathbf{u}^{(i)}}\right)^{-1} \mathbf{R}_{HB}\left(\mathbf{u}^{(i)}\right) \tag{2-39}$$

It is only an estimation because the neglected HOT are in reality nonzero if $\mathbf{R}_{HB}$ is nonlinear. In equation (2-39), the matrix $\frac{\partial \mathbf{R}_{HB}}{\partial \mathbf{u}}$ is called Jacobian and it collects all the partial derivatives of $\mathbf{R}_{HB}$ with respect to $\mathbf{u}$. Those partial derivatives can be computed analytically or using the finite difference method.

Analytical computation leads to a significant improvements in the computation cost and in the numerical precision and therefore should always be preferable when possible.

Since only an estimation of the correction is available, a recursive scheme must be implemented to bring the initial guessed solution to the actual one (within some tolerance margin). At each iteration, the updated guessed solution is given by

$$\mathbf{u}^{(i+1)} = \mathbf{u}^{(i)} + \Delta\hat{\mathbf{u}}^{(i)}. \tag{2-40}$$

The correction process only stops when $\left\|\mathbf{R}_{HB}\left(\mathbf{u}^{(i+1)}\right)\right\| < \varepsilon$, where ε is some given tolerance, or until the maximum amount of iteration is reached (convergence failed).

2.5 Alternating frequency-time scheme

In order to solve the Harmonic Balance equations defined in Eq. (2-36), the Newton-Raphson method is usually applied. In Eq. (2-39), R_{HB} and $\frac{\partial R_{HB}}{\partial \mathbf{u}}$ must be evaluated at each iteration during the recursive correction of the initial guess $\mathbf{u}^{(0)}$. In order to do that, the Fourier coefficients of the residual function defined in Eq. (2-31) and their respective derivatives must be computed several times. The Fourier coefficients of the residue were defined previously in Eq. (2-33), and they are repeated here for convenience:

$$\tilde{\mathbf{r}}_j^{(e)} = \mathbf{S}_j(\Omega)\tilde{\mathbf{q}}_j^{(e)} + \tilde{\mathbf{f}}_{nl,j}^{(e)}\left(\Omega, \left\{\tilde{\mathbf{q}}_k^{(e)}\right\}\right) - \tilde{\mathbf{f}}_{ex,j}^{(e)}(\Omega) \quad \text{for } j = 0, \ldots, H. \tag{2-41}$$

Each Fourier coefficient $\tilde{\mathbf{r}}_j^{(e)}$ is a sum of three terms: the Fourier coefficient of the linear force defined by $\mathbf{S}_j(\Omega)\tilde{\mathbf{q}}_j^{(e)}$, the Fourier coefficient of the nonlinear force, $\tilde{\mathbf{f}}_{nl,j}^{(e)}\left(\Omega, \left\{\tilde{\mathbf{q}}_k^{(e)}\right\}\right)$, and the Fourier coefficient of the external force, $\tilde{\mathbf{f}}_{ex,j}^{(e)}(\Omega)$. Equation (2-41) can be interpreted as the dynamic force equilibrium in frequency domain, evaluated at the j-th harmonic frequency. The computation of $\mathbf{S}_j(\Omega)$ does not present difficulties since it can be easily done knowing the matrices $\mathbf{M}$, $\mathbf{C}$ and $\mathbf{K}$. This linear term is harmonically-wise decoupled, which means that only the j-th harmonic coefficient of the periodic response contributes in the j-th harmonic coefficient of the residual. For the external force, the signal is usually given in upfront so that the Fourier coefficients $\left\{\hat{\mathbf{f}}_{ex,j}^{(e)}\right\}_{j=-H}^{H}$ can be computed using standard Fourier analysis. In general, the difficulty is restricted to the terms related to the nonlinear forces. Depending on the type of nonlinearity, the Fourier coefficients $\tilde{\mathbf{f}}_{nl,j}^{(e)}$ can not be calculated in a closed-form, or the process becomes too tedious when dealing with a high truncation order H. A popular approach to overcome this difficulty consists in compute $\tilde{\mathbf{f}}_{nl,j}^{(e)}(\Omega)$ numerically using the Alternating Frequency-Time

(AFT) scheme [43, 15, 44, 45, 46]. This technique is computationally efficient, especially when using the FFT algorithm. It can be summarize through the following three steps:

- Given the current guessed solution, $\mathbf{u}^{(i)}$, the Fourier coefficients $\tilde{\mathbf{q}}_k^{(e)}$ and the fundamental frequency Ω can be used to evaluate $\mathbf{q}_H(t)$. This change from frequency-domain to time-domain can be done theoretically using Eq. (2-30), or practically using the inverse Fast Fourier Transform (iFFT). The number of samples used to discretize $\mathbf{q}_H(t)$ over one period is equal to the total number of Fourier coefficients used in the iFFT. Therefore, to get a good discretization of the *Ansatz* in time-domain (high sampling frequency), a process of zero-padding in frequency domain is usually done. Assuming that $N \geq (2H+1)$ Fourier coefficients are used in the iFFT (some of them equal to zero by the zero-padding), the discrete signal $\mathbf{q}_{H,j} = \mathbf{q}_H(jh)$ for $j = 0, \ldots, N$ can be generated, where $h = \frac{2\pi}{N\Omega}$ is the sampling interval.
- From the sampled *Ansatz*, the discrete signal of the nonlinear force, $\mathbf{f}_{nl,j} = \mathbf{f}_{nl}(jh, \mathbf{q}_{H,j}, \dot{\mathbf{q}}_{H,j})$, can be computed according to the equation of motion. The samples of $\dot{\mathbf{q}}_{H,j}$ can be computed in the same way as $\mathbf{q}_{H,j}$, but multiplying the Fourier coefficients by $\mathbf{i}k\Omega$ before performing the iFFT (derivation in frequency-domain).
- The last step in the ATF scheme corresponds to transform the sampled nonlinear force $\mathbf{f}_{nl,j}$ (in time-domain) to $\tilde{\mathbf{f}}_{nl,j}^{(e)}$ (in frequency-domain). This can be easily done using the Fast Fourier transform (FFT). Notice that N Fourier coefficients are generated because of the zero-padding used in the first step. Only the coefficients related to harmonics with orders up to the H should be consider and the rest discarded.

A numerical example is presented now to illustrate these three steps of the AFT scheme. The chosen nonlinear force for this simple example corresponds to a restoring force from a pure cubic spring, i.e.,

$$f_{nl} = q^3(t). \tag{2-42}$$

The adopted truncation order of the *Ansatz* was chosen here to be 3, so that it can be written as

$$q_H(t) = \sum_{k=-3}^{3} \tilde{q}_k^{(e)} e^{\mathbf{i}k\Omega t}. \tag{2-43}$$

The fundamental frequency is known for this example and equals to $\Omega = 2\pi$, so that it is not part of the unknowns of the problem. Then, vector $\mathbf{u}$ becomes

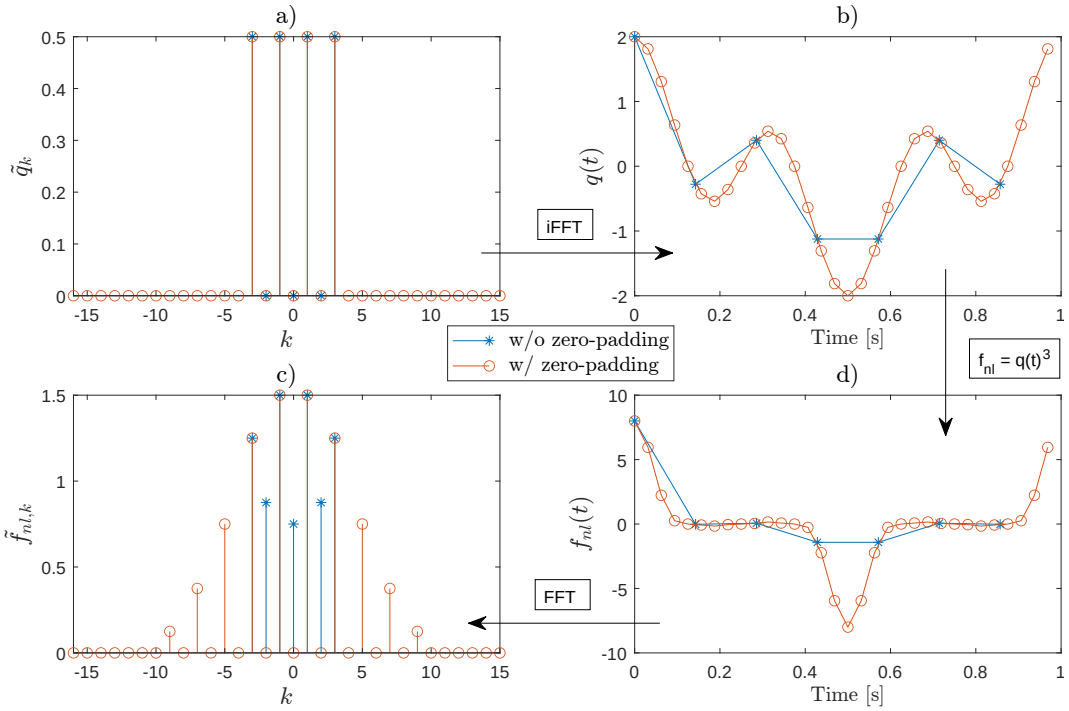

Figure 2.3: Numerical example of the ATF scheme.

$$\mathbf{u} = \begin{bmatrix} \tilde{q}_0 \\ \Re\left\{\tilde{q}_1^{(e)}\right\} \\ \Im\left\{\tilde{q}_1^{(e)}\right\} \\ \Re\left\{\tilde{q}_2^{(e)}\right\} \\ \Im\left\{\tilde{q}_2^{(e)}\right\} \\ \Re\left\{\tilde{q}_3^{(e)}\right\} \\ \Im\left\{\tilde{q}_3^{(e)}\right\} \end{bmatrix}. \tag{2-44}$$

The ATF scheme starts with the current guessed solution of the unknown, which in this case was arbitrarily chosen as

$$\mathbf{u} = \begin{bmatrix} 0 \\ 0.5 \\ 0 \\ 0 \\ 0 \\ 0.5 \\ 0 \end{bmatrix}. \tag{2-45}$$

From this guessed values of the unknowns, the Fourier coefficients of the guessed periodic solution can be computed. The result is presented in the top-left plot of Fig. 2.3 (blue). It is also presented the same Fourier coefficient with zero padding (red), which increases the total number of coefficients.

Once the Fourier coefficients are reconstructed from the vector of un-

knowns, the discrete time-domain signal of the guessed periodic solution can be computed using the iFFT. This represents the first step in the ATF scheme. The result is presented in the top-right plot of Fig. 2.3 for both cases, with and without zero-padding. Notice that the extra zero-valued Fourier coefficients added by the zero-padding did not modify the signal at all, but increased the sampling frequency. This is very important since it can be used latter to avoid aliasing, an error explained earlier at the end of section 2.1.

From the samples of the guessed periodic solution in the time-domain, the discrete time-domain signal of the nonlinear force can be computed following the nonlinearity expression, in this case, a cubic function of the periodic solution. This corresponds to the second step in the ATF scheme. The result is presented in the bottom-right plot of Fig. 2.3. The poor resolution of the discrete signal without zero-padding becomes more visible with this particular nonlinear force. The sampled signal (blue) with poor resolution misses an important part of the signal that contains high negative values of the force, which results in a wrong signal with a nonzero mean. This is no longer the case when the zero-padding is used in the first step and the sampling frequency becomes higher.

The importance of a good sampling frequency is highlighted at the last step of the ATF scheme, when the sampled signal of the nonlinear force is transformed from the time-domain to the frequency-domain using the FFT algorithm. Although the Fourier coefficients of the nonlinear force matches at the odd harmonics (up to the truncation order $H = 3$), some wrong nonzero even Fourier coefficients appear for the signal that was not zero-padded. This error is caused by *aliasing*. The Fourier coefficient of the harmonics above H (positive and negative) are not considered in the Harmonic Balance equation, so they should be discarded. Ideally, they should have a small value, but if this is not the case (as in this example), a higher truncation order of the *Ansatz* should be considered.

The Fourier coefficients of this simple polynomial nonlinear force have a closed-form expression, so it can be compared with the results from the ATF scheme. The guessed periodic solution can be written as a Fourier series from the vector on unknowns $\mathbf{u}$, which yielding in

$$q(t) = 0.5e^{-3\Omega t} + 0.5e^{-1\Omega t} + 0.5e^{\Omega t} + 0.5e^{3\Omega t}. \tag{2-46}$$

To evaluate the Fourier coefficient of the nonlinear force we need to compute

$q^3(t)$, which lead to

$$\begin{aligned} f_nl(t) &= \left(0.5e^{-3\Omega t} + 0.5e^{-1\Omega t} + 0.5e^{\Omega t} + 0.5e^{3\Omega t}\right)^3 \\ &= \frac{1}{8}e^{-9\Omega t} + \frac{3}{8}e^{-7\Omega t} + \frac{6}{8}e^{-5\Omega t} + \frac{10}{8}e^{-3\Omega t} + \frac{12}{8}e^{-\Omega t} \\ &\quad + \frac{12}{8}e^{\Omega t} + \frac{10}{8}e^{3\Omega t} + \frac{6}{8}e^{5\Omega t} + \frac{3}{8}e^{7\Omega t} + \frac{1}{8}e^{9\Omega t} \end{aligned} \tag{2-47}$$

A comparison between the expression in Eq. (2-47) and the bottom-left plot of Fig. 2.3 shows that the ATF scheme leads to the exact Fourier coefficients. If the nonlinear force had a higher dimension or a more complicated nonlinearity, the analytical process would become impossible or too tedious.

3
Shooting method

In the last chapter, the HBM was describe as a tool to solve the periodic boundary value problem described in Eq. (1-2). It used a weak formulation to approximate a solution in the form of a truncated Fourier series. This chapter addresses an alternative approach, known as the Shooting method [47, 48], which also deals with the periodic boundary problem numerically, integrating the differential equation directly in its strong formulation.

The idea behind the Shooting method is to search for an initial state that leads to a desired state after a defined period of time. When used to solve periodic boundary value problems, any difference between the initial and final states is treated as a residue, which can be minimized using a numerical method. To construct the residual function, the governing equation is first integrated numerically from a given initial state until a final state at a given time. This numerical integration can be done using any standard integration method, such as the Runge-Kutta or the Newmarks scheme.

When compared to the HBM, the Shooting method is much simpler. It only requires the implementation of a numerical integration scheme and a solver. It also deals with the periodic boundary value problem directly in its strong formulation, so the searched solution is only an approximation in the numerical sense, not because of its formulation. Nevertheless, since numerical integration is involved in the solution process, numerical instability and loss of accuracy can occur. The computational cost to evaluate the responses can also increase significantly when high dimensional systems are involved or if the solutions are not smooth (which requires a small time discretization). One main advantage of the Shooting method is its capacity to evaluate the instability of the solution (in a asymptotic sense) directly.

This chapter starts reviewing the Newmark scheme, the chosen integration method used here for the Shooting method. Then, the shooting residue is defined and a discussion of how to solve it using gradient based methods is defined. At the end, a method of how evaluate the asymptotic stability of periodic responses is presented.

3.1 Newmark Integrator

The integration method discussed in this section was first proposed by Newmark in 1959 [49] and underwent further developments in the following years [50, 51, 52]. It consists in a single-step integration formula that can integrate second-order differential equations of dynamic models directly. In another words, it does not require to recast the equation of motion in a first-order state-space form. The popularity of the method comes from the fact that it has two free parameters that can be used to adjust the numerical properties of the integration. For example, depending on the values of those two parameters, the integration becomes unconditionally stable, which means that the stability of the integration is not affected by the step size used.

The goal of the Newmark method is to find the state of the system at a time instant $t_{n+1} = t_n + v$ from a known state at the time instant t_n, where v is the time step size. In this chapter the Newmark method will be used to evaluate the final state of a system after a period of time $t = T$. The equation of motion (the same as Eq. (2-28)) and the respective initial conditions are given. In another words, the Newmark method will be used to solve a initial value problem.

Let a generic function $w(t)$ at a time instant t_{n+1} be expressed in a Taylor series expansion as

$$w(t_{n+1}) = w(t_n) + vw^{(1)}(t_n) + \frac{v^2}{2}w^{(2)}(t_n) + \cdots + \frac{v^s}{s!}w^{(s)}(t_n) + R_s \qquad (3\text{-}1)$$

where $w^{(s)}(t) = \frac{d^s w(t)}{dt^s}$ and R_s is the remainder of the development to the order s, defined as:

$$R_s = \frac{1}{s!}\int_{t_n}^{t_n+v} (t_n + v - \tau)^s \, w^{(s+1)}(\tau)d\tau \qquad (3\text{-}2)$$

Using the expressions (3-1) and (3-2), the displacement and velocity of the system at $t = t_{n+1}$ can be written as

$$\mathbf{q}_{n+1} = \mathbf{q}_n + v\dot{\mathbf{q}}_n + \int_{t_n}^{t_{n+1}} (t_{n+1} - \tau)\, \ddot{\mathbf{q}}(\tau)d\tau \qquad (3\text{-}3)$$

$$\dot{\mathbf{q}}_{n+1} = \dot{\mathbf{q}}_n + \int_{t_n}^{t_{n+1}} \ddot{\mathbf{q}}(\tau)d\tau, \qquad (3\text{-}4)$$

where $\mathbf{q}_n = \mathbf{q}(t_n)$ and $\mathbf{q}_{n+1} = \mathbf{q}(t_n + v) = \mathbf{q}(t_{n+1})$. The integral terms in Eq. (3-3) and Eq. (3-4) can then be approximated using a numerical quadrature.

The Taylor expansions of $\ddot{\mathbf{q}}_n$ and $\ddot{\mathbf{q}}_{n+1}$ around $\tau \in [t_n, t_{n+1}]$ is given by

$$\ddot{\mathbf{q}}_n = \ddot{\mathbf{q}}(\tau) + (t_n - \tau)\,\mathbf{q}^{(3)}(\tau) + \frac{(t_n - \tau)^2}{2}\mathbf{q}^{(4)}(\tau) + \dots \tag{3-5}$$

$$\ddot{\mathbf{q}}_{n+1} = \ddot{\mathbf{q}}(\tau) + (t_{n+1} - \tau)\,\mathbf{q}^{(3)}(\tau) + \frac{(t_{n+1} - \tau)^2}{2}\mathbf{q}^{(4)}(\tau) + \dots \tag{3-6}$$

Multiplying Eq. (3-5) by $(1-2\beta)$ and Eq. (3-6) by 2β, the sum of the resulting equations yields in

$$\ddot{\mathbf{q}}(\tau) = (1 - 2\beta)\,\ddot{\mathbf{q}}_n + 2\beta\ddot{\mathbf{q}}_{n+1} + \mathbf{q}^{(3)}(\tau)\,[\tau - 2v\beta - t_n] + \dots . \tag{3-7}$$

Repeating the same process, but now multiplying Eq. (3-5) by $(1-\gamma)$ and Eq. (3-6) by γ, the sum of the resulting equations yields in

$$\ddot{\mathbf{q}}(\tau) = (1 - \gamma)\,\ddot{\mathbf{q}}_n + \gamma\ddot{\mathbf{q}}_{n+1} + \mathbf{q}^{(3)}(\tau)\,[\tau - v\gamma - t_n] + \dots . \tag{3-8}$$

Substituting Eq. (3-7) and Eq. (3-8) in the integral terms of Eq. (3-3) and Eq. (3-4), respectively, the quadrature formulas are obtained:

$$\int_{t_n}^{t_{n+1}} (t_{n+1} - \tau)\,\ddot{\mathbf{q}}(\tau)d\tau = \left(\frac{1}{2} - \beta\right) v^2\ddot{\mathbf{q}}_n + \beta v^2\ddot{\mathbf{q}}_{n+1} + \mathbf{r}_\beta \tag{3-9}$$

$$\int_{t_n}^{t_{n+1}} \ddot{\mathbf{q}}(\tau)d\tau = (1 - \gamma)\,v\ddot{\mathbf{q}}_n + \gamma v\ddot{\mathbf{q}}_{n+1} + \mathbf{r}_\gamma \tag{3-10}$$

where $\mathbf{r}_\beta$ and $\mathbf{r}_\gamma$ are the error measures, defined as

$$\mathbf{r}_\beta = \left(\beta - \frac{1}{6}\right) v^3\mathbf{q}^{(3)}(\bar{\tau}) + O\left(v^4\mathbf{q}^{(4)}\right) \tag{3-11}$$

$$\mathbf{r}_\gamma = \left(\gamma - \frac{1}{2}\right) v^2\mathbf{q}^{(3)}(\bar{\tau}) + O\left(v^3\mathbf{q}^{(4)}\right) \tag{3-12}$$

for $t_n < \bar{\tau} < t_{n+1}$. Neglecting $\mathbf{r}_\beta$ and $\mathbf{r}_\gamma$ with the argument that they are higher-order functions of v, a family of time-integration schemes (Newmark's family) is obtained substituting Eqs. (3-9) and (3-10) into Eqs. (3-3) and (3-4), respectively:

$$\mathbf{q}_{n+1} = \mathbf{q}_n + v\dot{\mathbf{q}}_n + v^2\left(\frac{1}{2} - \beta\right)\ddot{\mathbf{q}}_n + v^2\beta\ddot{\mathbf{q}}_{n+1} \tag{3-13}$$

$$\dot{\mathbf{q}}_{n+1} = \dot{\mathbf{q}}_n + (1 - \gamma)\,v\ddot{\mathbf{q}}_n + \gamma v\ddot{\mathbf{q}}_{n+1} \tag{3-14}$$

The constants β and γ are the quadrature parameters. Common values of those parameters are: $\beta = \frac{1}{6}$ and $\gamma = \frac{1}{2}$, which corresponds to a linear interpolation of $\ddot{\mathbf{q}}(\tau)$ in $\tau \in [t_n,\ t_{n+1}]$, and $\beta = \frac{1}{4}$ and $\gamma = \frac{1}{2}$, which corresponds to the average of $\ddot{\mathbf{q}}(\tau)$ in $\tau \in [t_n,\ t_{n+1}]$.

From the Newmark's time-integration relationships, an implicit Newmark integration scheme can be constructed to integrate nonlinear systems. First,

the relationships established in Eq. (3-13) and Eq. (3-14) may be inverted in the following way:

$$\ddot{\mathbf{q}}_{n+1} = \frac{1}{\beta v^2}\left(\mathbf{q}_{n+1} - \hat{\mathbf{q}}_{n+1}\right) \tag{3-15}$$

$$\dot{\mathbf{q}}_{n+1} = \hat{\dot{\mathbf{q}}}_{n+1} + \frac{\gamma}{\beta v}\left(\mathbf{q}_{n+1} - \hat{\mathbf{q}}_{n+1}\right) \tag{3-16}$$

where $\hat{\mathbf{q}}_{n+1}$ and $\hat{\dot{\mathbf{q}}}_{n+1}$ may be seen as predictions of the displacement and velocity at t_{n+1} with $\ddot{\mathbf{q}}_{n+1} = \mathbf{0}$:

$$\hat{\mathbf{q}}_{n+1} = \mathbf{q}_n + v\dot{\mathbf{q}}_n + \left(\frac{1}{2} - \beta\right) v^2 \ddot{\mathbf{q}}_n \tag{3-17}$$

$$\hat{\dot{\mathbf{q}}}_{n+1} = \dot{\mathbf{q}}_n + (1-\gamma)\, v\ddot{\mathbf{q}}_n \tag{3-18}$$

The mechanical system been considered in this thesis are governed by the equation motion Eq. (2-28), repeated here for convenience:

$$\underbrace{\mathbf{M}\ddot{\mathbf{q}}(t) + \mathbf{C}\dot{\mathbf{q}}(t) + \mathbf{K}\mathbf{q}(t)}_{\text{Linear forces}} + \underbrace{\mathbf{f}_{nl}\left(t, \mathbf{q}(t), \dot{\mathbf{q}}(t)\right)}_{\text{Nonlinear forces}} = \underbrace{\mathbf{f}_{ex}(t)}_{\text{External forces}} . \tag{3-19}$$

Equations (3-15) and (3-16) can be substituted into the equation of motion to evaluate it at t_{n+1}. A residue (function of $\mathbf{q}_{n+1}$ only) can then be defined as:

$$\mathbf{r}_N(\mathbf{q}_{n+1}) = \left[\frac{1}{\beta v^2}\mathbf{M} + \frac{\gamma}{\beta v}\mathbf{C} + \mathbf{K}\right]\mathbf{q}_{n+1} + \mathbf{f}_{nl}\left(t_{n+1}, \mathbf{q}_{n+1}, \dot{\mathbf{q}}_{n+1}\left(\mathbf{q}_{n+1}\right)\right) - \mathbf{b} = 0 \tag{3-20}$$

where

$$\mathbf{b} = \left[\frac{1}{\beta v^2}\mathbf{M} + \frac{\gamma}{\beta v}\right]\hat{\mathbf{q}}_{n+1} - \mathbf{C}\hat{\dot{\mathbf{q}}}_{n+1} - \mathbf{f}_{ex}(t_{n+1}). \tag{3-21}$$

The implicit integration scheme consists in solving Eq. (3-20) for each time step using a solver (e.g. the Newton-Raphson method). Once the displacement $\mathbf{q}_{n+1}$ is found, the velocity and acceleration can be also computed using Eqs. (3-15) and (3-16) before moving forward to the next time step.

3.2 Shooting residue

To find the periodic solution of a nonlinear mechanical systems using the Shooting method, a shooting residual function must vanish. To define this residual, the equation of motion defined in Eq. (3-19) must be first recast into a state space form as:

$$\dot{\mathbf{y}}(t) = \mathbf{g}\left(\mathbf{y}(t), t\right) \tag{3-22}$$

where $\mathbf{y}(t) = \begin{bmatrix}\mathbf{q}^T(t) & \dot{\mathbf{q}}^T(t)\end{bmatrix}^T \in \mathbb{R}^{2n}$ is the state of the system and

$$\mathbf{g}\left(\mathbf{y}, t\right) = \begin{bmatrix}\mathbf{q} \\ \mathbf{M}^{-1}\left[-\mathbf{C}\dot{\mathbf{q}} - \mathbf{K}\mathbf{q} - \mathbf{f}_{nl}\left(t, \mathbf{q}, \dot{\mathbf{q}}\right) + \mathbf{f}_{ex}(t)\right]\end{bmatrix} \tag{3-23}$$

is the vector field. The time dependency of $\mathbf{y}$ and $\mathbf{q}$ in Eq. (3-23) has been omitted for simplicity. Just like in chapter 2, the external force $\mathbf{f}_{ex}$ and the nonlinear force $\mathbf{f}_{nl}$ are assumed here to be periodic if they are explicitly time dependent (non-autonomous systems). If no external force is applied, the system considered here must be conservative so that a periodic solution may exist. A residual function, also known as shooting residue, can be defined as the difference between the final state, $\mathbf{y}(T)$, and the initial state, $\mathbf{y}(0) = \mathbf{y}_0$:

$$\mathbf{R}_{sh}\left(\mathbf{y}_0, T\right) = \mathbf{y}(T) - \mathbf{y}_0. \tag{3-24}$$

where, T is the fundamental period of the periodic solution. Equation (3-24) highlights the dependence of the initial condition and the fundamental period in the residual function. The response is considered a solution of the periodic boundary value problem if

$$\mathbf{R}_{sh}\left(\mathbf{u}\right) = \mathbf{0}, \tag{3-25}$$

where $\mathbf{u} = \left[\mathbf{y}_0^T,\ T\right]$ corresponds to the unknowns of the problem. Equation (3-25) is analogous to the Eq. (2-36) for the HBM since the respective solutions define a periodic solution of the problem. Equation (3-25) can be solved with respect to the initial state and the fundamental period using any solver, for example, the same Newton-Raphson method described in section 2.4. The same comments made for the HBM solution are applied here: The initial guess of $\mathbf{u}$ must be close to the actual solution, otherwise convergence is not guaranteed. Also, if the period T is indeed an unknown (when no external excitation is applied), additional equations must be incorporated into $\mathbf{R}_{sh}$ to generate a unique solution. Those additional equations are responsible to define an energy level of the response using a amplitude normalization, which is postponed to the following chapters.

As shown in Eq. (2-39), the correction of a current guess $\mathbf{u}^{(i)}$ using the Newton-Raphson method requires the computation of the Jacobian matrix $\frac{\partial \mathbf{R}_{sh}}{\partial \mathbf{u}}$. This can be done analytically or numerically (e.g. through finite-difference). When $\mathbf{g}\left(\mathbf{y}, t\right)$ is not differentiable only the numerical approach is possible. The analytical approach is discussed here in more detail since it leads to a more efficient and precise computation of $\frac{\partial \mathbf{R}_{sh}}{\partial \mathbf{u}}$. For the Shooting method, the precise computation of this Jacobian matrix is particularly important since many of its entries can be used latter to evaluate the stability of the periodic responses.

Let's start with the differentiation of the residual function with respect to the initial conditions only. This leads to

$$\frac{\partial \mathbf{R}_{sh}}{\partial \mathbf{y}_0} = \left.\frac{\partial \mathbf{y}(t)}{\partial \mathbf{y}_0}\right|_{t=T} - \mathbf{I}_{2n}, \tag{3-26}$$

where $\mathbf{I}_{2n} \in \mathbb{R}^{2n\times 2n}$ is the identity matrix. The first term in the right-hand side of Eq. (3-26) corresponds to the variation in the state at $t = T$ after perturbations in the initial conditions, one at the time. This matrix can be computed by taking the derivative of the equation of motion in the state space form, Eq. (3-22), with respect to the initial conditions. This leads to

$$\frac{\partial}{\partial \mathbf{y}_0}\left[\dot{\mathbf{y}}(t)\right] = \frac{\partial}{\partial \mathbf{y}_0}\left[\mathbf{g}\left(\mathbf{y}(t), t\right)\right]. \tag{3-27}$$

Applying the chain rule on the right-hand side, it follows that

$$\frac{d}{dt}\left[\frac{\partial \mathbf{y}(t)}{\partial \mathbf{y}_0}\right] = \frac{\partial \mathbf{g}(\mathbf{y}(t), t)}{\partial \mathbf{y}}\frac{\partial \mathbf{y}(t)}{\partial \mathbf{y}_0}. \tag{3-28}$$

Equation (3-28) consists in an initial-value problem governed by ordinary differential equations and with initial condition given by $\frac{\partial \mathbf{y}(0)}{\partial \mathbf{y}_0} = \mathbf{I}_{2n}$. Therefore, to evaluate $\frac{\partial \mathbf{R}_{sh}}{\partial \mathbf{y}_0}$, one must first numerically integrate Eq. (3-28) to obtain $\frac{\partial \mathbf{y}(t)}{\partial \mathbf{y}_0}$ at $t = T$ and then substitute the result in Eq. (3-26).

The remaining terms in the Jacobian matrix are related to the differentiation of the residual function with respect to the fundamental period. This task is much easier and can be done using Eq. (3-22) evaluated at $t = T$ since

$$\frac{\partial \mathbf{R}_{sh}}{\partial T} = \left.\frac{\mathbf{y}(t)}{\partial t}\right|_{t=T} = \mathbf{g}\left(\mathbf{y}(T), T\right). \tag{3-29}$$

Once $\frac{\partial \mathbf{R}_{sh}}{\partial \mathbf{y}_0}$ and $\frac{\partial \mathbf{R}_{sh}}{\partial T}$ have been computed, the Jacobian can be built as:

$$\frac{\partial \mathbf{R}_{sh}}{\partial \mathbf{u}} = \begin{bmatrix}\frac{\partial \mathbf{R}_{sh}}{\partial \mathbf{y}_0} & \frac{\partial \mathbf{R}_{sh}}{\partial T}\end{bmatrix} \tag{3-30}$$

3.3 Stability analysis

When analyzing the steady state response of nonlinear vibration problems, the periodic solutions of the governing equations can be either stable or unstable. For the case of stable solution, it can be observed in an experimental setup while unstable solution can only be found numerically. The discussion of stability is restricted here to autonomous systems that can be described by a first-order ordinary differential equation. In the case of non-autonomous systems where the time dependency is periodic (with known period), the same approach for stability analysis is still possible by adding additional variables into the state vector, transforming the non-autonomous system in an autonomous one.

The discussion here is restricted to the concept of asymptotic stability: a periodic solution (a limit cycle) is asymptotically stable if any trajectory that starts sufficiently close to it, remain close to it until it converges to the actual

limit cycle as time progresses. Since the stability analysis is restricted here to small perturbations around the periodic solution, linear approximations for the perturbed solutions can be applied.

Let the periodic solution $\mathbf{y}(t)$ be written as $\mathbf{y}(t, \mathbf{y}_0)$ to emphasize the dependence of the response in the initial condition. By perturbing the initial condition with a significant small amount $\Delta\mathbf{y}_0$, the perturbed response after one period can be written in a Taylor expansion as

$$\mathbf{y}\left(T, \mathbf{y}_0 + \Delta\mathbf{y}_0\right) = \mathbf{y}\left(T, \mathbf{y}_0\right) + \left.\frac{\partial \mathbf{y}(t, \mathbf{y}_0)}{\partial \mathbf{y}_0}\right|_{t=T} \Delta\mathbf{y}_0 + HOT \tag{3-31}$$

For small perturbations the higher order terms (HOT) can be neglected, so the perturbation in the solution becomes

$$\Delta\mathbf{y}(T) = \left.\frac{\partial \mathbf{y}(t, \mathbf{y}_0)}{\partial \mathbf{y}_0}\right|_{t=T} \Delta\mathbf{y}_0 = \mathbf{\Phi}(T, \mathbf{y}_0)\Delta\mathbf{y}_0, \tag{3-32}$$

where $\mathbf{\Phi}(T, \mathbf{y}_0)$ is the monodromy matrix. It describes how small perturbations around $\mathbf{y}_0$ evolves in the solution after one period of oscillation. One of the greatest benefits of the Shooting method over the HBM is the fact that the monodromy matrix is already computed during the process, so the stability analysis is done without significant amount of extra computation.

Using the result of Eq. (3-32), the perturbation in the periodic solution after m oscillations can then be approximated by

$$\Delta\mathbf{y}(mT) = \left[\mathbf{\Phi}(T, \mathbf{y}_0)\right]^m \Delta\mathbf{y}_0, \tag{3-33}$$

which shows that the stability of the periodic solution depends on the eigenvalues of the monodromy matrix, also known as Floquet multipliers. The set of eigenvalues provides the exponential variation of the perturbation along the eigendirections of the monodromy matrix [53]. If a Floquet multiplier has magnitude above one, the perturbation grows exponential as time increases in that eigendirection. Therefore, the periodic solutions are considered stable only if all the Floquet multipliers lies within the unit circle in the complex plane.

4
Numerical path continuation

In chapters 2 and 3, two numerical methods capable of solving periodic boundary value problems were described. The knowledge of just one periodic solution of a nonlinear systems is usually not enough to cover all the dynamic characteristics that the system might have. For example, small changes in the initial conditions can lead to a total different dynamic behavior since those initial conditions may be located at different basin of attractions. Furthermore, one could also be interest in understand the qualitative and quantitative changes of some periodic solution under the variation of a certain parameter, here referred to as free parameter. Numerical path continuation is a consistent and effective method to accomplish this type of analysis through the computation of solutions paths (branches of solutions).

In structural dynamics, path continuation are commonly applied for several types of analysis. Two important ones that are covered in this thesis are:

- The construction of nonlinear frequency response curves (NFRCs), where the excitation frequency becomes the free parameter and the periodic solutions are evaluated at different frequencies.
- Nonlinear modal analysis, where modal parameters such as nonlinear normal modes (NNM) and the respective fundamental frequencies are computed for an increasing level of energy.

Generally, the construction of a solution path is restricted to a predefined interval of the free parameter. This free parameter is then allowed to vary within the predefined interval with a fixed increment, a process known as sequential method, or using a more flexible parameterization restriction, a process known as continuation method. In both cases, the most common strategy to compute the solution path follows a predictor-corrector scheme [54]. In this case, the initial guess for a new periodic solution is given using information from the previous known solution (prediction phase). This initial guess is usually close to the actual solution, but not exact. A correction is then needed and it is usually done using a solver (e.g. the Newton-Raphson method).

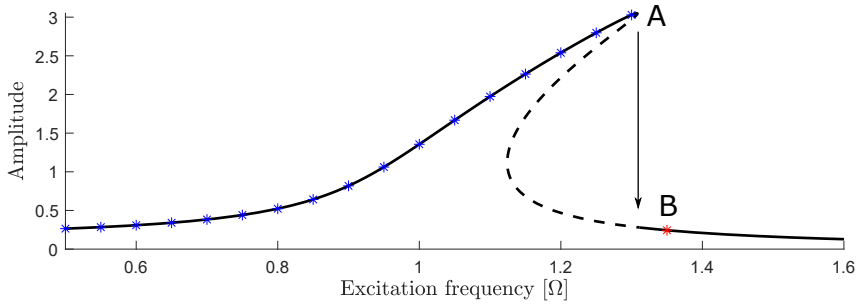

Figure 4.1: Illustration of a sequential continuation procedure to compute a NFRC of a Duffing oscillator.

When using the sequential method, numerical problems can arise when facing turning points, which is a common type of bifurcation when dealing with nonlinear systems. Such problem is illustrated in Fig 4.1. In this example, a NFRC of a Duffing oscillator is presented. The respective equation of motion is given by:

$$\ddot{x} + 0.05\dot{x} + x + 0.1x^3 = 0.2\sin(\omega_f t)\,. \tag{4-1}$$

For this analysis, the solution branch was computed using the excitation frequency as free parameter and restricting it to the interval $\omega_f \in [0.5,\ 1.6]$. Here, the amplitude in the plot corresponds to the root mean square value (RMS) of the periodic oscillations. The black lines (solid and dashed) correspond to the actual solution branch. The blue dots shows the results for a sequential continuation that started at $\omega_f = 0.5$ and had the fixed frequency increment of $\Delta\omega_f = 0.05$. The process undergo smoothly until the turning point A is reached. Following the sequential strategy, the next theoretical solution point should be B, a point that cannot be computed in most cases. The main cause of this failure is the fact that solutions A and B are quite different from each other. The prediction using information from solution A is not close enough to B, so that the convergence in the correction phase was not guarantee (Newton method is a local method and requires good initial guesses). Therefore, an evident limitation of the sequential method is its inability to transpass a turning point. In Fig. 4.1, additional solution points that compose the NRFC are represented by the dashed line. Some of those solutions could indeed be obtained if the sequential continuation was done in a decreasing direction, from high to low frequencies, but some parts of the NFRC would still not be computed.

This severe limitation motivates the use of numerical path continuation instead of the sequential continuation [55]. Although it increases the computational complexity, the robustness in finding the solution paths compensates the cost. If one has the previous knowledge that no turning point (or any kind of bifurcation) exists, the sequential continuation can become a preferable choice since it reduces the computational cost. In the following sections, different

methods for prediction and correction are discussed. The combination of those methods allows the creation of a robust and efficient continuation method. The nonlinear frequency response curves (NFRCs) of three systems with different nonlinear properties are used to illustrate the continuation method. Since nonlinear normal modes are the main subject of this thesis, their calculation using continuation methods will be developed in the dedicated chapter 5.

4.1 Continuation methods

Let the problem under analysis be defined as

$$\begin{aligned} \text{Solve} \quad & \mathbf{R}\left(\bar{\mathbf{u}}\right) = \mathbf{0} \\ \text{with respect to} \quad & \bar{\mathbf{u}} = \begin{bmatrix} \mathbf{u}^T & \lambda \end{bmatrix}^T \\ \text{for the interval} \quad & \lambda^s \leq \lambda \leq \lambda^f \\ \text{where} \quad & \mathbf{u} \in \mathbb{R}^{n_u},\ \lambda \in \mathbb{R},\ \mathbf{R} : \mathbb{R}^{n_u+1} \rightarrow \mathbb{R}^{n_u}. \end{aligned} \tag{4-2}$$

Function $\mathbf{R}$ corresponds to the residual functions. Those functions were defined by Eq. (2-36) when solving the periodic solutions with the HBM and by Eq. (3-24) when solving with the Shooting method. The vector of unknowns $\mathbf{u}$ corresponds to the Fourier coefficient of the *Ansatz* when using the HBM or the initial conditions when using the Shooting method. The fundamental period (or fundamental frequency) of the periodic solution can also be incorporated in the vector of unknowns in many situations (e.g. when computing NNMs). Sometimes, it becomes a known parameter when the excitation frequency is given (e.g. when computing the NFRCs).

The parameter λ corresponds to the free parameter in which the continuation analysis is based on. It can be any parameter of the system or excitation. For example, it becomes the excitation frequency in the frequency response analysis, or the system's energy in the NNMs, or a damping parameter in the analysis of self-excited limit cycles and etc. The continuation analysis is restricted to a predefined interval of the free parameter, limited by the lower bound λ^s and upper bound λ^f.

4.1.1 Predictor

To follow a solution branch, a prediction of the next point is necessary using the properties of at least one previous solution. Let's assume that a solution $\bar{\mathbf{u}}_i$ for the problem in Eq. (4-2) is known, usually at the starting point λ^s. A prediction for the next solution in the branch can be obtained as

$$\hat{\bar{\mathbf{u}}}_{j+1} = \bar{\mathbf{u}}_j + s_j \mathbf{p}_j, \tag{4-3}$$

where $\mathbf{p}_j$ is the direction vector and s_j is the step size. The direction vector is assumed here to have unit norm. The direction vector can be evaluated in two different manners, using the secant or the tangent methods. Both approaches are illustrated in Fig. 4.2a.

Direction vector with secant method: the direction vector is defined using two previous known solution points and extrapolating the solution path linearly. This leads to

$$\mathbf{p}_j = \frac{\bar{\mathbf{u}}_j - \bar{\mathbf{u}}_{j-1}}{\|\bar{\mathbf{u}}_j - \bar{\mathbf{u}}_{j-1}\|}. \tag{4-4}$$

Higher order extrapolations can also be used, but it would requires the knowledge of even more previous points and an extension of Eq. (4-3) would also be necessary to account for the higher order terms.

Direction vector with tangent method: the direction of the straight line that is tangent to the solution branch at $\mathbf{u}_j$ is defined solving the following linear system of equations:

$$\left.\frac{\partial \mathbf{R}}{\partial \bar{\mathbf{u}}}\right|_{\bar{\mathbf{u}}_j} \bar{\mathbf{p}}_j = \mathbf{0}. \tag{4-5}$$

A unique tangent direction is guaranteed only if $rank\left\{\frac{\partial \mathbf{R}}{\partial \bar{\mathbf{u}}}\right\} = n_u$. This criterion fails if more than one solution branch crosses at $\bar{\mathbf{u}}_j$ (e.g. transcritical and pitchfork bifurcations). Since Eq. (4-5) has n_u equations and $n_u + 1$ unknowns, it is underdetermined. Therefore only the directions of $\bar{\mathbf{p}}_j$ is obtained, not its length and orientation. This can be overcome by adding an extra normalization equation to the system in Eq. (4-5). An example of such normalization is given by

$$\mathbf{e}_k^T \bar{\mathbf{p}}_j = 1, \tag{4-6}$$

where $\mathbf{e} \in \mathbb{R}^{n_u+1}$ is a unit vector with all entries equal to zero except the k-th, which equals one. This is not the only possible normalization, but it has the benefit to maintain the problem linear. The tangent direction $\bar{\mathbf{p}}_j$ can then be computed through

$$\begin{bmatrix} \left.\frac{\partial \mathbf{R}}{\partial \bar{\mathbf{u}}}\right|_{\bar{\mathbf{u}}_j} \\ \mathbf{e}_k^T \end{bmatrix} \bar{\mathbf{p}}_j = \mathbf{0} \tag{4-7}$$

A further normalization can be applied later on $\bar{\mathbf{p}}_j$ to make it a unit vector, i.e.,

$$\mathbf{p}_j = \frac{\bar{\mathbf{p}}_j}{\|\bar{\mathbf{p}}_j\|}. \tag{4-8}$$

Throughout this thesis, the tangent predictor will be used. Once the normalization is made, its direction can be defined to ensure the continuation in the solution path, avoiding it to return to previous points. In Fig. 4.2a, $\mathbf{p}_j$

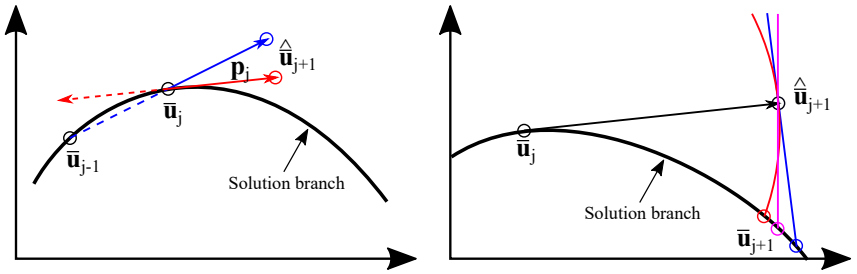

Figure 4.2: a) prediction estimation with secant (blue) and tangent (red) methods. b) Different parameter restrictions during correction phase

is represented by the dashed and solid red arrows. Both are tangent to the solution branch and have unit norm. But only the solid arrow continues in the right direction of the branch and therefore should be the one chosen in Eq. (4-3).

Step size: The value of s_j represents (indirectly) the resolution of the solution path. It can be defined as a constant or it can be adaptive (which is recommended). When a big step size is used, it is more likely for the prediction point to move away from the actual solution. As a consequence, a higher amount of iterations is necessary to correct the prediction to the actual solution, or even worst, the convergence can be lost. If a small step size is used, a higher number of solution points is necessary to cover all the predefined interval of the free parameter, which becomes time consuming. A common strategy is to adjust the step size in terms of the number of iterations required to correct the previous predicted solution. This can be accomplished by the following equation

$$s_j = \frac{N_c}{N_*} s_{j-1}, \tag{4-9}$$

where N_c is the number of iterations used to correct the last predicted solution to the actual solution (correction) and N_* is an ideal number, chosen by the user. Additionally, the step size is usually limited by a upper bound value to ensure a minimum resolution of the branch. This strategy is illustrated in Fig 4.3. Notice that the points near higher curvatures tend to have a smaller step size. This occurs because the predictions (from tangent or secant method) are not so accurate around those regions, resulting in a higher number of iterations to correct them.

4.1.2 Correction

Once the predicted solution is calculated from Eq. (4-3), some corrections are needed to find the actual solution (within some tolerance) of Eq. (4-2). To

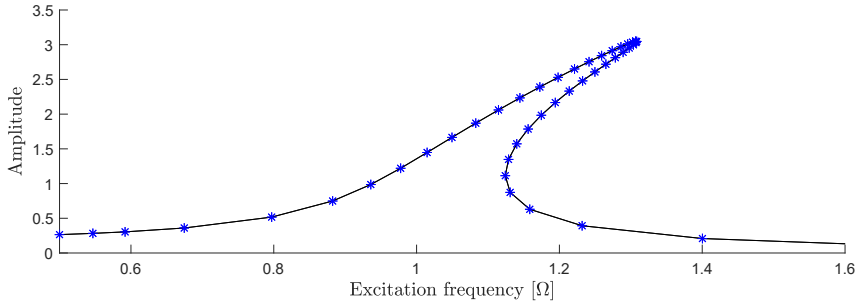

Figure 4.3: Illustration of a continuation procedure with the step size adjustment as function of the number of iteractions in the correction phase.

guarantee that this new solution also maintains the continuation of the branch, a parametric restriction is necessary. A parameterization consists in some kind of measure that defines the position of the solution points along the branch. From a given parameterization, it is possible to set a restriction that guarantees the continuation along the branch. Without this restriction, the prediction could return to previous known solutions, which hinders the continuation of the solution. The restriction in the parameterization will be given here by the additional equation $h(\bar{\mathbf{u}}_{j+1}) = 0$, which must be solved simultaneously with Eq. (4-2). In other words, one must solve the following system of algebraic equations during the correction phase:

$$\begin{bmatrix} \mathbf{R}\left(\bar{\mathbf{u}}_{(j+1)}\right) \\ h(\bar{\mathbf{u}}_{j+1}) \end{bmatrix} = \begin{bmatrix} \mathbf{0} \\ 0 \end{bmatrix}, \tag{4-10}$$

which corresponds to $n_u + 1$ equations with $n_u + 1$ unknowns. The equations are usually nonlinear and are solved using a numerical method. The process of finding the solution (within some tolerance) of Eq. (4-10) corresponds to the correction of the predicted solution. The initial guess is given by $\hat{\bar{\mathbf{u}}}_{j+1}$ (from Eq. (4-3)) and can be updated using the Newton-Raphson method. The number of iterations N_c used by the solver is important to update the step size used to predict next solution point, as showed by Eq. (4-9).

Different types of parameterization are possible. For example, one can use the components of $\bar{\mathbf{u}}$ or the arclength from some reference point. Figure 4.2b illustrates three types of restrictions that will be discussed now in more detail. Any of them can be used to replace $h(\bar{\mathbf{u}}_{j+1})$ in Eq. (4-10).

Local restriction: Using the components of $\bar{\mathbf{u}}$ to parameterize the solution branch, a restriction in the new solution point can be made by imposing the value of one of its components, e.g. the local parameter $u_{k,(j+1)}$, where $1 \leq k \leq n_u + 1$. One can restrict its value by adding a fixed increment from the previous solution $u_{k,j}$, i.e.,

$$h_{\text{loc}}(\bar{\mathbf{u}}_{j+1}) = u_{k,j+1} - (u_{k,j} + \xi) = 0, \tag{4-11}$$

where ξ is the fixed increment. Notice that u_k can be any component of $\bar{\mathbf{u}}$, including the free parameter λ. The choice of the index k is free to change at each new solution point. If $k \leq n_u$, the local parameter is a component of $\mathbf{u}$, which means that the new solution can also move perpendicular to λ. This allow the continuation to overcome turning points. If $k = n_u + 1$, the local parameter becomes λ and the continuation method approaches the sequential one. The performance of the corrector depends on the choice of k. One way of defining it is by setting k equal to the index of the largest component in $\mathbf{p}$, i.e.,

$$p_k = \max\left\{\|p_1\|, \|p_2\|, \ldots, \|p_{n_u+1}\|\right\}. \tag{4-12}$$

The increment size ξ depends in the index k, as well as the current location on the solution path. One possibility is to relate it with the step size s_j, defining it as

$$\xi = s_j p_{k,j}. \tag{4-13}$$

The benefit of this approach is that ξ becomes also adaptive along the continuation (with small values nearby turning points).

This parameterization restriction is shown in Fig. 4.2b with the correction path represented by the magenta line. In this example, $k = n_u + 1$ so that the local parameter is the free parameter λ. The increment ξ is used as defined in Eq. (4-13). This parameterization restriction forces the correction path to be travel perpendicular to the λ axis.

Orthogonal restriction Another way to restrict the new solution point is by forcing the correction path to be perpendicular to $\mathbf{p}_j$, the direction vector in the predictor phase. This is accomplished by defining the restriction function as

$$h_{\text{ort}}(\bar{\mathbf{u}}_{j+1}) = \mathbf{p}_j^T \left(\hat{\bar{\mathbf{u}}}_{j+1} - \bar{\mathbf{u}}_{j+1}\right) \tag{4-14}$$

This type of restriction is illustrated with the blue correction path in Fig. 4.2b. This restriction strategy can face problems when dealing with turning points, specially if a large step size is used in the prediction phase (computing $\hat{\bar{\mathbf{u}}}_{j+1}$ through Eq. (4-3)). The main advantage of this method is that it is linear.

Arclength restriction Another way to parameterize the solution branch is by measuring its arclength from a given reference point. When the reference point is defined as the last known solution point $\bar{\mathbf{u}}_j$, the arclength to the predicted point is given by the step size s_j. To maintain this distance along the correction path, one can define the restriction function $h(\bar{\mathbf{u}}_{j+1})$ as

$$h_{\text{arc}}(\bar{\mathbf{u}}_{j+1}) = \sum_{k=1}^{n_u+1} (u_{k,j+1} - u_{k,j})^2 - (s_j)^2 = 0 \tag{4-15}$$

This strategy is robust against turning points, which justifies its popularity. Throughout this thesis, the arclength corrector will be used. In the schematic example showed in Fig. 4.2b, the corrector path with the arclenght restriction is illustrated with the red curve.

4.1.3 Algorithm

An algorithm to compute the continuation of periodic solutions based on the prediction-correction scheme is now presented. The same algorithm works for the HBM and the Shooting method and it is described in Fig. 4.4. The subscripts HB and sh in the residual equations have been removed since both methods are contemplated by the same algorithm. The main steps of the algorithm are summarize as following:

1. First, some input parameters must be given. This includes an initial guess $\hat{\mathbf{u}}_0$ for the first periodic solution point $\mathbf{u}_0$ to be found at the starting value of the free parameter λ^s. It also includes an initial step size s_0 for the continuation and the ideal number of iterations in correction phase N_*. The initial guess of the first periodic solution can be sometimes the hardest part in the entire algorithm. A good strategy is to look for a first periodic solution that is close to the periodic solution of the underlying linear system, which can be easily calculated. This represents, for example, choosing a first periodic solution that is away from the resonance when computing the NFRC, or choosing a first periodic solution that has low energy levels when computing the NNM so that it is similar to the LNM. The values of s_0 and N_* require some experience since it can varies significantly depending on the type of problem.

2. Before correcting the given initial guess for the first solution point, a special parameterization restriction must be created for this first solution point. It should force the correction iterations to maintain the same value of the free parameter. This can be done imposing

$$h(\bar{\mathbf{u}}_0) = \lambda - \lambda_s. \tag{4-16}$$

   Such parameterization restriction can be seen as the local one, as described in section 4.1.2, where the $k = n_u + 1$ (i.e., the free parameter is restricted), $u_{k,j} = 0$ (there is no previous point) and $\xi = \lambda^s$.

3. Given the initial parameterization restriction, the periodic solution can be found solving Eq. (4-10) using the Newton-Raphson method and using the $\hat{\tilde{\mathbf{u}}}_0 = \left[\hat{\mathbf{u}}_0^T, \lambda_s\right]$ as initial guess.

4. Knowing at least one periodic solution (the first one or any other), the next periodic solution in the solution branch can be predicted using Eq. (4-3). It requires the computation of the unit direction vector $\mathbf{p}_j$, which depends in the prediction method used. It can be computed with Eq. (4-4) for the secant method and with Eqs. (4-5) and (4-8) for the tangent method. When only the first periodic solution is known ($j = 0$), the tangent method is the only possible choice since the secant method requires at least two solution points.

5. After computing the unit direction vector, the prediction of the next periodic solution is computed using Eq. (4-3) and the current step size s_j. Such prediction is used as initial guess of the solver during the correction phase.

6. Before correcting the initial guess of the next periodic solution, the parameterization restriction must be updated from the knowledge of the previous periodic solution. Three different methods were discussed in section 4.1.2. The parameterization restriction is defined by Eq. (4-11) for the local restriction, by Eq. (4-14) for the orthogonal restriction and by Eq. (4-15) for the arc-length restriction.

7. Knowing the parameterization restriction and the initial guess (predicted solution), the next periodic solution can be found solving Eq. (2-39) with the Newton-Raphson method. An important parameter to observe this time is the number of iterations required by the solver, defined as N_c.

8. Knowing N_c and the target number N_*, the step size for the next prediction can be adjust using Eq. (4-9).

9. From the last known periodic solution, it is possible to check if the free parameter λ already reached the λ^f, which represents the higher boundary value of the predefined interval. If it has reached, the continuation can stop. Otherwise, a new solution point should be found repeating steps 4 to 8.

Besides the steps described above, additional mechanisms should be added to the algorithm to create a more robust code. If the correction of the predicted solution fails (no convergence), a new trial should be conducted estimated a new prediction with a smaller step size, for example, half of

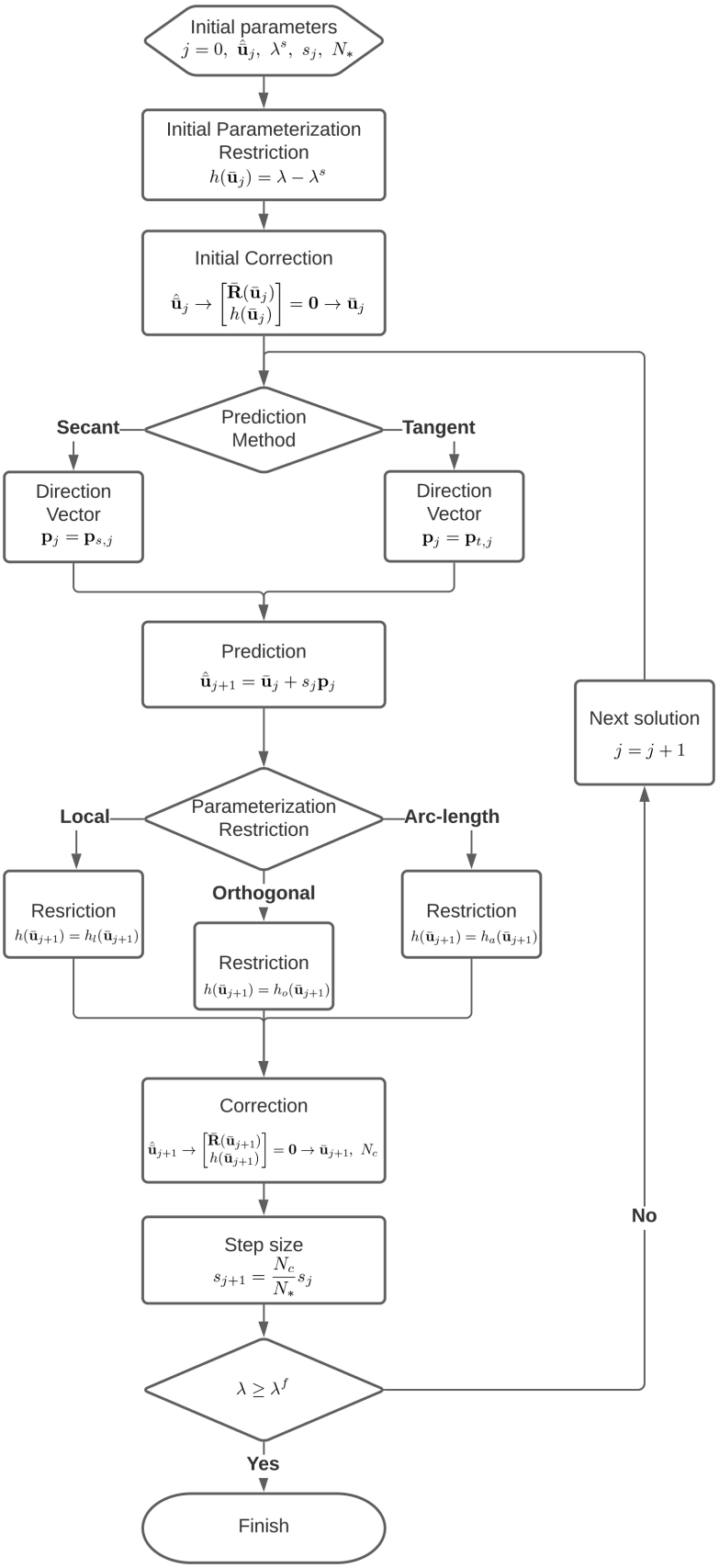

Figure 4.4: Algorithm to compute the NNM and NFRC.

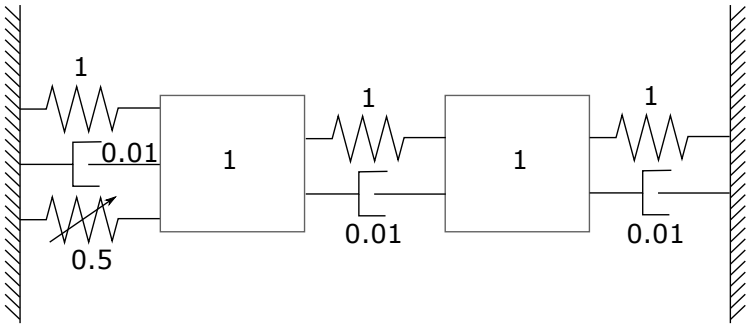

Figure 4.5: Two degrees of freedom system with local nonlinear spring.

the current size. Also, the solver can face some numerical problems when dealing with unknowns with different orders of magnitude. This can be solved preconditioning the problem, as explained in [56].

4.2 Nonlinear frequency response curves

To exemplify the numerical path continuation method described in the last section, in combination with the HBM and the Shooting method described in chapters 2 and 3, the frequency response of nonlinear mechanical systems will be presented now. It consists in calculate the response of the system harmonically excited at different frequencies, usually nearby the resonance region (where the nonlinear effects becomes more apparent). Therefore, the free parameter in this continuation analysis becomes the fundamental frequency for the HBM and the oscillation period for the Shooting method. In the examples here, the frequency response is evaluated with different levels of excitation to highlight the energy dependency in the response of nonlinear systems.

When dealing with linear systems that are excited with a sinusoidal force, the responses are also sinusoidal and with equal frequency. The differences are restricted to changes in the amplitude and phase. The frequency response can then be easily defined as the ratio between the response over the excitation at each frequency. This is no longer possible for nonlinear systems since the response is not (in general) sinusoidal anymore, i.e., higher and lower harmonics usually arise in the periodic solution because of the nonlinear terms [34, 42]. Therefore, a different scalar quantity must be used to characterize the response as function of the excitation frequency. The most common ones are the root mean square (rms), the peak-to-peak or the maximum value of the periodic oscillation.

4.2.1 Example 1: 2 DOF oscillator with cubic spring

The first example discussed here is the 2 DOF oscillator with a nonlinear stiffness as illustrated in Fig. 4.5. This mechanical system is often used as benchmark in the study of nonlinear normal modes [53, 56, 57]. The main goals of this example are: a) show that the HBM and the Shooting method can lead to the same periodic responses, b) show the characteristics of cubic spring elements, c) show the results of a stability analysis and d) show that the implemented path continuation method can easily pass through turning points.

The equations of motion for this system is given by

$$\begin{aligned} \ddot{q}_1 + 0.02\dot{q}_1 - 0.01\dot{q}_2 + 2q_1 - q_2 + 0.5q_1^3 &= P_1 \sin(\omega_f t) \\ \ddot{q}_2 + 0.02\dot{q}_2 - 0.01\dot{q}_1 + 2q_2 - q_1 &= P_2 \sin(\omega_f t), \end{aligned} \tag{4-17}$$

where q_1 and q_2 are the displacements of the left and right masses, respectively.

The NFRCs were evaluated around both natural frequencies of the underlying linear system (1 and $\sqrt{3}$ rad/s). The responses were calculated for a sinusoidal excitation with magnitude (P_1 or P_2) varying from 0.01 to 0.16 with an increment of 0.05. The forces were applied at each DOF, one at the time (first $P_1 = \{0.01; 0.06; 0.11; 0.16\}$ and $P_2 = 0$, then $P_1 = 0$ and $P_2 = \{0.01; 0.06; 0.11; 0.16\}$). The responses were evaluated at both DOF and the RMS of the periodic solutions were calculated. In total, four families of NFRCs were generated for each frequency interval. The results are presented in Fig. 4.6 and 4.7. The periodic solutions were calculated using the HBM and the Shooting method. When using the HBM, the truncation order was set up to the 7-th harmonic. An analysis of the stability of the responses was also done using the Floquet multipliers (only when using the Shooting method), as described in section 3.3. All figures show a perfect agreement between both methods. They also show the expected bending of the resonance peak to the right as consequence of the hardening effect caused by the cubic stiffness term [42]. For the responses in Fig. 4.6, unstable responses were found even for low levels of excitation and before turning points (see $NFRC_{12}$ and $NFRC_{22}$), which shows the importance of performing the stability analysis to predict unexpected behavior. Regarding the numerical path continuation, the methods used here (tangent predictor with arclength corrector) were able to handle turning points with not problem, so that the response in all frequency band of interest was evaluated.

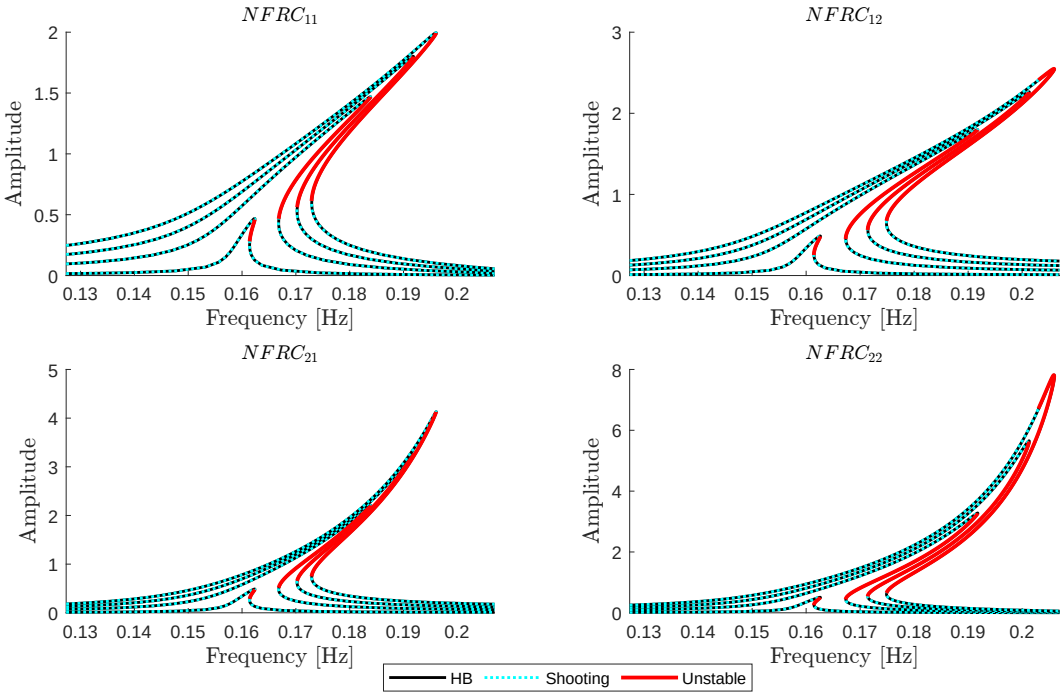

Figure 4.6: Nonlinear frequency response curves around the first resonance region of the 2 DOF system

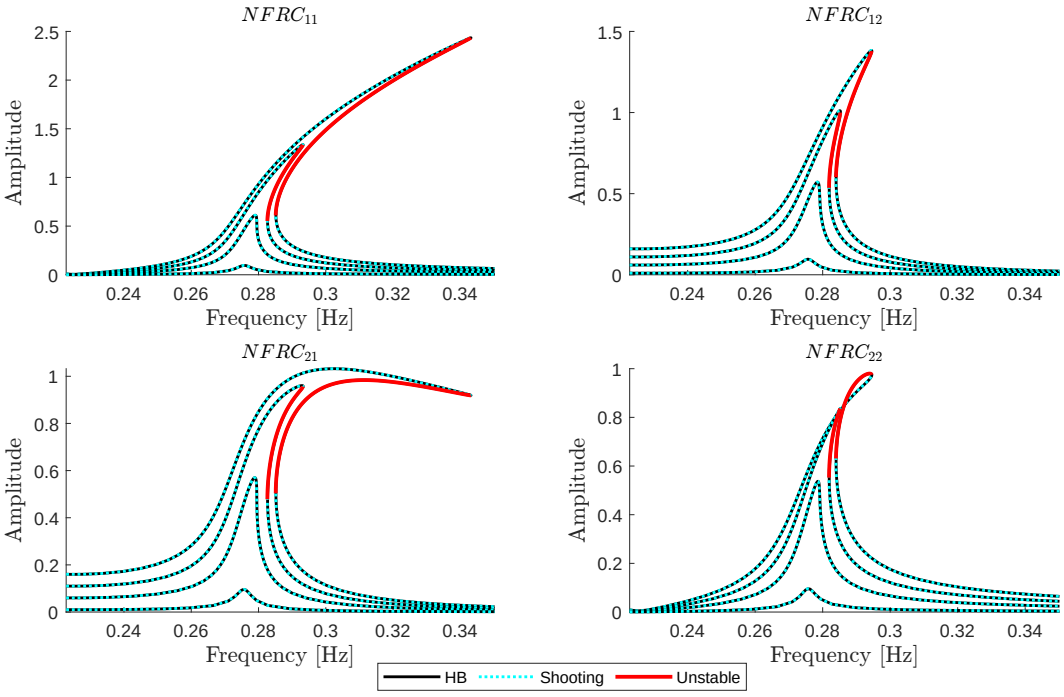

Figure 4.7: Nonlinear frequency response curves around the second resonance region of the 2 DOF system

Length (m)	Width (m)	Thickness (m)	Young's mod. (N/m^2)	Density (kg/m^3)
1	0.038	0.0036	185e9	7830

Table 4.1: Geometric and material properties of the cantilever beam with dry friction.

4.2.2 Example 2: Cantilever beam with dry friction

For the second example, a finite element model of a continuous structure is used. It consists in a clamped-free beam with a dry-friction element at its free end. The goals of this example are: a) to show the dynamical behavior of a different nonlinear element (dry friction) and b) to show different changes in the NFRCs as function of excitation level. The beam's geometric and material properties are summarized in table 4.1. It was spatially discretized using FEM with 10 Euler-Bernoulli elements.

The system was excited by a sinusoidal force at the middle of the beam (as shown in Fig. 4.8) with an amplitude varying from 0.1 to 10.1N with an increment of 0.5N. The displacement was evaluated at the same position where the force was applied. The dry-friction element was smoothed using a hyperbolic tangent function described as follows:

$$f_{nl} = 2\tanh\left(\frac{\dot{q}_{nl}}{0.05}\right), \tag{4-18}$$

where f_{nl} is the nonlinear force generated by the dry-friction and $\dot{q}_{nl}$ is the transverse velocity of the beam's free end. In addition to the dry-friction element, the beam was simulated having a viscous damping matrix that leads to a damping ratio of 1% for all modes of the underlying linear model (clamped-free boundary conditions).

The NFRC was defined here as the ratio between the displacement RMS and excitation RMS, in a way that the respective NFRCs are some how normalized by the force intensity (similar to the FRF in the linear case). Figure 4.8 shows the NFRCs for all the excitation levels. The dashed lines represents the FRF of the linear models of the beam (without the dry-friction element) under different boundary conditions. The red-dashed line represents a linear clamped-free beam, while the blue represents the clamped-pinned beam. This two lines appears as boundary limits for all NFRCs with dry-friction element. For low excitation (solid-blue lines), the transverse velocity at the free end is low, so the resistance imposed by the dry-friction element is proportionally high. Therefore, those curves resemble the clamped-pinned linear FRF, with the highest amplitude around 78rad/s. As the excitation level

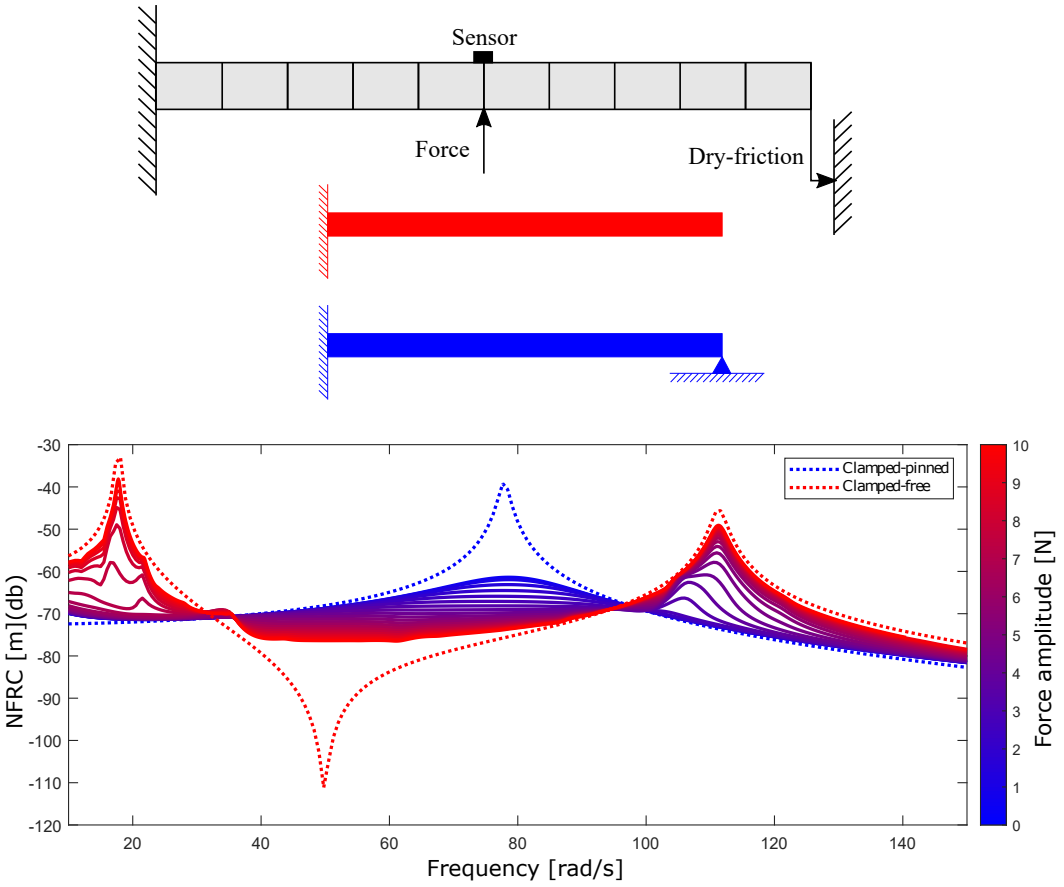

Figure 4.8: Nonlinear frequency response curves of a beam with dry-friction

increases, the velocity at the free end also increases, which makes the friction force to stay at its constant asymptotic value (2N as defined by Eq. (4-18)) for most part of the oscillating period. This makes the resistance force at the free-end proportionally low, so that the respective NFRCs becomes similar to the FRF associated to the linear clamped-free model. This example exposes how the NFRCs of nonlinear systems can drastically change their characteristics with the variation in the energy.

4.2.3 Example 3: Cantilever beam with unilateral spring

The last example of this chapter deals with the same beam of the previous example, but switching the dry-friction element by an unilateral spring with a gap at its free end. The unilateral spring model is linear with the stiffness coefficient equal to 500N/m and positioned with a 0.1m gap from the free end in the transverse direction (see Fig. 4.9). Let $q_{nl}(t)$ be the transverse displacement of the free end of the beam. The nonlinear force is then given by

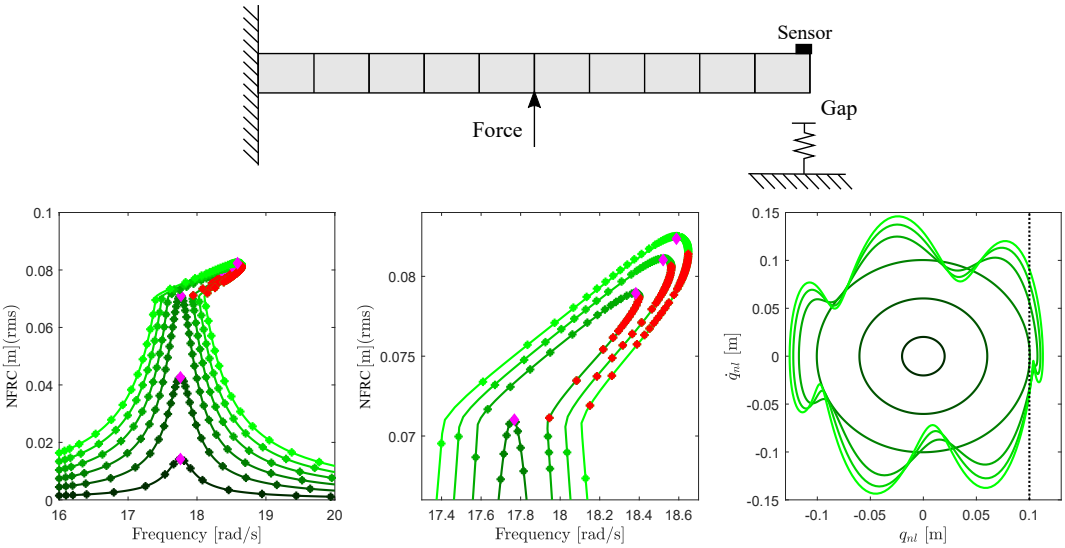

Figure 4.9: Nonlinear frequency response curves of a beam with spring gap at the free end.

$$f_{nl} = \begin{cases} 500\,(q_{nl} - 0.1)\,, & \text{if } q_{nl} \geq 0.1 \\ 0, & \text{if } q_{nl} < 0.1 \end{cases} \tag{4-19}$$

The goals of this example are: a) to show the behavior of the structure under another nonlinear element and b) to show the influence of the truncation order in the computation of the periodic solution with the HBM. This latter topic (although important for all the previous examples) was postponed until now because the nonlinear spring with gap creates a discontinuity in the model. As discussed in chapter 2, periodic functions with discontinuity usually requires a high number of harmonics to well represent it. Therefore, the importance of a correct truncation order becomes more clear in this example.

The NFRCs in this example corresponds to the RMS value of the periodic solutions, evaluated between 16 and 20rad/s. The excitation was applied at the middle of the structure with a sinusoidal force with amplitude varying from 0.1 to 1.1N with an increment of 0.2N. The system response was evaluated only at the free end of the beam. The left plot in Fig. 4.9 shows all the computed NFRCs, where the solid lines represent the solutions with the HBM and the dots the solutions with the Shooting method. For the low excitation levels (up to 0.5N), the displacement at the free end is smaller than the gap between the structure and the unilateral spring (0.1m). Hence, the structure behaves as a simple clamped-free beam. The highest value of each NFRC is marked with a magenta diamond, and the corresponding phase plane is presented in the right plot of Fig. 4.9. As expected, the response in the phase plane for those linear solutions corresponds to ellipses. For the high excitation levels, the unilateral spring becomes activated, causing the local nonlinearity in the system. This

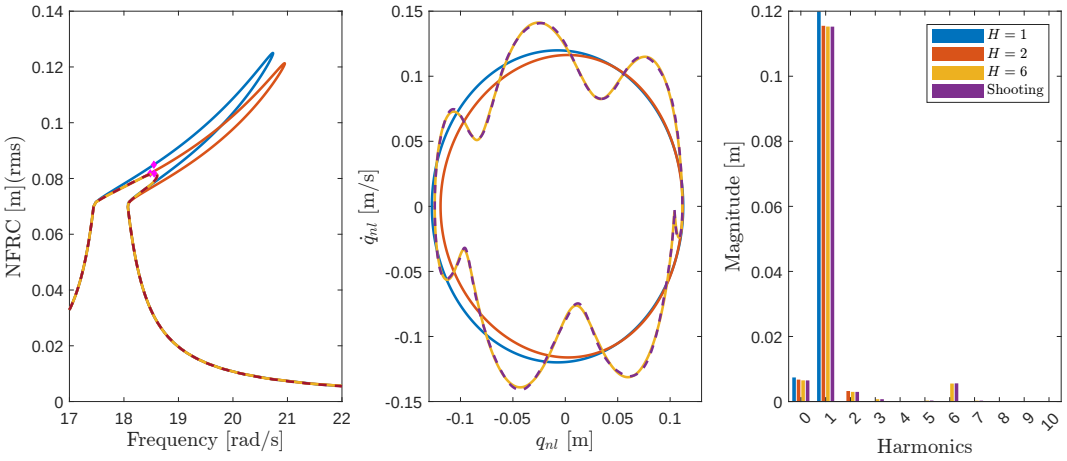

Figure 4.10: Influence of the harmonic truncation order in the periodic response.

sudden increase of stiffness causes the peaks in the NFRCs to bend to the right direction when reaching RMS values higher than $0.1/\sqrt{2}$. The responses become non sinusoidal and instability may occur. The middle plot in Fig. 4.9 shows the same NFRCs with focus at the bent peaks. A stability analysis was done in the Shooting method, evaluating the eigenvalues of the monodromy matrix (section 3.3). All the unstable solutions are marked with red dots. The nonlinear behavior of the beam becomes clear by looking the responses at the phase plane, since they all deviate significantly from ellipses. The black dashed line in the right hand-side plot of Fig. 4.9 separates the phase plane and shows the region where the unilateral spring is in contact with the beam (right part) and where it is not (left part).

Let us focus now in the importance of the truncation order of the HBM. Since the system analyzed has a discontinuity in its model, the response can become non-smooth at high energy levels. As explained in chapter 2, non-smooth periodic functions require more harmonic terms (Fourier coefficients) to well approximate them. This is shown here by calculating once again the NFRC at a high energy level (force equal to 1.1N) with different truncation orders, i.e., with $H = 1$, 2 and 6. The quality of the responses can be evaluated when comparing it with the NFRC obtained using the Shooting method. Figure 4.10 shows the NFRCs, as well as the response in the phase plane of the periodic solutions marked with magenta diamonds. It is clear that the periodic solutions with $H = 1$ or 2 lead to wrong solutions. The reason is shown in the right hand-side plot of Fig. 4.10. The Fourier series coefficients of the periodic solution of with the Shooting method show a significant contribution of the 6th harmonic, which is only contemplated by the HBM if the truncation order is equal or higher than 6.

5
Nonlinear normal modes

Modal analysis is perhaps the most common analysis tool used in structural dynamics. Its popularity comes from its wide field of applications, such as: model reduction, response prediction, system identification, finite element updating, structural modification, vibration control, troubleshooting, substructure coupling and structure health monitoring [58, 59, 60, 41, 61, 62, 63]. Several additional references on modal analysis can be found in the Proceedings of the International Modal Analysis Conferences (IMAC). Modal analysis is formulated and restricted to linear systems. The linear assumption enjoys the benefits of great simplifications, which justify its use. A vector basis built with linear modes can be used to decompose linear systems and write them as uncoupled single degree-of-freedom systems governed by the respective eigensolutions. The free or (periodically) forced solution of a linear system can then be written as a linear combination of the modal solutions, a property known as modal superposition. Also, if the system's free motion is initially restricted to only one mode (from special initial conditions), it will continue to have the motion restricted to that mode indefinitely. There is no energy transfer between modes. This property is known as invariance.

Although modal analysis is a very mature and sophisticated tool for linear systems, it does not exist for nonlinear system. This is mainly explained by the lack of modal superposition property and by the energy-dependency of nonlinear systems, a characteristic that imposes additional difficulties. Although the first contribution related to nonlinear normal modes is attributed to Rosenberg back in the 1960s ([21, 22]), it is still an active field of research with significant contributions in the recent years. Major efforts have been made in the computation of nonlinear normal modes (NNM) of high-dimensional systems [64, 65], of non-conservative system [66, 67, 68, 46, 69] and in the application of nonlinear normal modes for model reductions [70, 71]. The experimental identification of NNM is also under development, where the traditional experimental modal analysis is being adjusted to nonlinear systems [57, 72, 73, 74, 75, 76]. Review articles covering the latest developments in the computation and identification of NNM can be found in [13, 77, 78, 79].

This chapter initiates with the definition of nonlinear normal modes ac-

cording to Rosenberg. The relationship between LNMs and NNMs is discussed and the respective properties of NNM are presented. Later, the computation of the NNM (based on the Rosenberg's definition) is addressed using the tools previously developed in chapters 2, 3 and 4. Several examples are used to illustrate the computations and properties of NNM.

5.1 Nonlinear normal modes: Rosenberg's definition

Rosenberg is responsible for the first definition of nonlinear normal modes (NNM). He defines NNM as a vibration in unison of the system, which restricts the motion of all DOF to reach their extreme values and pass through zero simultaneously (synchronous motion). It is a direct extension of modes for linear conservative natural systems, the linear normal modes (LNM). The equation of motion for those type of systems are given by

$$\mathbf{M}\ddot{\mathbf{q}}(t) + \mathbf{K}\mathbf{q}(t) = \mathbf{0}, \tag{5-1}$$

where $\mathbf{M}$ and $\mathbf{K} \in \mathbb{R}^n$ are the symmetric mass and stiffness matrices of the system, $\mathbf{q}(t) \in \mathbb{R}^n$ represents the displacements of the DOFs. LNMs are found searching for synchronous motion of the system. An *Ansatz* having separated time and space terms is then proposed for this synchronous motion in the following form:

$$\mathbf{q}(t) = \tilde{\mathbf{q}}e^{st}. \tag{5-2}$$

where $\tilde{\mathbf{q}}$ is a constant vector and s is a constant scalar, respectively. Substituting this *Ansatz* in the equation of motion, an eigenvalue problem is obtained:

$$\mathbf{K}\tilde{\mathbf{q}} = \lambda\mathbf{M}\tilde{\mathbf{q}}, \tag{5-3}$$

where $\lambda = -s^2$. A detailed review in the properties of the eigensolutions of this problem is presented in Appendix A. Here, it is important to emphasize that the engensolutions $\{\lambda_k, \tilde{\mathbf{q}}_k\}_{k=1}^n$ are independent of the energy, i.e., they do not change their values with respect to the amplitude of the synchronous motion described by $\mathbf{q}(t)$. The eingenvalues $\{\lambda_k\}_{k=1}^n$ are the squares of the natural frequencies, $\{\omega_{n,k}\}_{k=1}^n$, and the eigenvectors $\{\tilde{\mathbf{q}}_k\}_{k=1}^n$ are the LNMs of the system. Each LNM brings the information about the ratio between the displacements of all DOF. Such relationship is constant along the synchronous motion. This means that, when moving according a certain LNM, the displacement of all DOFs can be written in terms of a single reference DOF.

From one eigensolution pair $(\omega_{n,k}^2, \tilde{\mathbf{q}}_k)$, a family of synchronous motion

can be defined as (see appendix A):

$$\mathbf{q}_k(t) = a_k\tilde{\mathbf{q}}_k e^{\mathbf{i}\omega_k t} + a_k^*\tilde{\mathbf{q}}_k e^{\mathbf{i}\omega_k t} \quad (5\text{-}4)$$

$$= A\cos(\omega_k t + \phi)\,\tilde{\mathbf{q}}_k \quad (5\text{-}5)$$

where A is an amplitude parameter, and therefore dictates the energy in the synchronous motions, and ϕ is a phase parameter. a_k is a complex constant and the product $a_k\tilde{\mathbf{q}}_k$ could be seen as the Fourier coefficient of the fundamental (and only) harmonic of $\mathbf{q}_k(t)$, so it has the information regarding the amplitude and phase of the synchronous motion. All of those parameters could be defined if one state of the system was given at any time. Usually the initial state is used for simplicity. What is important to note is that: a) there are infinite synchronous motions related to k-th eigensolution pair since A and ϕ can be any real number and a_k any complex number. b) the natural frequency and the LNM do not depend on A or $|a_k|$, i.e., they do not depend on the energy of the synchronous motions.

Equation (5-5) describe periodic functions, so it could be seen as solutions of the following periodic boundary value problem:

$$\begin{cases} \mathbf{M}\ddot{\mathbf{q}}_k(t) + \mathbf{K}\mathbf{q}_k(t) = \mathbf{0}, \quad t \in [0, T_k] \\ \mathbf{q}_k(0) = \mathbf{q}_k(T_k) \\ \dot{\mathbf{q}}_k(0) = \dot{\mathbf{q}}_k(T_k) \end{cases} \quad (5\text{-}6)$$

The process of solving this periodic boundary value problem is much more expensive than the process of solving the eigenvalue problem defined by Eq. (5-3), so no one takes this path to compute natural frequencies and LNM in practical situations. It also have infinite solutions, unless the amplitude A and phase ϕ (or a_k) are somehow restricted. This could be done adding two restriction equations into Eq. (5-6):

$$\begin{cases} \mathbf{M}\ddot{\mathbf{q}}_k(t) + \mathbf{K}\mathbf{q}_k(t) = \mathbf{0}, \quad t \in [0, T_k] \\ \mathbf{q}_k(0) = \mathbf{q}_k(T_k) \\ \dot{\mathbf{q}}_k(0) = \dot{\mathbf{q}}_k(T_k) \\ \eta_a(\mathbf{q}_k(0), \epsilon) = 0 \\ \eta_p(\mathbf{q}_k(0)) = 0 \end{cases}, \quad (5\text{-}7)$$

where η_a represents an amplitude restriction of $\mathbf{q}_k(t)$ at $t = 0$, ϵ is a term related to the energy level of the periodic solution and η_p is a phase restriction of $\mathbf{q}_k(t)$. Both restrictions are equivalent to set an initial condition to Eq (5-5). Once the unique periodic solution $\mathbf{q}_k(t)$ is obtained, the natural frequency could be

calculated since $\omega_k = \frac{2\pi}{T_k}$ and T_k becomes a known parameter. The LNM could also be calculated considering the ratio between the entries of $\mathbf{q}_k(t)$ at any time (since the ratio is constant along the oscillation).

Moving now to nonlinear systems, if any *Ansatz* having separated space and time is proposed to find synchronous motion, no eigenvalue problem can be created because of the nonlinear terms. So, there is no *easy way* to obtain the synchronous motion of the system. The definition of Rosenberg's NNM then follows the alternative approach mentioned above: solve a periodic boundary value problem. For a periodic solution to exist, the system must be conservative. Therefore, the computation of NNMs according Rosenberg corresponds in solving the following problem:

$$\begin{cases} \mathbf{M}\ddot{\mathbf{q}}(t) + \mathbf{K}\mathbf{q}(t) + \mathbf{f}_{nl}\left(\mathbf{q}(t)\right) = \mathbf{0}, \quad t \in [0, T] \\ \mathbf{q}(0) = \mathbf{q}(T) \\ \dot{\mathbf{q}}(0) = \dot{\mathbf{q}}(T) \end{cases}, \tag{5-8}$$

where $\mathbf{f}_{nl}$ represents the nonlinear forces in the system. As for the case of linear systems, there are an infinite number of solutions for this problem, each one related to a different amplitude (energy level) and phase. Therefore, a amplitude and a phase restriction for the periodic solution must be also added to the problem to solve it uniquely:

$$\begin{cases} \mathbf{M}\ddot{\mathbf{q}}(t) + \mathbf{K}\mathbf{q}(t) + \mathbf{f}_{nl}\left(\mathbf{q}(t)\right) = \mathbf{0}, \quad t \in [0, T] \\ \mathbf{q}(0) = \mathbf{q}(T) \\ \dot{\mathbf{q}}(0) = \dot{\mathbf{q}}(T) \\ \eta_a(\mathbf{q}(t), \epsilon) = 0 \\ \eta_p(\mathbf{q}(t)) = 0 \end{cases}, \tag{5-9}$$

Those restrictions are better discussed in section 5.3. From a known periodic solution (at a certain energy level ϵ), one can define the fundamental frequency of the periodic solution and the ratios between the displacements of all DOFs. The ratios now are time dependent, which means that they change along $t \in [0, T]$. The fundamental frequency and ratios between the displacements of the DOF are also energy dependent, so the periodic solution should be evaluated for several energy levels ϵ to thoroughly understand the dynamics of the system. This stimulates the implementation of a numerical path continuation of the periodic solution with respect to the energy level in the system. The dependency of energy in the periodic solutions of nonlinear conservative system was already illustrated by Fig. 1.1c in chapter 1.

To illustrate the differences between NNM and LNM according to Rosen-

berg's definition, regarding the energy dependency of them, the underlying conservative version of the 2-DOF system presented in section 4.2.1 is analyzed once again here. The equations of motion correspond to

$$\begin{aligned} \ddot{q}_1 + 2q_1 - q_2 + 0.5q_1^3 &= 0 \\ \ddot{q}_2 + 2q_2 - q_1 &= 0, \end{aligned} \tag{5-10}$$

and its underlying linear version around the equilibrium point ($q_1 = 0$ and $q_2 = 0$) is given by

$$\begin{aligned} \ddot{q}_1 + 2q_1 - q_2 &= 0 \\ \ddot{q}_2 + 2q_2 - q_1 &= 0. \end{aligned} \tag{5-11}$$

The first NNM of the nonlinear systems (extension of the first LNM of the underlying linear system) can be calculated from solutions of a periodic boundary value problem at different energy levels. A method to compute it is presented later in section 5.3. Modal lines can be constructed by plotting the displacement $q_2(t)$ with respect to $q_1(t)$ along one period of the solutions, so that they show the ratio between the displacements of all DOFs. Figure 5.1 shows the results for an energy level in the system varying from 10^{-4} to approximately 10^3J. The ratio between the displacements of the DOFs is constant and independent of the energy level for the linear system, hence only one curve is displayed at the left plot. It corresponds to an in-phase mode since both DOF move in the same direction and with the same value, so the ratio is always 1. The modal lines are straight and the ratio is defined by the angular coefficient of it. For the nonlinear system, the modal lines start also as straight lines (equal to the linear case) for low energy levels but deviate from it as the energy level increases. This occurs because at low energy levels, the displacement $q_1(t)$ is small and the nonlinear term $q_1^3(t)$ becomes negligible. As the energy increases, the term $q_1^3(t)$ becomes relevant.

Those modal lines bring information regarding the ratio between displacements but no information regarding the period of the solution (fundamental frequency of the oscillation). A common way to graphically represent this information is through the frequency-energy plots (FEP)[80]. It shows solution branches of the respective fundamental frequencies of the periodic solutions as function of the total energy in the system. Usually, modal lines are also displayed at some key points to better understand the changes in the ratios of the displacements, and this way transmitting all important information about the NNMs. For this 2 degrees of freedom example, the FEP is presented

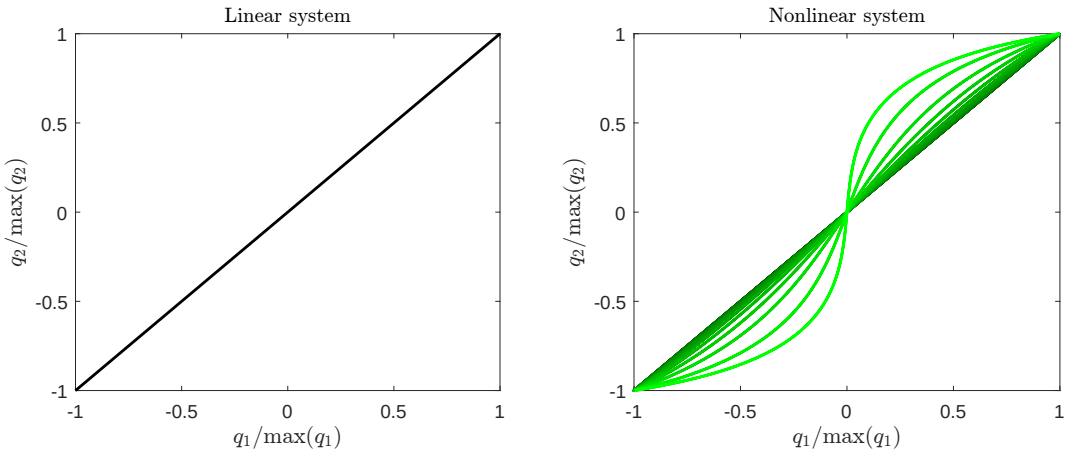

Figure 5.1: Modal lines of the first mode of the nonlinear (right plot) and underlying linear system (left plot) for different energy levels

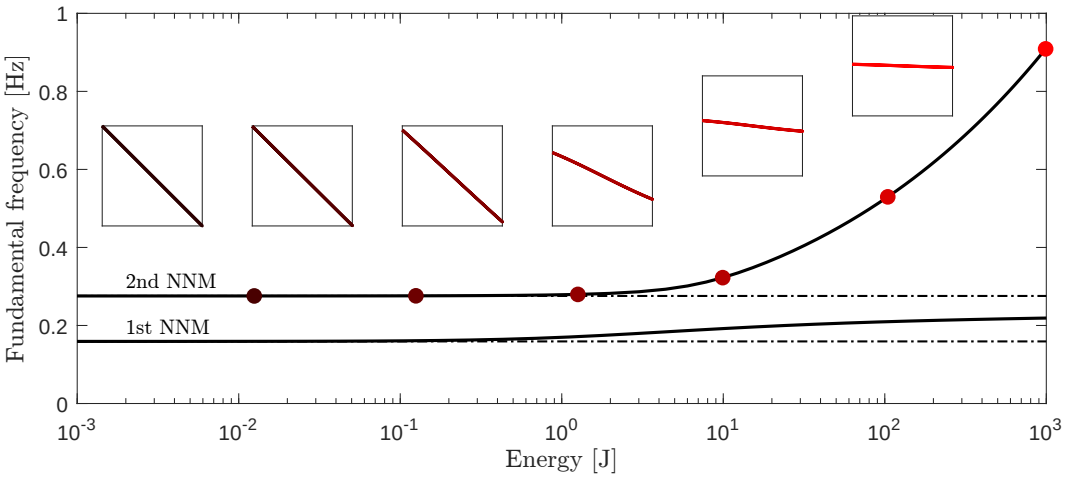

Figure 5.2: Frequency-energy plot on the NNM of the 2 DOF oscillator

in Fig. 5.2. It shows the fundamental frequency of the first (in-phase) and second (out-phase) NNMs as function of the energy in the system. For simplicity, only the modal lines of the second NNM are presented at some key points. The dashed lines represent the FEP of the underlying linear system, which corresponds to horizontal lines since linear systems are not energy dependent. The FEP is a useful tool to determine if a linear model is suitable or not under some given energy level. In this example, the solution branches stay at constant values (equal to the LNMs) until approximately 10^{-1} J. A linear model may then lead to good results when dealing with motions below this energy level. In other words, the LNM and the NNM are approximately the same. When working above this "threshold", the linear models should be abandoned for the sake of accuracy.

5.2 Properties of nonlinear normal modes

Next, two important properties of NNMs besides their energy dependency are discussed. Both have no counterpart in linear systems.

5.2.1 Modal interactions

Another exclusive property of NNMs is their capacity to interact with each other. It allows the energy exchange between modes, a feature that can be beneficial and desirable under some conditions. In the literature, the transference of energy between modes was already studied for vibration absorbers [81]. The interaction between modes is only possible in nonlinear systems because:

- the motion that characterize the NNMs contains higher harmonics and not just the fundamental one as in the LNMs.
- the fundamental frequencies are energy dependent, as discussed in section 5.1, so their value can change (usually not in the same rate) as function of the energy in the system.

When the i-th mode has a fundamental frequency that is k times the fundamental frequency of some other mode, let say the j-th mode, the k-th harmonic of the j-th mode can excite the i-th mode and exchange energy between them. Thanks to the energy dependency of the fundamental frequency, the interaction of modes occurs only at some particular energy levels.

The NNM interaction can be better explained using an example. Once again the same 2 DOF oscillator described by Eq. (5-10) is used. The same FEP presented in Fig. 5.2 is repeated in Fig. 5.3, but this time extending the energy levels to higher values. As highlighted in the figure, several new solution branches emanate from the first NNM branch. This is a consequence of bifurcations. Those new solution branches are sometimes called tongues and are responsible for the interactions between the first and second NNMs. At low energies, the ratio between the fundamental frequencies of the second and first NNMs starts as $\sqrt{3}$, but rapidly increases with the energy level. This is a consequence of the energy dependency of NNMs and the fact that the fundamental frequency of the second NNM increases faster than the fundamental frequency of the first NNM. When the ratio between those fundamental frequencies becomes 3, the frequency of the 3-rd harmonic of the first NNM equals the fundamental frequency of the second NNM, resulting in an internal resonance. This behavior repeats for all integer ratios between the

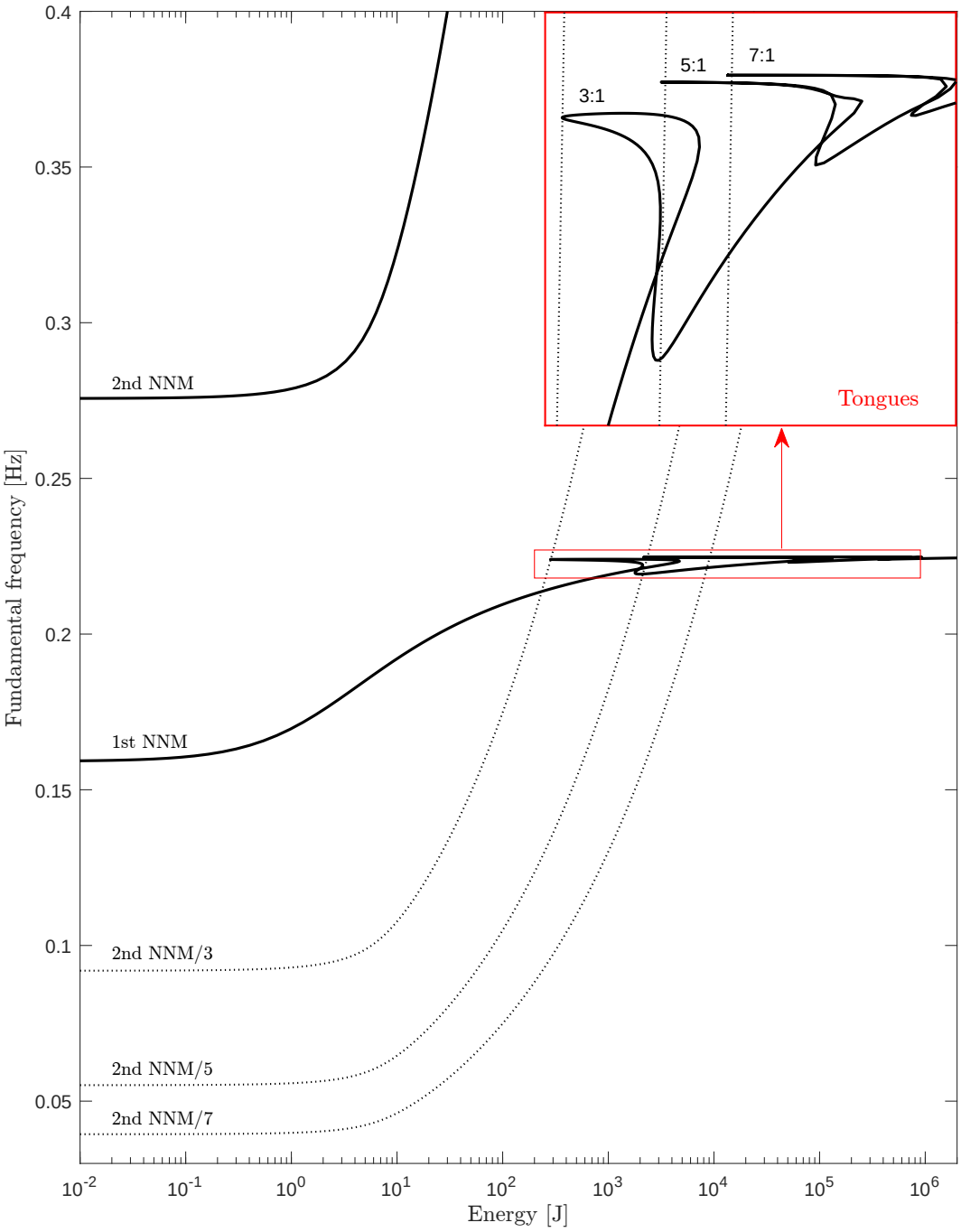

Figure 5.3: Example of mode interaction for the 2 DOF oscillator

fundamental frequencies of the first and second NNMs. Figure 5.3 shows only the 3:1, 5:1 and 7:1 interactions, but more of them exist and were not computed. To better visualize the ratio between the fundamental frequencies, several dashed lines were introduced in the figure and represent the fundamental frequency of the second NNM divided by integers.

Figure 5.4 illustrates the 3:1 mode interaction between the modes. It shows the modal curves at some key points on the solution branch of the first NNM and in the 3:1 interaction tongue. The modal curves show a gradual shift from the first NNM to a pure second NNM and then back to the first NNM. Also, it is possible to see that this pure second NNM motion occurs at a fundamental frequency that is exactly 3 times smaller than the actual second NNM fundamental frequency. This means that if the system is excited at this particular low frequency and energy, a significant part of the resulting motion will have a frequency 3 times the excited one.

5.2.2 Stability

One second exclusive property of NNMs is the fact that they can be stable or unstable (in the asymptotic sense) depending on the energy level, which is different from LNMs that are strictly stable. The instability in a NNM corresponds to a loss in its oscillatory motion. Therefore, only stable NNM can be physically realizable. The stability analysis of NNMs can be done numerically or analytically. Figure 5.5 shows the stability analysis of the first NNM mode of the 2 DOF system described by Eq. (5-10). Such stability analysis was done numerically through the assessment of the Floquet multipliers. Since the systems analyzed under the Rosenberg's definition of NNMs are conservative, the NNM is characterized by periodic solutions so that the monodromy matrix can be evaluated as described in section 3.3.

A stability analysis can be beneficial in many situations, specially for the detection of bifurcation points. As highlighted in Fig. 5.5 with a black circle, the first NNM suffers a change in its stability, which characterizes the presence of a bifurcation point. Since this highlighted point is not a turning point, it is possible that another branch emanates from it, creating a pitchfork bifurcation point. Indeed, a 2:1 non symmetric internal resonance tongue emanates at this point, as showed in references such as [53, 64, 57].

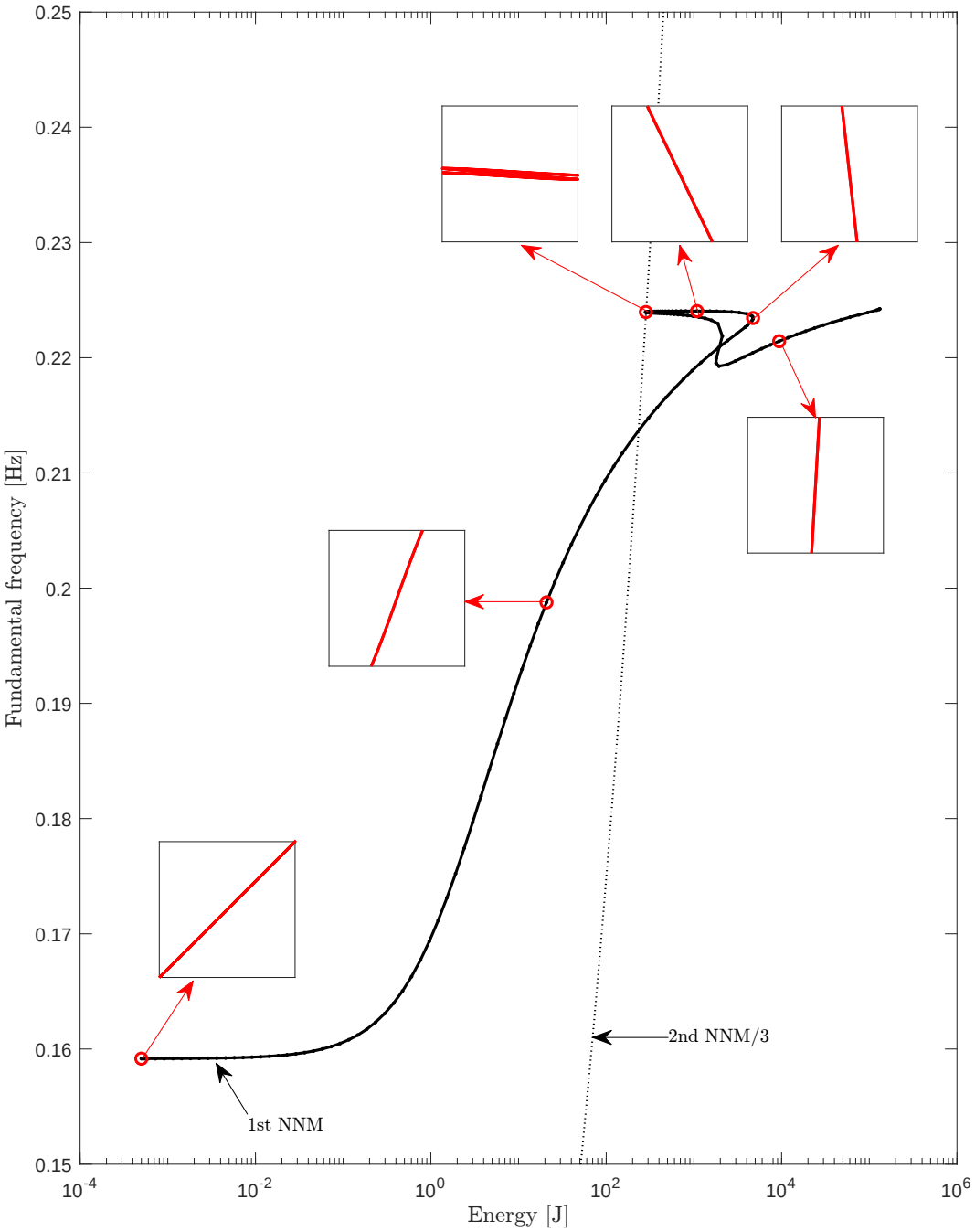

Figure 5.4: Example of 3:1 interaction of the in/out of phase modes for the 2 DOF oscillator

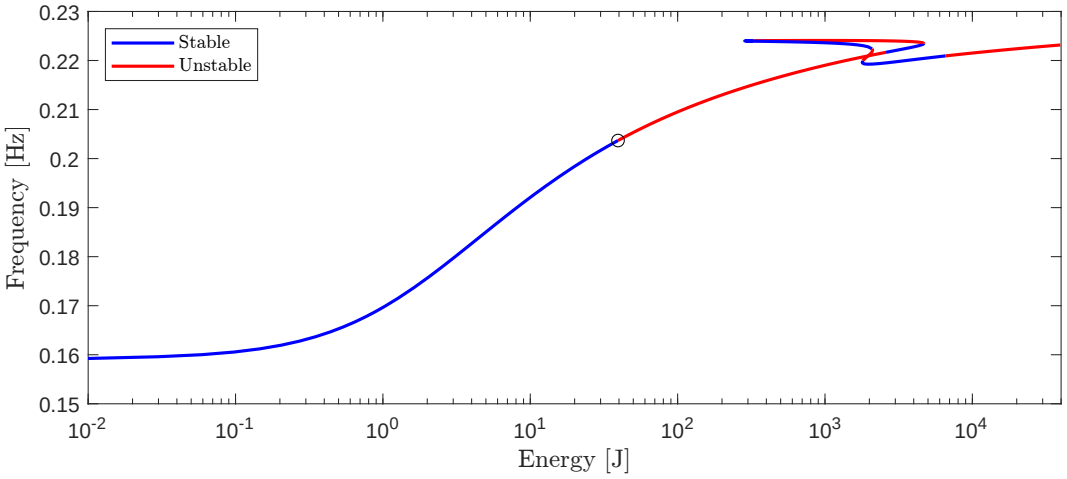

Figure 5.5: Stability analysis of the in phase NNM of the 2 DOF oscillator.

5.3 Numerical computation of nonlinear normal modes

A numerical procedure that allows the computation of NNM for mechanical systems according Rosenberg's definition is discussed now. Only spatially discretized systems are considered here. The goal is to find the solutions of periodic boundary value problem defined in Eq. (5-9) for different levels of energy ϵ. This is accomplished here combining two techniques previously presented in this thesis: computation of periodic solution using the HBM (chapter 2), or Shooting method (chapter 3), and the numerical path continuation to track the variations of those periodic solution as function of the energy in the system (chapter 4). This numerical approach was proposed by Peeters [64] using the Shooting method. Krack [56] used the same methodology with the HBM and proposed an extension to account also for non conservative systems [46].

As discussed in chapters 2 and 3, solutions of periodic boundary value problems are found by solving a system of residual equations in the form of $\mathbf{R}(\mathbf{u}) = \mathbf{0}$. The residual equations and the respective unknown parameters depend on the method used. When using the HBM, the residual equations are defined by Eq.(2-36) and $\mathbf{u}$ corresponds to the Fourier coefficients and the fundamental frequency of the periodic solution. When using the Shooting method, the residual equations are defined by Eq. (3-25) and $\mathbf{u}$ corresponds to the initial conditions and the period of the solution.

The residual equations, $\mathbf{R}(\mathbf{u}) = \mathbf{0}$, for this problem consists in a underdeterminated system of equations because there are an infinite number of periodic solutions that could satisfy the free vibration of the mechanical system, as already discussed in this chapter. It lacks a amplitude and phase restriction.

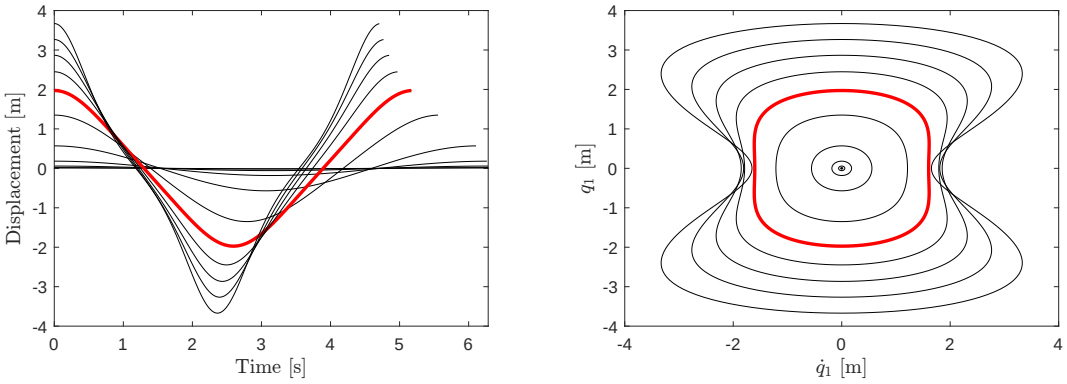

Figure 5.6: Several periodic solution to illustrate the necessity of an amplitude normalization.

The necessity of an amplitude and a phase restrictions for the computation of NNMs is discussed now using an example. Again, the 2 DOF system defined by the equation of motion in Eq. (5-10) is used. The motion of the first DOF according to the first NNM is presented in Fig. 5.6 for several periodic solutions, each with a different amplitude (energy levels). All of them satisfy the residual equations $\mathbf{R}(\mathbf{u}) = \mathbf{0}$, which shows the underdetermination of the problem. An amplitude normalization is then necessary to restrict the periodic solution to a unique energy level, for example, the one represented by the red curve in Fig. 5.6. Such energy level is related to a unique trajectory in the phase plane. Although the energy level is defined with the amplitude restriction, the starting point of such trajectory still not defined and can be any point on the trajectory. All the periodic solutions that lead to the same trajectory satisfy the residual equations for the same energy level, so that the problem still underdeterminated. In other words, any periodic solution that defines the NNM at a certain energy level can be shifted in time and continues to be the same periodic solution, i.e., representing the same trajectory. This underdetermination is illustrated in Fig. 5.7. It shows two equivalent periodic solutions (belong to the same trajectory), but with different initial conditions (represented by the blue and red dots). This underdetermination can be removed by adding a phase restriction to the problem. A common phase restriction consists in imposing zero initial velocity for one DOF of the system.

Next, the amplitude restriction, redefined here as $\eta_a(\mathbf{u}, \epsilon)$, and the phase restriction, redefined here as $\eta_p(\mathbf{u})$, defined in Eq. (5-9) will be presented for the HBM and Shooting methods. Notice that both restrictions where written now as functions of $\mathbf{u}$ instead of a function of $\mathbf{q}(t)$, as in Eq. (5-9). This is equivalent since the unknown parameters $\mathbf{u}$ defines the periodic solution $\mathbf{q}(t)$. Together, the residual functions $\mathbf{R}(\mathbf{u}) = \mathbf{0}$, the amplitude restriction $\eta_a(\mathbf{u}, \epsilon)$ and the phase restriction $\eta_p(\mathbf{u})$ lead to a unique periodic solution when they

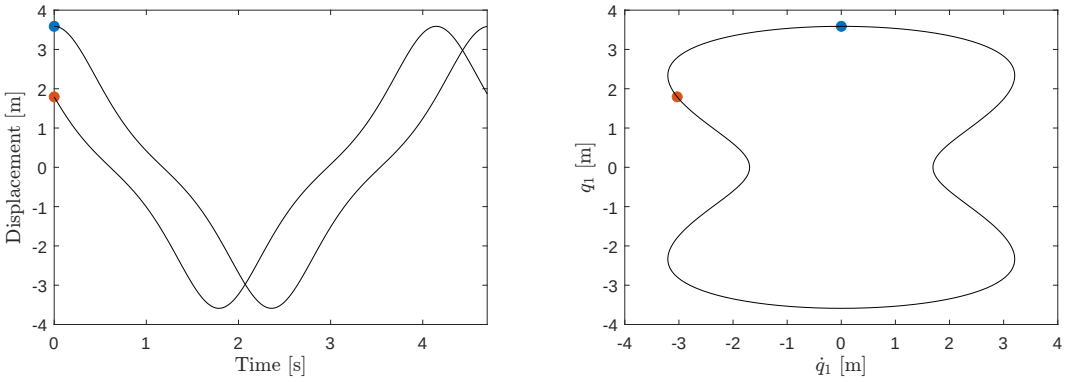

Figure 5.7: Several periodic solution to illustrate the necessity of an amplitude normalization.

are solved simultaneously for a given value of energy ϵ. This periodic solution represents a NNM of the system at that energy level.

5.3.1 Computation using the HBM

When using the HBM, the residual equations are defined by Eq. (2-36), repeated here for convenience:

$$\mathbf{R}_{HB}\left(\mathbf{u}\right) = \begin{bmatrix} \tilde{\mathbf{r}}_0^{(e)}\left(\mathbf{u}\right) \\ \Re\left\{\tilde{\mathbf{r}}_1^{(e)}\left(\mathbf{u}\right)\right\} \\ \Im\left\{\tilde{\mathbf{r}}_1^{(e)}\left(\mathbf{u}\right)\right\} \\ \vdots \\ \Re\left\{\tilde{\mathbf{r}}_H^{(e)}\left(\mathbf{u}\right)\right\} \\ \Im\left\{\tilde{\mathbf{r}}_H^{(e)}\left(\mathbf{u}\right)\right\} \end{bmatrix} = \mathbf{0}, \tag{5-12}$$

where $\mathbf{u} = \left[\tilde{\mathbf{q}}_0^{(e)}, \Re\left\{\tilde{\mathbf{q}}_1^{(e)}\right\}, \Im\left\{\tilde{\mathbf{q}}_1^{(e)}\right\}, \ldots, \Re\left\{\tilde{\mathbf{q}}_H^{(e)}\right\}, \Im\left\{\tilde{\mathbf{q}}_H^{(e)}\right\}, \Omega\right]$. Only the real and imaginary parts of the non-negative Fourier coefficient are considered as unknowns because the negative ones can be reconstructed from the positive ones knowing that they share the conjugate mirror property. Equation (5-12) shows that the Fourier coefficients of the residual must be zero up to the *Ansatz* order H. Again, only the non-negative Fourier coefficients must be verified because of the conjugate mirror property. The Fourier coefficients of the residual are defined as

$$\tilde{\mathbf{r}}_j^{(e)}\left(\mathbf{u}\right) = \mathbf{S}_j(\Omega)\tilde{\mathbf{q}}_j^{(e)} + \tilde{\mathbf{f}}_{nl,j}^{(e)}\left(\Omega, \left\{\tilde{\mathbf{q}}_k^{(e)}\right\}\right), \text{ for } j = 0, \ldots, H. \tag{5-13}$$

$\mathbf{S}_j(\Omega)$ is the dynamic stiffness matrix of the underlying linear system and $\tilde{\mathbf{f}}_{nl,j}^{(e)}$ is the Fourier coefficients of the nonlinear terms, usually computed using the Alternating Time-Frequency method (see chapter 2). The main advantage of the residual equations defined in Eq. (5-12) is the absence

of numerical integration, which can accelerate the computation and avoid numerical instability. On the other hand, the size of the system can become substantially large if a high truncation order H is needed in the computation of periodic solutions of a system with a large number of DOF. This situation can be faced when dealing with geometrically complex structures discretized with FEM and having a non-smooth nonlinearity.

Regarding the required amplitude restriction $\eta_a(\mathbf{u}, \epsilon)$, a modal mass normalization considering all harmonics is adopted here [56]. It is similar to the modal mass normalization used in linear systems, but in this case considering all harmonics that compose the periodic solution. Those additional harmonics are necessary because the Fourier coefficients related to the fundamental harmonic can diminish during an internal resonance. The amplitude normalization for the HBM is then defined here by the following equation:

$$\eta_{a,HB}(\mathbf{u}, \epsilon_{HB}) = \sum_{l=0}^{H} \left(\tilde{\mathbf{q}}_{-l}^{(e)}\right)^T \mathbf{M}\tilde{\mathbf{q}}_{l}^{(e)} - \epsilon_{HB} = 0, \tag{5-14}$$

where ϵ_{HB} is the modal mass, a parameter that is related to the energy in the system. Therefore, this parameter will be used later as free parameter in the continuation method to compute the branches of periodic solutions (NNMs).

For the phase normalization $\eta_p(\mathbf{u})$, the initial velocity of some generic DOF is imposed to be zero. This restriction can be done through the following equation:

$$\eta_{p,HB}(\mathbf{u}) = \sum_{l=1}^{H} l\mathbf{e}_i^T \Im\left\{\tilde{\mathbf{q}}_{l}^{(e)}\right\} = 0, \tag{5-15}$$

where $\mathbf{e}_i \in \mathbb{R}^n$ is a unit vector with all components equal to zero except the i-th entry, which equals one. It points to the DOF that will have the initial velocity restricted to zero.

In summary, the periodic solution related to the NNM of a mechanical system can be found (when using the HBM) solving the following extended system of algebraic equations:

$$\bar{\mathbf{R}}_{HB}(\mathbf{u}, \epsilon_{HB}) = \begin{bmatrix} \mathbf{R}_{HB}(\mathbf{u}) \\ \eta_{a,HB}(\mathbf{u}, \epsilon_{HB}) \\ \eta_{p,HB}(\mathbf{u}) \end{bmatrix} = \mathbf{0}. \tag{5-16}$$

Such a problem can be solved numerically using the Newton-Raphson method.

5.3.2 Computation using the Shooting method

When using the Shooting method, the residual equations are defined by Eq. (3-25) and represents the difference between the initial state and the final state at the unknown fundamental period T, i.e.,

$$\mathbf{R}_{sh}\left(\mathbf{u}\right) = \mathbf{y}(T) - \mathbf{y}_0 = \mathbf{0} \tag{5-17}$$

where $\mathbf{y}^T = \begin{bmatrix}\mathbf{q}^T & \dot{\mathbf{q}}^T\end{bmatrix}$ is the state of the system and $\mathbf{u} = \begin{bmatrix}\mathbf{y}_0^T & T\end{bmatrix}$ is the vector of unknowns, composed by the initial state and the fundamental period. Such residual is much more simple and compact than the one using the HBM, but it requires a numerical integration over one period of oscillation.

A possible and simple way to restrict the amplitude of the periodic solution for the Shooting method is by imposing a certain value for the displacement of any DOF. Therefore, the amplitude normalization can be given as

$$\eta_{a,sh}(\mathbf{u}, \epsilon_{sh}) = \begin{bmatrix}\mathbf{e}_i^T & \mathbf{0}_n^T\end{bmatrix}\mathbf{y}_0 - \epsilon_{sh} = 0 \tag{5-18}$$

where $\mathbf{0}_n$ is a $n \times 1$ zero vector and ϵ_{sh} is the initial displacement of the i-th DOF. Once again $\mathbf{e}_i$ points to which DOF the restriction is applied. As the modal mass in the amplitude restriction for the HBM, ϵ_{sh} is related to the energy in the system. Therefore, this parameter will be used later as free parameter in the continuation scheme.

The phase restriction is also simpler and can be defined through the equation

$$\eta_{p,sh}(\mathbf{u}) = \begin{bmatrix}\mathbf{0}_n^T & \mathbf{e}_i^T\end{bmatrix}\mathbf{y}_0 = 0. \tag{5-19}$$

This equation imposes a zero value to the i-th DOF. It can be the same DOF used in the amplitude normalization or any other.

Just like for the HBM, the periodic solution related to the NNM of a mechanical system can be found (when using the Shooting method) solving the following extended system of algebraic equations:

$$\bar{\mathbf{R}}_{sh}\left(\mathbf{u}, \epsilon_{sh}\right) = \begin{bmatrix}\mathbf{R}_{sh}(\mathbf{u}) \\ \eta_{a,sh}\left(\mathbf{u}, \epsilon_{sh}\right) \\ \eta_{p,sh}(\mathbf{u})\end{bmatrix} = \mathbf{0}, \tag{5-20}$$

where, once again, the solution can be found numerically using the Newton-Raphson method.

5.3.3 Continuation

The extended system of equations defined in Eq. (5-16) and in Eq. (5-20) is responsible for evaluating the periodic solution of the NNM at some energy level ϵ. Such unique solution is not enough to fully understand the behavior of the respective NNM and a continuation method is necessary to compute the entire solution branch. This can be accomplished using the predictor-corrector scheme described in chapter 4. In this case, the free parameter λ should be related some how to the energy in the system. Therefore, it can be the modal

mass ϵ_{HB}, when using the HBM, or the the initial displacement ϵ_{sh} of a chosen DOF, when using the Shooting method.

The only difference between the algorithm presented in section 4.1.3 and the one needed to solve the NNM branch is the substitution of the residual function, $\mathbf{R}(\bar{\mathbf{u}})$, by the extended one, $\bar{\mathbf{R}}(\bar{\mathbf{u}}, \epsilon)$, where the amplitude and phase normalization are added. For the first periodic solution in the continuation scheme, the initial guess could be the LNM of the underlying linear system. For this guess to be close to the actual periodic solution of $\bar{\mathbf{R}}(\mathbf{u}, \epsilon)$, a low energy level ϵ should be use, i.e., λ^s should have a small value.

5.4 Numerical examples

Next, the NNMs of three systems are computed as examples. Each of them illustrates different concepts. All the NNM computations were done using the tangent method for the prediction phase and the arc-length parameterization restriction in the correction phase.

5.4.1 2 DOF oscillator with cubic spring

The first example corresponds to the 2 DOF system widely used throughout this chapter. The governing equation is given by Eq. (5-10). Since all the properties of this system were already discussed in detail in the previous sections, the idea here is to just show the agreement between NNMs computed using the HBM and the Shooting method. Figure 5.8 shows the in-phase and the out-phase FEP computed using both methods. As expected, no significant difference can be seen between the results. For the HBM, the *Ansatz* was set with a truncation order H up to the 9-th harmonic, although a smaller order would also give good results. This "high" value of H was justified by the low dimension of the system, which imposes low computational cost. Hence, some extra harmonics were used to ensure that the *Ansatz* already converged to the actual periodic solution. For the Shooting method, 400 time samples were used during the numerical integration along one period. The numerical integration is the only approximation of the Shooting method, so one must be aware of its stability and precision. Increasing the number of samples leads to better results but with a significant computational cost.

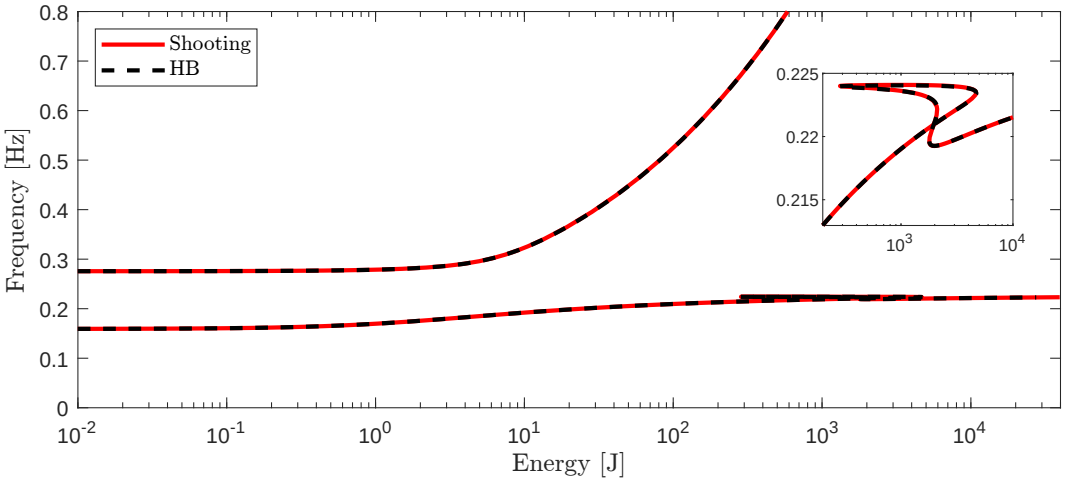

Figure 5.8: FEP of the 2 DOF oscillator with cubic spring computed using the HBM and the Shooting method.

Length (m)	Width (m)	Thickness (m)	Young's mod. (N/m^2)	Density (kg/m^3)	Nonlin. coeff. (N/m^3)
0.7	0.014	0.014	2.05e11	7800	6e9

Table 5.1: Geometric properties, material properties and nonlinear coefficients of the cantilever beam with cubic spring.

5.4.2 Cantilever beam with cubic spring

The second example deals with a more challenging system. The computation of the NNM becomes more intense because the system dimension is increased. It corresponds to a cantilever beam with a cubic spring attached at its free end. This system represents an actual benchmark for nonlinear identification used during the European Action COST F3 [72]. Its NNMs were also computed and presented in [57, 64, 53]. The geometric and material properties, as well as the nonlinear coefficients are presented in table 5.1. Ten Euler-Bernoulli elements were used to spatially discretize the system. Giving the clamp-free boundary conditions, the number of DOF in the system becomes 20, which is still a low size problem compared to the full scale airplane model analyzed in [65], but it is already 10 times higher than the first example.

In this example, only the Shooting method was used. The numerical integration was conducted with 5000 time samples along each period. The FEP of the first mode is presented in Fig. 5.9. The NNM motion along one period is also shown at six key points of the branch. The first point corresponds to a low energy motion where the NNM and the LNM are basically the same one. At the second point, the NNM mode shows a little increment in its fundamental frequency because of the hardening effect of the cubic spring, although the

motion continues to be similar to the respective LNM. Points 3, 4, and 5 were selected along the tongue that represents a 5:1 internal resonance between the first two modes. A smooth transition from the first mode to the second one can be seen in the point 3, followed by a pure second mode motion at point 4, and back to a smooth transition from the second mode to the first mode at point 5. Point 6 shows a pure first mode once again, but now with a higher fundamentl frequency.

5.4.3 Cantilever beam with unilateral spring

In this last example, the same cantilever beam with unilateral spring analyzed in section 4.2.3 is once again studied. However, the spatial discretization of the beam was refined to 20 Euler-Bernoulli elements to get more accurate results for the higher modes. Also, the gap between the beams free end and the unilateral spring was reduced to 0.05m. The geometric and material properties of the beam are kept the same and are summarized in table 4.1. An illustration of the beam with the new discretization and spring gap is given in Fig. 5.10. This time only the HBM will be used to compute the NNM. The goals of this example are: a) to show that the NNM computation is still possible even when the system presents some sort of discontinuity in the model, b) to show that the unilateral spring can be used to excite internal resonances in a system and c) to show the importance of the truncation order when dealing with mode interactions. As mentioned in chapter 2, periodic solutions computed using the HBM are only approximations that converge to the actual solution as the truncation order increases. This is particular important when dealing with internal resonances since higher frequencies components can appear in a NNM with low fundamental frequency.

To have a broad picture of the system's NNMs, the first three modes were computed using a truncation order up to $H = 20$. This high truncation order allows most of the modes interactions to be computed, although it is important to keep in mind that some of the interactions related to higher NNMs could have been neglected during the numerical continuation (filtered out by the truncation order or skipped by the a high step size). If the computation of all interactions is essential to the analysis, perhaps the Shooting method is a more suitable choice. All three computed NNM are presented in Fig. 5.11. The mode shapes at the interaction tongues are also illustrated to better understand the solution branches.

The first important characteristic illustrated by the FEP is the fact that all NNMs start as horizontal lines, i.e., equal to the respective LNMs of the

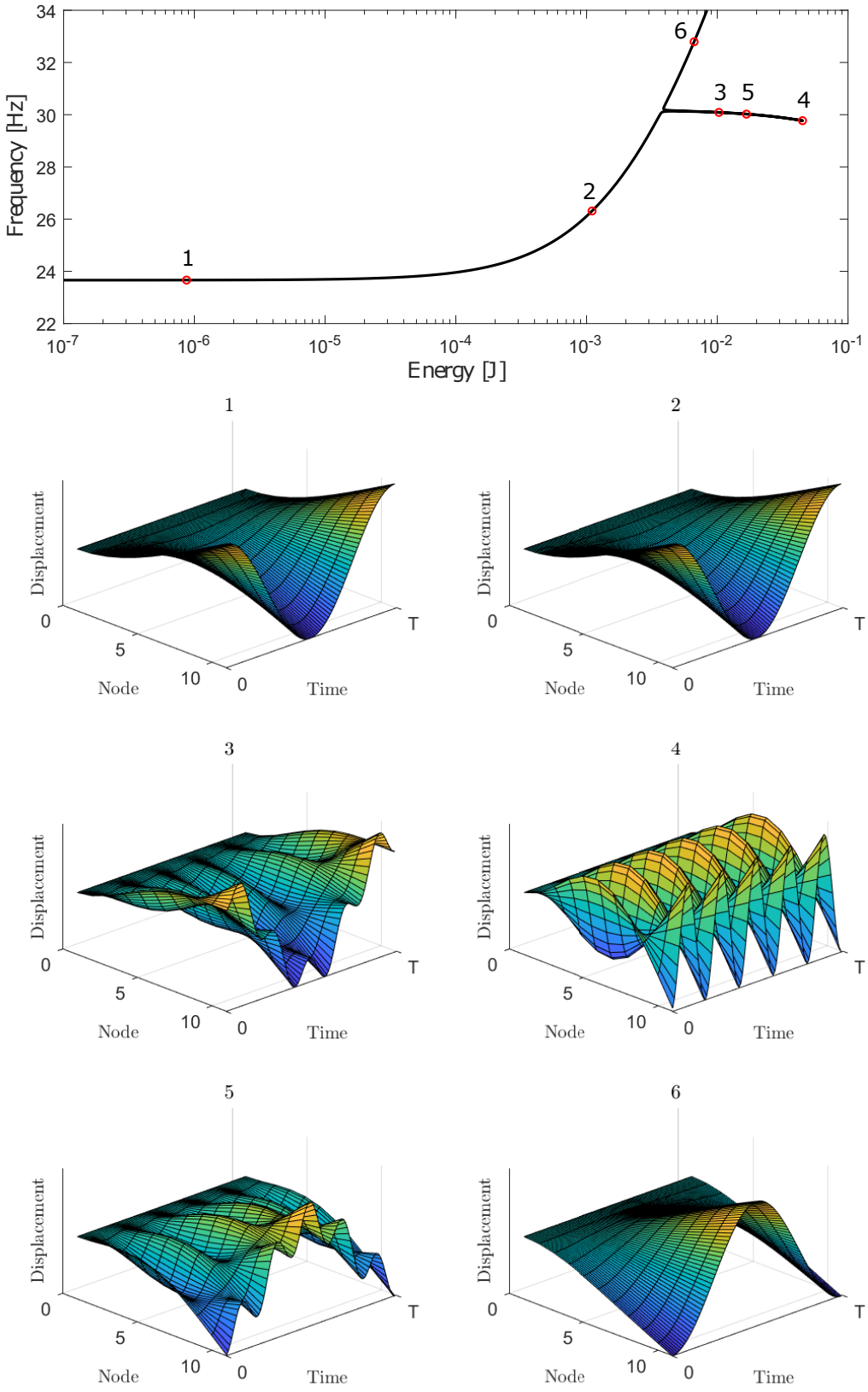

Figure 5.9: FEP of the first NNM of the cantilever beam with cubic spring

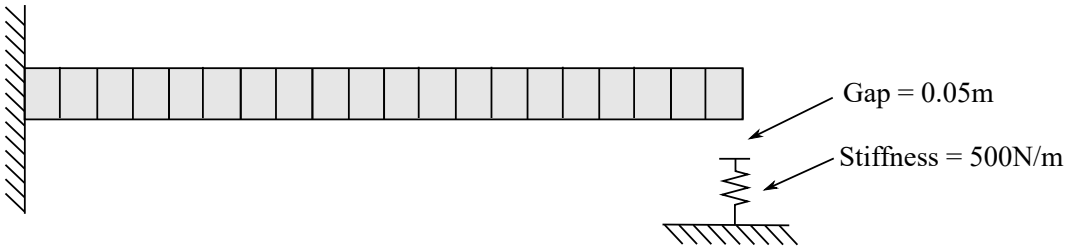

Figure 5.10: Illustration of the beam with unilateral spring used to compute the NNMs.

beam without the nonlinear element. With low energies, the motion at the free end is below the unilateral spring gap, so the motion is indeed linear. As soon as the energy grows and the beam's free end overcomes the gap, a sudden increment in the NNM fundamental frequency is observed. The additional stiffness of the unilateral spring is responsible for this frequency increment. Also, since the unilateral spring is placed at the free end of the beam, the energy required for the motion to become nonlinear increases monotonically with respect to the mode order. That is, the first NNM will begin its nonlinear motion (touches the unilateral spring) with an energy $\approx 10^{-1}J$, which is lower than the energy required by the second NNM, $\approx 3 \times 10^{0}J$. In the mean time, the third NNM requires an energy $\approx 2 \times 10^{1}J$, which is higher than the required for the first and second NNM to begin its nonlinear motion. Therefore, as illustrated in Fig. 5.11, the first NNM shows a quick increment in its fundamental frequency while all the others NNM frequencies continues with constant values (in their linear range). This interesting characteristic increases the chances of internal resonances between modes. It becomes more likely that the fundamental frequency of the first NNM crosses some ratio of the fundamental frequency of some others NNMs. In addition, the unilateral spring imposes a nonlinearity in the model that is more likely to generate a NNM motion with a high amount of harmonics, which is essential to create mode interactions.

Following the FEP of the first NNM, three internal resonances were computed: a 17:1 between the third and first modes, and two interactions between second and first modes, a 5:1 and a 6:1. At the extreme points of the respective tongues, marked by red circles, the motion becomes the second and third LNM mode in the vicinity of becomes nonlinear (except the 5:1 interaction between second and first modes). Therefore, those points share the same energy level where each mode leaves the linear range and starts to have increases in the fundamental frequency. This characteristic is highlighted by the two dashed lines, pointing that the second and third NNM leave the linear motion at the same energy level of the extreme interaction points. Following

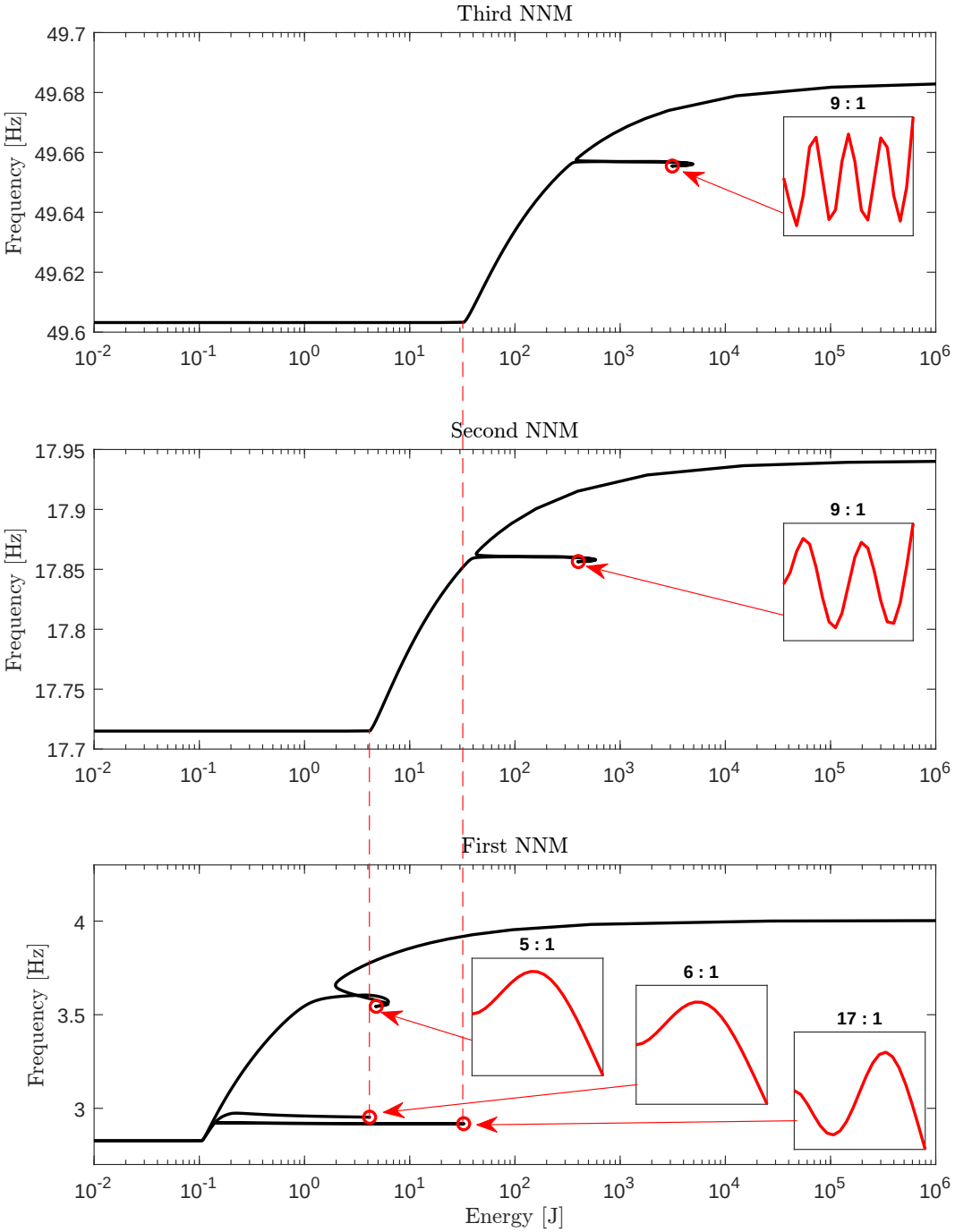

Figure 5.11: FEP of the first three NNM of the cantilever beam with unilateral spring.

now the second NNM FEP, a 9:1 interaction between the fifth and second mode was computed. The computed FEP of the third NNM shows a similar behavior, but with a 9:1 mode interaction between the eighth and third mode. For all the computed NNM, stabilization in the fundamental frequency value is also observed at high energy levels. As the mode order increases, the shift between the fundamental frequency at low energy levels (linear case) and the stabilized fundamental frequency at high energy level becomes smaller. For the first NNM this shift on the fundamental frequency was from 2.8Hz to 4Hz, i.e., a shift of 1.2Hz. For the second NNM, the shift was already reduced to 0.23 Hz, and for the third NNM the shift was almost negligible (0.08Hz).

All the NNM computations in this example were done using the HBM. An important parameter in this method is the truncation order H of the *Ansatz*. When dealing with mode interaction, this parameter becomes even more important since higher frequency components can emerge and dominate the motion. To illustrate how the parameter H contributes in the computation of the NNM branches, the FEP of the first NNM was computed again using $H = 5$. The result is presented in Fig. 5.12. As mentioned earlier, the NNM shows a 6:1 and a 5:1 interaction between the first and second modes. This means that when the NNM reaches the 6:1 interaction tongue, the 6th harmonic of the fundamental frequency becomes significant and must be considered in the *Ansatz*. If this was not the case, the 6:1 mode interaction would not be considered and it would be filtered out from the solution branch. The same filter effect occurs for the 17:1 mode interaction between the first and third mode since it requires at least $H \geq 17$ to compute the interaction tongue. In Fig. 5.12, the right hand-side plot shows the filtered FEP, where the 6:1 and the 17:1 interactions were eliminated.

Another point that was postponed until now is the fact that the computation of NNM according to Rosenberg's definition (periodic solutions) can still be useful to analyze weakly damped systems. To this end, a damping matrix was added to the model and it generates a damping ratio of 1% at all modes in the linear regime. The NFRCs of the beam's free end was computed using the HBM as described in chapter 4. The excitation was applied at the middle of the beam with an amplitude varying from 0.1N to 2.9N. The first NNM with $H = 5$ was then overlapped to the NFRCs and presented in Fig 5.13. It shows that the respective NNM represents the backbone of the NFRCs and shows the bending direction of the resonance peaks. The knowledge of the backbone of the NFRCs can be extremely beneficial, especially to detect and compute isolated resonance curves, the subject of the appendix C.

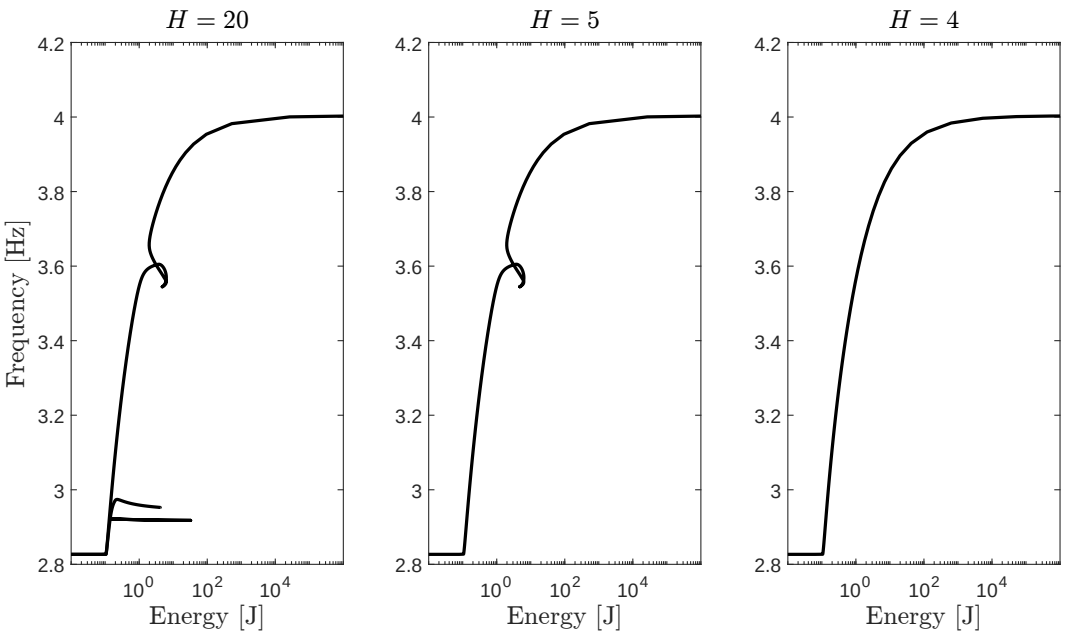

Figure 5.12: Influence of the truncation order H in the computation of NNM using the HBM

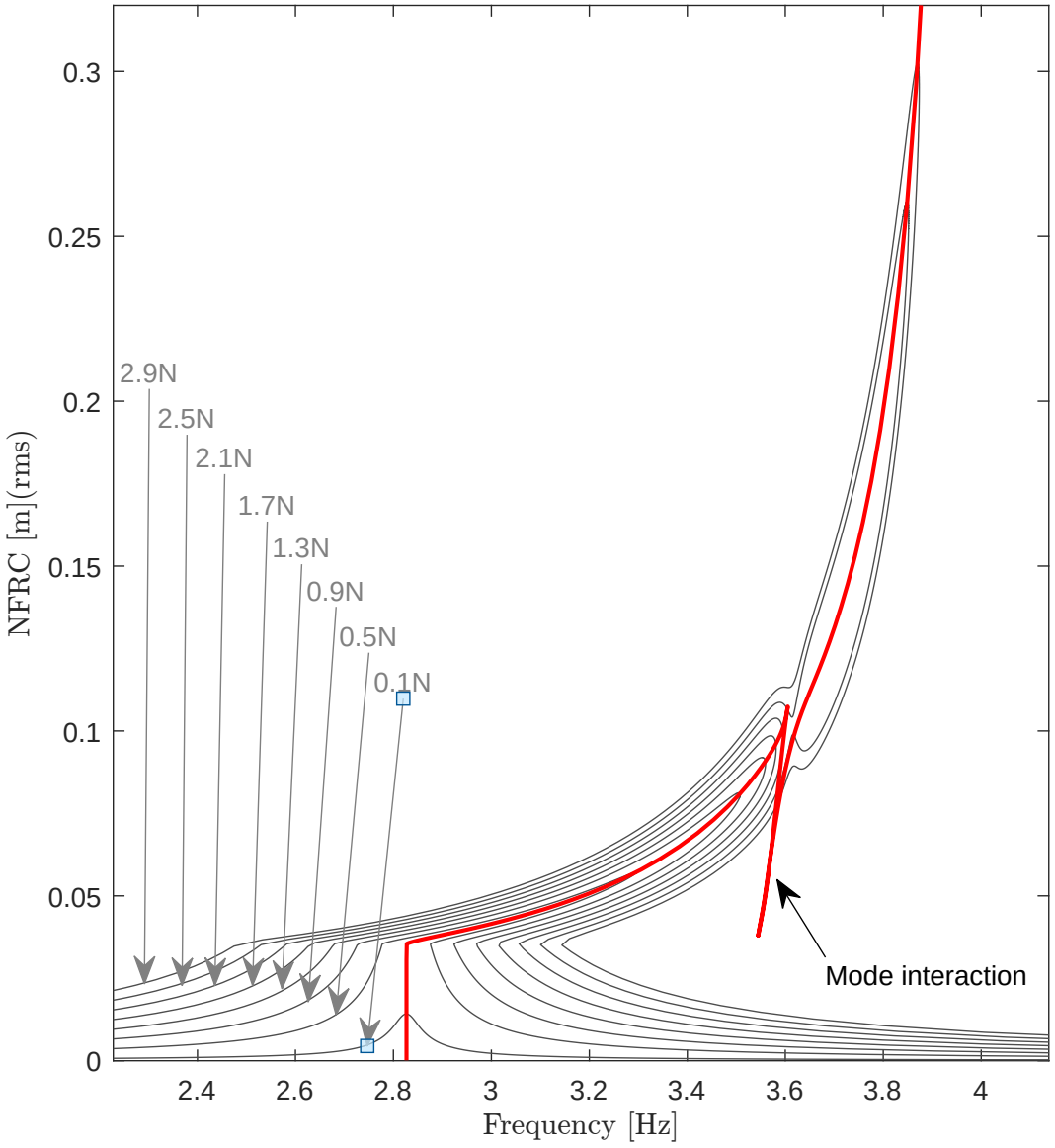

Figure 5.13: NNM as backbone of NFRCs for the catilever beam with unilateral spring.

6
NNMs of flexible beams

Flexible beams are usually modeled under the assumption of large displacements, finite rotations, but with small strains. Such hypothesis allows the equation of motion to be built using co-rotational finite elements. The co-rotational formulation decomposes the total motion of a structural element into two parts: a rigid body displacement and an elastic (small) deformation. Each element has its own local frame that follows it according to its rigid body part of the motion. The elastic deformation is then written with respect to the local frame using traditional linear finite elements (since small strain hypothesis are been used), and later transformed to the global coordinate system, which generates the geometric nonlinearity of the model.

This chapter starts describing the kinematics of the co-rotation beam elements. Then the finite element formulation adopted in this thesis is presented. Several researches have already analyzed the dynamic responses of flexible beams using co-rotational finite elements [82, 83, 84, 85]. The main differences between the several formulations lies in the choice of the interpolation functions used in the local frame when computing the energies of the system. In [84], the authors showed that linear interpolation leads to the classical linear and constant Timoshenko mass matrix when deriving the inertial terms of the model. However, they also highlighted that this linear interpolation leads to a shear locking problem, a phenomenon that adds virtual stiffness to the model when the beam elements become too thin. Therefore, they proposed a cubic interpolation for the derivation of the elastic forces, generating a locking-free beam element [86]. Since numerical examples show a satisfactory rate of convergence using this approach, it will be adopted in this thesis. A similar approach was used in [87] for plane beam models and in [88] for spacial beam models. In [89], the authors proposed a cubic interpolation to derive also the inertial term. Although this approach leads to a better convergence, the computational time becomes greater due to the complexity.

With this co-rotational model, the NNM are then computed using the HBM and the prediction-correction continuation method as discribed in the previous chapters. Numerical examples are given to evaluate the proposed method. It starts analyzing the frequency-energy dependency of the oscillations

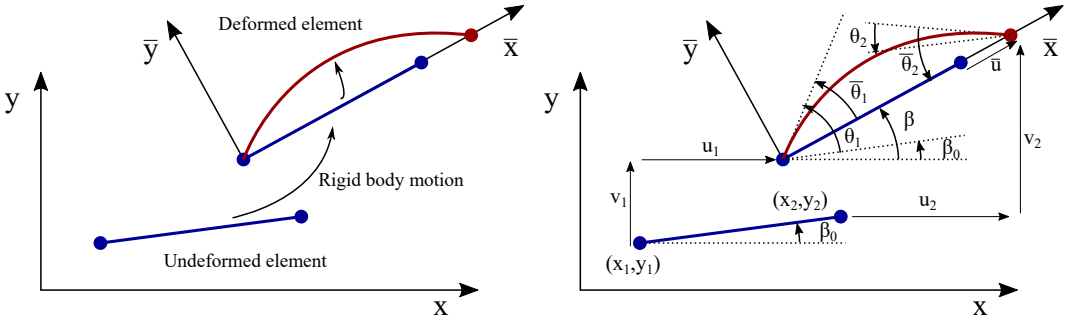

Figure 6.1: Co-rotational beam element kinematics.

in two simple nonlinear systems. From those simple results, it becomes easier to understand the source of nonlinearities expected in flexible beams and the impact that they have in the NNMs. Two flexible beams are then analyzed. The first one, a bi-supported beam, illustrates the computation of the first NNM and shows how the uncertainty in the boundary condition can affect the results (changing it from a softening behavior to a hardening one). The second example corresponds to a co-rotational bi-clamped beam. It illustrates once again the computation of the first NNM, but in this case with a mode interaction. A convergence analysis of the fundamental frequency with respect to the number of co-rotational elements is also performed.

6.1 Dynamic model

An illustration of the two-node co-rotational beam element that will be considered in this thesis is presented in Fig. 6.1. The rigid body motion and the linear elastic deformation that compose the total motion of the element are highlighted in the figure. To help in the computation of the kinetic and potential energy of the element, the kinematics will be introduced first. Then, the hypotheses (order of the interpolation functions) used in the computation of the element's energies are discussed. The equation of motion is then derived using the Lagrange's equation.

6.1.1 Beam's kinematics

The position of nodes 1 and 2 in the undeformed configuration, written with respect to the global frame (x, y), is defined as (x_1, y_1) and (x_2, y_2), respectively. The vector of generalized coordinates of the element is given as

$$\mathbf{q}_e = \begin{bmatrix} u_1 & v_1 & \theta_1 & u_2 & v_2 & \theta_2 \end{bmatrix}^T, \tag{6-1}$$

where u and v represent the horizontal and vertical displacements of the nodes and θ represents the rotation of the cross sections. The local coordinate system $(\bar{x}, \bar{y})$ is defined with the origin coinciding with the first node and with the $\bar{x}$ axis connecting both nodes at all times (follows the element rigid body motion). Following this definition, the axial and transverse displacements of the first node and the transverse displacement of the second node are zero at all times in the local frame. Therefore, the generalized coordinates in the local frame reduces to

$$\bar{\mathbf{q}}_e = \begin{bmatrix} \bar{u} & \bar{\theta}_1 & \bar{\theta}_2 \end{bmatrix}^T, \tag{6-2}$$

where

$$\bar{u} = l - l_0 \tag{6-3}$$
$$\bar{\theta}_1 = \theta_1 - \beta + \beta_0 \tag{6-4}$$
$$\bar{\theta}_2 = \theta_2 - \beta + \beta_0. \tag{6-5}$$

Equations (6-3), (6-4) and (6-5) establish the nonlinear relationship between the local and global coordinates. The terms l and l_0 represent the current and the undeformed length of the element, respectively, and are defined as

$$l = \left[(x_2 + u_2 - x_1 - u_1)^2 + (y_2 + v_2 - y_1 - v_1)^2 \right]^{1/2} \tag{6-6}$$
$$l_0 = \left[(x_2 - x_1)^2 + (y_2 - y_1)^2 \right]^{1/2}. \tag{6-7}$$

The angle between the local and global frame is defined as β and can be computed from either of the following equations:

$$\cos\beta = \frac{1}{l}(x_2 + u_2 - x_1 - u_1) \tag{6-8}$$
$$\sin\beta = \frac{1}{l}(y_2 + v_2 - y_1 - v_1) .. \tag{6-9}$$

The transformation from the local frame to the global frames is given by the rotation matrix

$$\mathbf{R}_{rot} = \begin{bmatrix} c & -s \\ s & c \end{bmatrix} \tag{6-10}$$

where $c = \cos\beta$ and $s = \sin\beta$.

The differentiation of the current length of the element can be derived from Eq. (6-6), resulting in

$$\delta l = \begin{bmatrix} -c & -s & 0 & c & s & 0 \end{bmatrix} \delta\mathbf{q}_e = \mathbf{w}\delta\mathbf{q}_e. \tag{6-11}$$

Taking the differentiation of Eqs. (6-6), (6-8) and (6-9), the differentiation of the angle β can be expressed as

$$\delta\beta = \frac{1}{l}\begin{bmatrix} s & -c & 0 & -s & c & 0 \end{bmatrix}\delta\mathbf{q}_e = \frac{1}{l}\mathbf{z}\delta\mathbf{q}_e. \tag{6-12}$$

At last, the differentiation of Eqs. (6-3) to (6-5) yields

$$\delta\bar{\mathbf{q}}_e = \mathbf{B}\delta\mathbf{q}_e \tag{6-13}$$

where

$$\mathbf{B} = \begin{bmatrix} \mathbf{b}_1 \\ \mathbf{b}_2 \\ \mathbf{b}_3 \end{bmatrix} = \begin{bmatrix} -c & -s & 0 & c & s & 0 \\ -s/l & c/l & 1 & s/l & -c/l & 0 \\ -s/l & c/l & 0 & s/l & -c/l & 1 \end{bmatrix}. \tag{6-14}$$

6.1.2 Strain energy

Since small strain is considered here, the linear theory can be applied in each finite element to describe their elastic deformations with respect to the local frames. The beam element considered here for the computation of the strain energy corresponds to the Interdependent Interpolation Element (IIE) [86], although any other beam element could be used. The IIE element interpolates the transverse displacement with a cubic function and the cross section rotation with a quadratic function. It is formulated to solve the (homogeneous) equilibrium equation of the Timoshenko beam theory exactly at the nodal points. For the axial displacement, linear interpolation is used. An important property of the IIE is that it is a locking-free shear element, which means that accurate models are given even for slim elements (typically founded in flexible beams)[86]. Hence, this element is commonly found in co-rotational formulations [84, 89, 90].

Since the axial displacement of the first node and the transverse displacements of both nodes are zero with respect to the local coordinate system, the stiffness matrix of the element can be significantly reduced. The potential energy from the element strain is then given by

$$\mathcal{V}_e = \frac{1}{2}\bar{\mathbf{q}}_e^T\mathbf{K}_e\bar{\mathbf{q}}_e \tag{6-15}$$

where

$$\mathbf{K}_e = \begin{bmatrix} \frac{EA}{l_0} & 0 & 0 \\ 0 & (4+12\Omega)\mu & (2-12\Omega)\mu \\ 0 & (2-12\Omega)\mu & (4+12\Omega)\mu \end{bmatrix} \tag{6-16}$$

$$\Omega = \frac{EI}{GAK_s l_0^2} \tag{6-17}$$

$$\mu = \frac{1}{1+12\Omega} \tag{6-18}$$

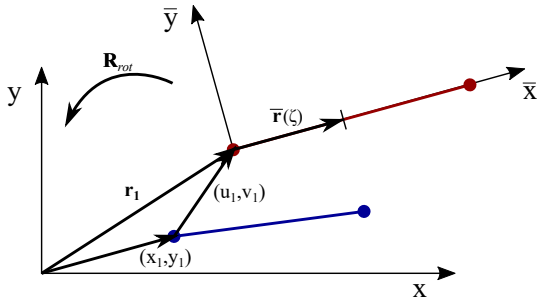

Figure 6.2: Co-rotational beam element kinematics.

The coefficients E and G stand for elastic and shear modulus, while A and I stand for first and second moments of area. K_s is the coefficient for the shear correction, originated from the hypothesis in Timoshenko's theory of constant shearing stress along the beam's cross section. It was assumed in Eq. (6-15) that the beam element is uniform and composed by a isotropic material. A complete description of how to compute this element stiffness matrix is found in [84] and [86].

6.1.3 Kinetic energy

For the kinetic energies, the classical linear Timoshenko element is adopted [84]. This means that linear interpolations are used in the local frame, simplifying the derivation of the inertia term latter when building the equation of motion. The linear interpolation assumes that the transverse displacement is zero along the element, which is only accurate if a significant amount of elements are used to spatially discretize the structure. Higher order interpolations can be used, as showed in [89], leading to a more accurate result. The cost, on the other hand, comes from the significant increment in complexity when deriving the equations of motion.

Let $\mathbf{r}$ be the position vector of the cross-section centroid along the element, written with respect to the global frame. As shown in Fig. 6.2, it can be expressed as

$$\begin{aligned}\mathbf{r}(\zeta) &= \mathbf{r}_1 + \mathbf{R}_{rot}\bar{\mathbf{r}}(\zeta) \\ &= \begin{bmatrix} x_1+u_1 \\ y_1+v_1 \end{bmatrix} + \begin{bmatrix} c & -s \\ s & c \end{bmatrix} \begin{bmatrix} \frac{l}{l_0}\zeta \\ 0 \end{bmatrix} \\ &= \begin{bmatrix} \left(1-\frac{\zeta}{l_0}\right)(x_1+u_1) + \frac{\zeta}{l_0}(x_2+u_2) \\ \left(1-\frac{\zeta}{l_0}\right)(y_1+v_1) + \frac{\zeta}{l_0}(y_2+v_2) \end{bmatrix}\end{aligned} \tag{6-19}$$

where $\mathbf{r}_1$ is the current position of the first node, also written with respect to the global frame. Vector $\bar{\mathbf{r}}$ corresponds to position of the cross-section centroid

with respect to the local frame and $\zeta \in [0, l_0]$ is the element domain. The velocity of the cross section centroid along the element is first obtained by taking the time derivative of Eq. (6-19), which results in

$$\begin{aligned} \dot{\mathbf{r}}(\zeta) &= \dot{\mathbf{r}}_1 + \dot{\mathbf{R}}_{rot}\bar{\mathbf{r}}(\zeta) + \mathbf{R}_{rot}\dot{\bar{\mathbf{r}}}(\zeta) \\ &= \begin{bmatrix} \left(1 - \frac{\zeta}{l_0}\right)\dot{u}_1 + \frac{\zeta}{l_0}\dot{u}_2 \\ \left(1 - \frac{\zeta}{l_0}\right)\dot{v}_1 + \frac{\zeta}{l_0}\dot{v}_2 \end{bmatrix}. \end{aligned} \tag{6-20}$$

Since the rotation of the cross section is also interpolated linearly across the element, the angular velocity is given by

$$\dot{\theta}(\zeta) = \left(1 - \frac{\zeta}{l_0}\right)\dot{\theta}_1 + \frac{\zeta}{l_0}\dot{\theta}_2. \tag{6-21}$$

From Eq. (6-20) and (6-21), the kinetic energy can be expressed as

$$\begin{aligned} \mathcal{T}_e &= \frac{1}{2}\int_0^{l_0} \left(\rho A \dot{\mathbf{r}}^T\dot{\mathbf{r}} + I\dot{\theta}^2\right) d\zeta \\ &= \frac{1}{2}\dot{\mathbf{q}}_e^T\mathbf{M}_e\dot{\mathbf{q}}_e \end{aligned} \tag{6-22}$$

where

$$\mathbf{M}_e = l_0 \begin{bmatrix} \frac{\rho A}{3} & 0 & 0 & \frac{\rho A}{6} & 0 & 0 \\ 0 & \frac{\rho A}{3} & 0 & 0 & \frac{\rho A}{6} & 0 \\ 0 & 0 & \frac{I}{3} & 0 & 0 & \frac{I}{6} \\ \frac{\rho A}{6} & 0 & 0 & \frac{\rho A}{3} & 0 & 0 \\ 0 & \frac{\rho A}{6} & 0 & 0 & \frac{\rho A}{3} & 0 \\ 0 & 0 & \frac{I}{6} & 0 & 0 & \frac{I}{3} \end{bmatrix}. \tag{6-23}$$

$\mathbf{M}_e$ corresponds to the classic and constant Timoshenko mass matrix.

6.1.4 Equation of motion

The Lagrangian approach is used here to derive the equation of motion of the system. Defining the Lagrangian function of one beam element as $L = \mathcal{T}_e - \mathcal{V}_e$, the Lagrangian equation becomes

$$\frac{d}{dt}\left(\frac{\partial \mathcal{T}_e}{\partial \dot{\mathbf{q}}_e}\right) + \frac{\partial \mathcal{V}_e}{\partial \mathbf{q}_e} = 0 \tag{6-24}$$

Performing the respective differentiations, the equation of motion becomes

$$\mathbf{M}\ddot{\mathbf{q}}_e + \underbrace{\mathbf{B}^T\mathbf{K}_e\bar{\mathbf{q}}_e}_{\mathbf{f}_{nl,e}(\mathbf{q}_e)} = 0, \tag{6-25}$$

where $\mathbf{f}_{nl,e}(\mathbf{q})$ corresponds to the nonlinear elastic force vector and takes into account the finite displacement and rotation of the element, i.e., the

geometric nonlinearity of the flexible beam. For several types of analysis considering nonlinear structures (static or dynamic), a linearization around a given configuration is usually required. This is the case, for example, when performing numerical integration of the nonlinear equation of motion with a modified Newmark scheme, as shown in section 3.1. Therefore, the tangent stiffness matrix, defined as $\mathbf{K}_{e,s} = \frac{\partial \mathbf{f}_e}{\partial \mathbf{q}}$, must also be computed, preferably analytically to guarantee numerical precision and computational efficiency. For the co-rotational finite element considered here, this tangent stiffness matrix becomes

$$\mathbf{K}_{e,s} = \mathbf{B}^T \mathbf{K}_e \mathbf{B} + \frac{1}{l} \mathbf{z}^T \mathbf{z} \mathbf{e}_1 \mathbf{K}_e \bar{\mathbf{q}} + \frac{1}{l^2} \left(\mathbf{w}^T \mathbf{z} + \mathbf{z}^T \mathbf{w} \right) \mathbf{e}_2 \mathbf{K}_e \bar{\mathbf{q}} \tag{6-26}$$

where

$$\mathbf{e}_1 = \begin{bmatrix} 1 & 0 & 0 \end{bmatrix} \tag{6-27}$$

$$\mathbf{e}_2 = \begin{bmatrix} 0 & 1 & 1 \end{bmatrix}. \tag{6-28}$$

The equation of motion described in Eq. (6-25) was derived for just one co-rotational beam element. An equation of motion for the entire structure (considering all elements, the respective connectivities and boundary conditions) should be assembled using the traditional finite element procedure. Giving a mapping between the degrees of freedom of the entire structure and of each element, the global equation of motion can be written as

$$\mathbf{M}\ddot{\mathbf{q}}(t) + \mathbf{f}_{nl}\left(\mathbf{q}(t)\right) = \mathbf{0}, \tag{6-29}$$

where $\mathbf{M} \in \mathbb{R}^{n \times n}$ is the global mass matrix, while $\mathbf{q}$ and $\mathbf{f}$ correspond to the generalized coordinates of the entire structure and the global elastic force vector, respectively. n is the number of degrees of freedom of the system. Given the linear interpolation used in the derivation of the kinetic energy of each element, a convergence analysis should be conducted to evaluate the adopted spacial discretization.

To compute the NNMs of flexible beams, the equation of motion defined by Eq. (6-29) should be replaced in the periodic boundary value problem defined in Eq. (5-9). The solution follows the methodology presented in section 5.3. The main difficulty when dealing with flexible beams is the fact that $\mathbf{f}_{nl}\left(\mathbf{q}(t)\right)$ is in general nonzero for all DOF. This has a consequence in the computational cost and in the numerical stability of the method.

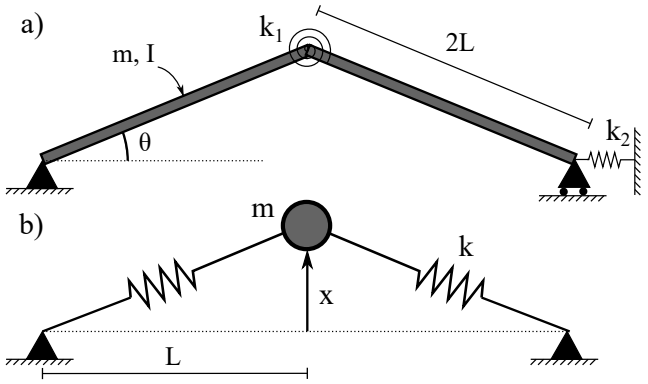

Figure 6.3: SDOF systems with different nonlinearities to analyze the influence in the periodic oscillations.

m [**kg**]	**I** [**kg.m²**]	**L** [**m**]	**k₁** [**N/rad**]
3.925	0.327	1	2748

Table 6.1: Parameters used in the SDOF systems.

6.2 Numerical examples

Before dealing directly with different examples of flexible beams governed by Eq. (6-29), two single degree of freedom systems are first analyzed. The fundamental frequency of the periodic solutions are analyzed for different energy levels. Those simplified systems contain nonlinearities that are likely to be found in flexible beams, which motivates this analysis. The idea is to understand through simplified systems how the nonlinear terms can affect the fundamental frequency. Both systems analyzed here are illustrated in Fig. 6.3. The bars are assumed to be rigid body elements. The parameters used in the computation of the periodic solutions are summarized in Tab. 6.1. The equations of motion for both systems were obtained using the Lagrange's equation, and correspond to

$$\left(mL^2 + I\right)\ddot{\theta} + 2k_1\theta + 4\sin^2\theta\ddot{\theta} + 8k_2L^2\left(1 - \cos\theta\right)\sin\theta = 0 \qquad (6\text{-}30)$$

$$m\ddot{x} + 2kx - \frac{2kLx}{\sqrt{x^2 + L^2}} = 0. \qquad (6\text{-}31)$$

Equation (6-30) represents the equation of motion of system a) and the nonlinearities come from the finite rotation of the bars. A horizontal spring was added at the right boundary condition to understand how this possible elastic element can modify the dynamics of the system. Boundary conditions are elements that have a high degree of uncertainties in many practical cases, which motivates this analysis. Equation (6-31) represents the equation of motion of system b) and the nonlinearity comes from the springs angle with respect to

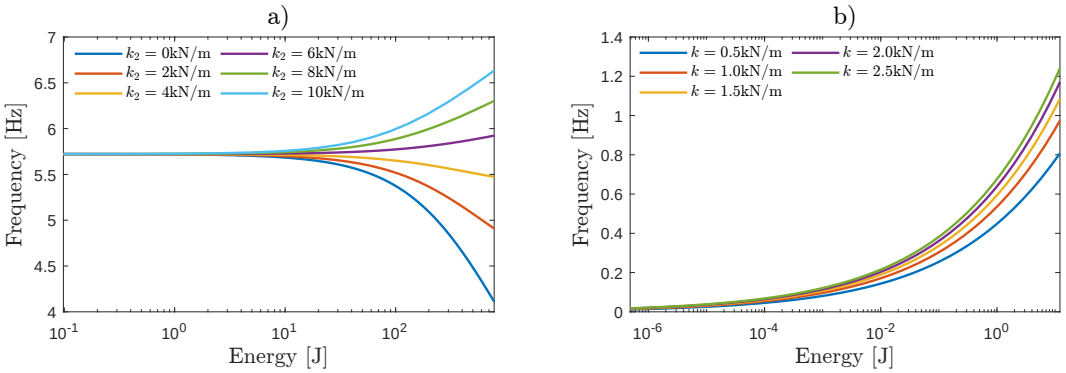

Figure 6.4: FEP of both SDOF systems.

the motion of the mass particle [106].

The computation of the periodic solutions was done using the HBM with an *Ansatz* truncated at the 5th harmonic ($H = 5$). The Fourier coefficients of the nonlinear terms were computed using the AFT method. A total of 128 samples were used to discretize the period of oscillation in time-domain. The predictor-corrector scheme using the tangent method and the arc-length parameterization described in section 4.1 was used to compute the periodic solution branch. The results are displayed in Fig. 6.4 in the form of frequency-energy plots. For the system (a), different values for the spring coefficients k_2 were used. When $k_2 = 0$ (no spring), a reduction in the fundamental frequency is observed at high energy levels. By increasing the spring stiffness, the fundamental frequency increases proportionally and becomes even higher than the frequency at low energy levels (which is the natural frequency of the underlying linear system). This means that the system changes from a softening to a hardening behavior. For the system (b), different spring stiffnesses were also used in the analysis. For small displacements (low energy levels), the influence of the springs is negligible, which reduces the equation of motion to a simple mass system. Hence, the fundamental frequency goes to zero in all analyzed cases. At higher energies, a hardening effect was observed. A quicker increment in the fundamental frequency is found for the systems with higher springs stiffnesses. This nonlinearity can be latter related to the axial strain of the co-rotational beam elements.

Considering now to the computation of NNMs of flexible beams, the first structure analyzed corresponds to a slim bi-supported beam, as shown in Fig. 6.5. The right hand-side boundary condition was allowed to move freely in the horizontal direction. However, a spring was introduced to connect the free end of the beam to the ground, similarly to the analyzed SDOF system (a). The beam is made of steel and have rectangular and uniform cross sections. The geometric and material properties are summarized in Tab. 6.2.

Figure 6.5: Slender bi-supported beam representation.

Mass density	**Elasticity modulus**	**Shear modulus**	**Length**	**Height**	**Thickness**
$7850kg/m^3$	$200GPa$	$76.92GPa$	$2m$	$0.01m$	$0.05m$

Table 6.2: Beam's material and geometric properties.

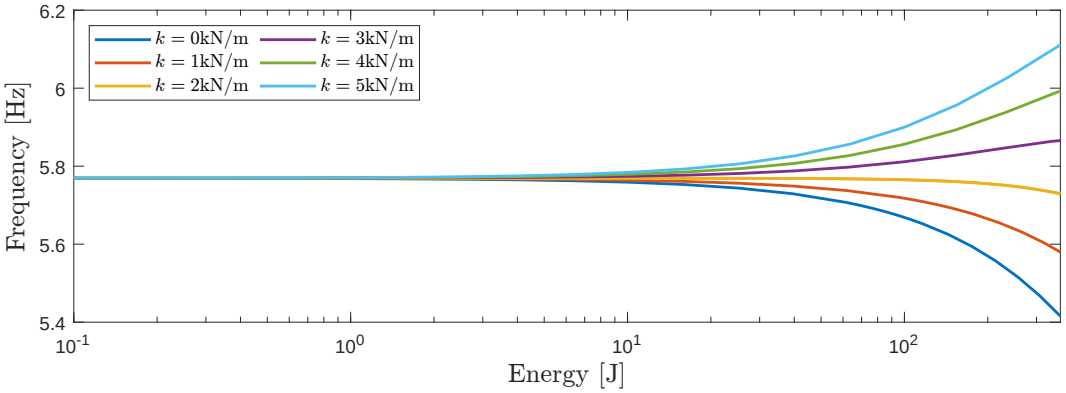

Figure 6.6: Frequency-energy plot of the slim bi-supported beam.

Only the fist NNM is analyzed here because it is the most likely mode to exhibit large displacements and rotations. The *Ansatz* in the HBM was set as a Fourier series truncated up to the 8th harmonic. The number of samples used in the ATF method was kept the same as the previous examples, i.e. 128 samples per period. The resulting frequency-energy plot of the first NNM is presented in Fig. 6.6. A similar behavior in comparison to the SDOF system (a) is observed. When no spring is attached to the right hand-side boundary condition ($k = 0$), the fundamental frequency of the first NNM reduces with the increase of the energy level, i.e., presenting a softening behavior. As the spring stiffness in the boundary condition increases, the fundamental frequency also increases, becoming even higher than the natural frequency of the underlying linear system, i.e., presenting a hardening behavior.

To understand the contribution of each harmonic in the solution path of this NNM, the participation of the relevant harmonics (the ones that are different from zero) in the horizontal and vertical motion of the beam's middle node is presented in Fig. 6.7. Only the case of $k = 0$ is considered in this analysis since the results are similar in all analyzed cases. For the vertical motion, only the first harmonic contributes significantly to the periodic solution. A small participation of the third harmonic is noticed at high energy levels. In the other hand, for the horizontal motion, only the DC term and

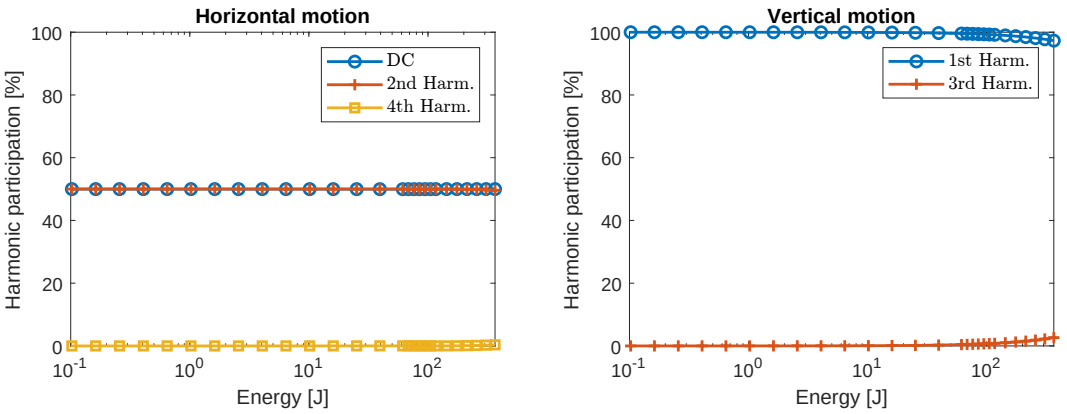

Figure 6.7: Harmonic participation in the vertical and horizontal motion of the middle node of the beam.

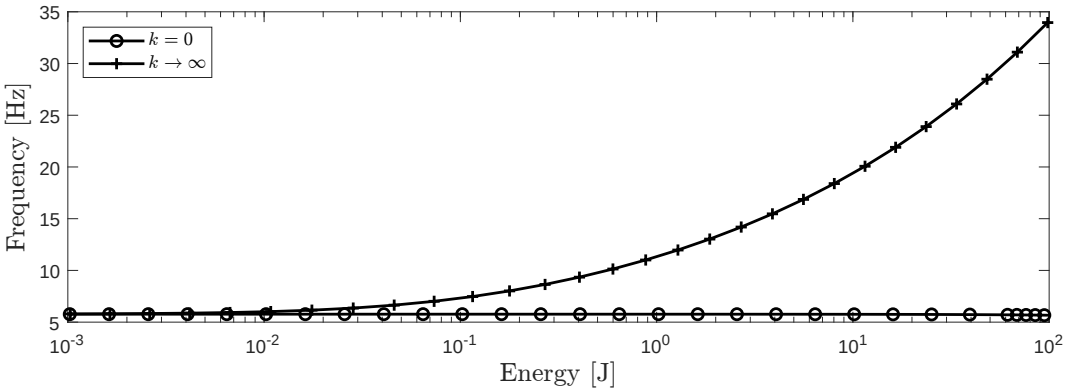

Figure 6.8: Frequency-energy plot of the slim bi-supported beam with $k = 0$ N/m and $k \to \infty$.

the second harmonic equally contribute in the periodic solutions at all energy levels. All the beam's nodes move only to the right hand-side direction with respect to the equilibrium configuration, which explains the presence of a DC term. Also, for each oscillation in the vertical direction, two oscillations in the horizontal direction are necessary, which explains the second harmonic term. With this result, it is possible to reduce the *Ansatz* truncation order to a lower value (e.g. $H = 4$) to reduce the computational cost.

At the limiting condition, where the spring stiffness tends to infinity, i.e. when the horizontal displacement at the right hand-side boundary condition is not allowed, the first NNM exhibits a hardening effect similar to the one observed in the SDOF system (b). The frequency-energy plot for $k = 0$ and $k \to \infty$ is shown in Fig. 6.8. The hardening effect with $k \to \infty$ is much higher than the softening behavior found for $k = 0$.

The second example analyzed here corresponds to a clamp-clamp flexible beam. The geometric and material properties are the same as the previous example (summarized in Tab. 6.2). Given the symmetry of the problem, only

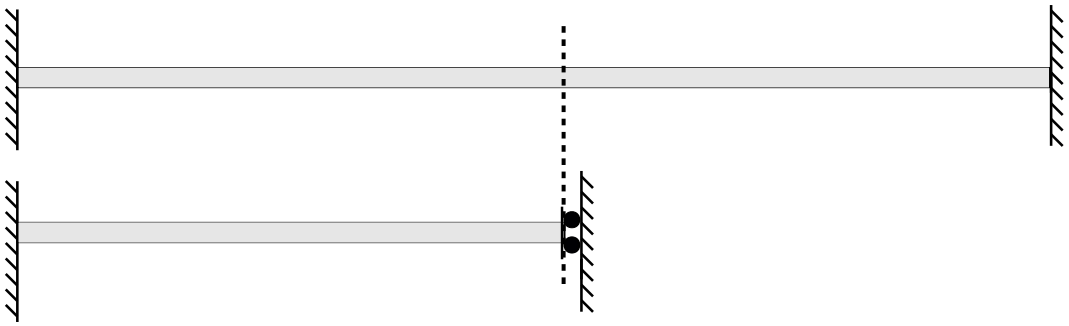

Figure 6.9: Schematic representation of the clamp-clamp thin beam. Only half of the beam domain is used given the symmetry of the problem.

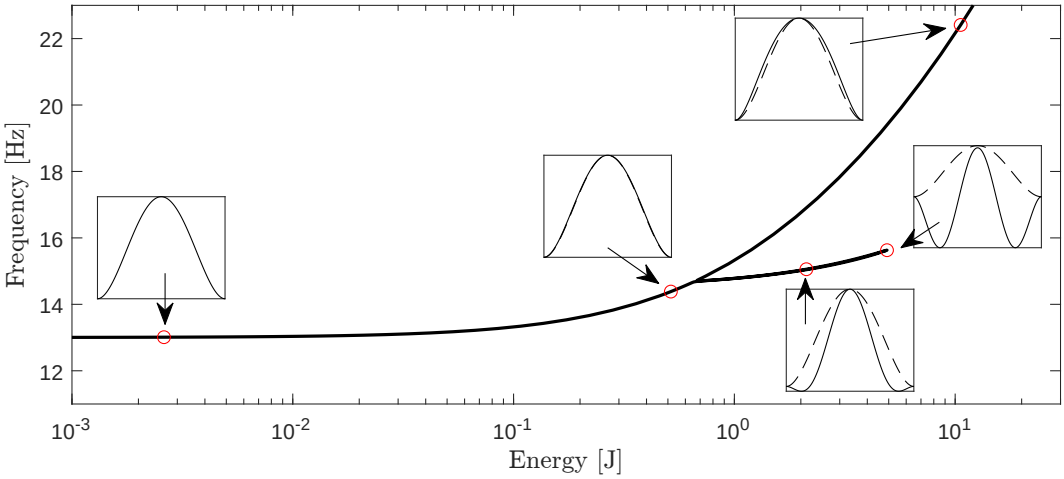

Figure 6.10: Frequency energy plot of the clamp-clamp beam modeled with 10 co-rotational finite elements.

half of the beam's domain is analyzed. The spacial discretization is done using 10 co-rotational elements. This time, the HBM is implemented with the *Ansatz* truncated at the 6th harmonic. The number of samples used to evaluate the Fourier coefficients of the nonlinear terms with the ATF method are increased to 512 samples.

Again, only the first NNM is analyzed. The frequency-energy plot of the clamped-clamped flexible beam is presented in Fig. 6.10. The mode shapes (solid lines) are also displayed at some key points together with the first linear normal mode (dashed lines) of the undelying linear system (under the hypothesis of small displacements). Besides the main solution branch, a tongue representing a 5:1 mode interaction between the first and the third NNMs was computed. As expected from the SDOF system (b), the fundamental frequency of the First NNM presents a stiffening effect caused by the axial strain.

As any continuous structure that are spatially discretized with the finite element method, a convergence study is necessary to evaluate the adopted mesh. This is especially important for the co-rotational finite element proposed

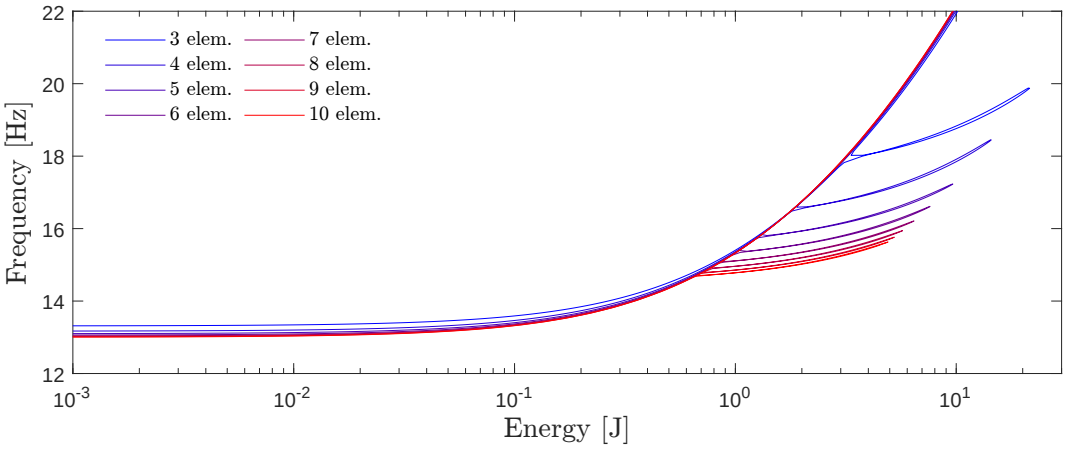

Figure 6.11: Convergence analysis of the first NNM.

in this paper since it uses a linear interpolation to simplify the computation of the inertial terms in the equation of motion. To this end, the computation of the first NNM was also done using a different number of elements (3 to 10). The resulting frequency-energy plot of the beam with these different meshes are overlapped in Fig. 6.11. The purpose of this plot is to illustrate the convergence of the fundamental frequency of the mode in its main branch as well as in the interaction tongue. It is clear that the main branch reaches convergence quicker and with a low amount of elements. For the mode interaction tongue, a much higher amount of elements (at least 10) was necessary to reach a convergence, which is explained by the fact that it also depends on the convergence of the third NNM. In general, higher modes require higher number of elements to converge, even when dealing with linear models.

7
Conclusions

The necessity of lighter and longer structures have been requiring the consideration of nonlinearities during the design stage of new mechanical systems. The analysis of nonlinear structures is in general more complex because it has physical phenomena that have no counterpart in linear systems. The dynamics is usually richer and complex, but on the other hand allows the structural limits to be extended. Therefore, nonlinear structure is an interesting and active field of research in the academy and industry.

This thesis felt into this topic with the emphasis in nonlinear normal modes (NNM), one of the underdevelopment analysis tool for structural dynamics. Although many references about it are found in the literature for a few decades, new application of NNM still appearing. The novelty of this thesis explored the application of NNM to flexible beams.

This thesis started with a detailed presentation of two mathematical methods developed to compute periodic solutions of periodic boundary value problems. In chapter 2, the Harmonic Balance method (HBM) was first introduced. The representation of periodic functions as Fourier series is essential to the comprehension of this method and therefore was initially reviewed. The HBM was then presented as a particular case of a family of weighted residual approaches. Then, it was described in more detailed to mechanical systems using a Fourier-Galerkin projection. The exponential representation of the Fourier series was used. Traditionally, the HBM is presented using the trigonometric form when dealing with mechanical systems. However, in the author perspective, the exponential form was more comprehensive and efficient. Additional care was required during the implementation of the method in a Matlab script. The problem of finding periodic solution was then summarized as a solution of a nonlinear system of algebraic equations. The respective solutions was found numerically using the Newton-Raphson method. Depending on the type of nonlinearity, there is no close form for their Fourier coefficients, so a numerical approach known as Alternating Frequency-Time (AFT) was considered. Given its versatility and efficiency, such numerical approach had excellent performance.

The second and equivalent method covered in this thesis corresponds

to the well known Shooting method. It also seeks for solutions of periodic boundary value problems, but evaluating the difference between the initial and final state of the system after one period. Hence, it requires the implementation of a numerical integration scheme. Chapter 3 started reviewing a modified version of Newmark integrator, which allowed the integration of nonlinear models efficiently. The residual functions of the Shooting method and the corresponding partial derivatives were then defined, allowing the solution to be found using a Newton type solver. The partial derivatives were shown to be related to the asymptotic stability of the periodic solution, contributing significantly in the comprehension of the dynamics of the systems.

Chapter 4 was the last chapter of this theses in which the mathematical tools were described. It focused on the numerical continuation of the periodic solutions. Nonlinear systems are energy-dependent, so that the periodic solutions evolve with the energy level in the system. Tracking those changes was important when evaluating the dynamic behavior of the nonlinear system. The prediction-correction scheme was therefore presented. Different prediction methods and parameterizations restrictions were considered. An efficient algorithm was presented and adopted throughout the rest of the thesis. To exemplify the implementation of the code, the computation of NFRCs was performed for several numerical examples. Each one of them presented a different type of local nonlinearities (cubic spring, friction damping and unilateral spring) to illustrate the versatility of the algorithm. The code was implemented in a format that account for periodic solutions computed either by the HBM or the Shooting method. Both of them were used in the numerical examples and the results showed the equivalence between them.

Chapter 5 was responsible for the definition and computation of NNMs. The two well known definition of NNMs in the literature were presented. Comparison between linear and nonlinear modes was also performed. Important properties that have no counterpart in linear modes were discussed, including the energy dependency, internal resonances and stability. Such properties were also illustrated with a simple 2 DOF nonlinear system. Additional beam examples with local nonlinearities were also considered, showing the capability of the algorithm and its correct implementation. Again, the HBM and the Shooting method were considered to highlight the equivalence between them.

7.1 Contribution

The concept of NNM as the backbone curve of the NFRCs was showed in the last example of chapter 5. Such property was exploited in more datail

in the Appendix C. It was used as starting point for the computation of isolas. A cantilever beam with strong nonlinearity originated from a unilateral spring was considered. As far as this author knows, the computation of isolas of such system using NNM data was not yet done, so it becomes part of the novelty of this thesis.

Chapter 6 represented the main originality of this monograph. It synthesized the content of all previous chapters through the computation of NNMs of flexible beams. The generated geometric nonlinearity was modeled using the co-rotation finite element framework. Such model was developed under the assumption of large displacement, finite rotation and small strain. The strain energy was computed using the Interdependent Interpolation Element (IIE), which uses cubic interpolation for the transverse displacement and quadratic interpolation for the cross section rotation. It was chosen since it solves the homogeneous governing equation of the Timoshenko beam theory exactly at the nodal points and because it is a locking-free element, a desirable property when dealing with thin beam elements. For the kinetic energy, a linear interpolation was used to simplify the formulation of the inertial terms when deriving the equation of motion. Such simplification is often used in the literature and lead to convergent result with a suitable amount of elements.

From the derived equation of motion, the NNM were computed based on the Rosemberg's definition. A periodic restriction was incorporated to the problem to generate a periodic boundary value problem, in which the solution was approximated with the HBM. The computation of the Fourier coefficients of the nonlinear term is the main part of the proposed method and was done numerically using the Alternating Frequency-Time method. The tangent method and the arc-length parametrization were adopted in the predictor-corrector scheme to perform the continuation of the periodic solution at different energy levels. The overall system of nonlinear algebraic equation built during the corrector phase was solved numerically using a Newton type solver.

Two numerical examples were used to investigate the possibility of combining all of the numerical techniques (co-rotational finite elemnts, Harmonic Balance, Alternating Frequency-Time, Arc-length continuation and Newton type solver) to compute the NNMs of flexible beams. In both cases, the computation of the NNM was possible. A bi-supported beam was first considered, where an equivalent spring was added to one of the boundary conditions in order to investigate the effect of this uncertain stiffness in the fundamental frequency of the NNM. It exhibit an interesting change from softening to hardening behavior as the spring stiffness was increased. In the second exam-

ple, a bi-clamped beam was considered. For this system, a mode interaction was found. The NNM was computed repetitively with an increasing number of elements to evaluate the convergence of the NNM. The frequency-energy plot showed a quicker convergence of the main solution branch (around 5 elements), while the mode interaction tongue required more elements (around 10 elements). Since the mode interaction depends also on the convergence of higher NNMs, it requires more elements to converge.

7.2 Future works

When combining a high amount of degrees of freedom and a high truncation order of the *Ansatz* of the HBM, the computational cost of the NNM becames an issue when using the proposed method. Given the different orders of magnitudes between the unknowns (axial displacement, transversal displacements, cross section rotation and the fundamental frequency), it was necessary to preconditioning the system of algebraic equations. Without precondition the system, the different orders of magnitude slowed down or even impeded convergence of the solver. A better preconditioning of the solver should be implemented in future works to allow the application of the proposed method to system with higher dimensions.

The implemented method used in this thesis was focused on the computation of NNM of flexible beams. Only uniform beams were considered at this stage. Nevertheless, an extension to more complex structures is straightforward. For example, nonuniform beams could be analyzed if the mass and stiffness matrices were modified in the local coordinate system of the co-rotational formulation. Also, other types of flexible structures could be implemented. For example thin-shells could be considered since co-rotational finite element formulations for dynamic analysis have already been proposed in the literature [91].

Bibliography

[1] YAZDCHI, M.; CRISFIELD, M.A.. **Non-linear dynamic behaviour of flexible marine pipes and risers**. International Journal for Numerical Methods in Engineering, 54(9):1265–1308, 2002.

[2] ALBINO, J.C.R.; ALMEIDA, C.A.; MENEZES, I.F.M.; PAULINO, G.H.. **Co-rotational 3d beam element for nonlinear dynamic analysis of risers manufactured with functionally graded materials (fgms)**. Engineering Structures, 173:283–299, 2018.

[3] WHITE, S.W.; KIM, S.M.; BAJAJ, A.K.; DAVIES, P.; SHOWERS, D.K.;LIEDTKE, P.E.. **Experimental techniques and identification of nonlinear and viscoelastic properties of flexible polyurethane foam**. Nonlinear Dynamics, 22(3):281–313, 2000.

[4] SCHULTZE, J.F.; HEMEZ, F.M.; DOEBLING, S.W.; SOHN, H.. **Application of non-linear system model updating using feature extraction and parameter effects analysis**. Shock and Vibration, 8:581978, 2001.

[5] SINGH, R.; DAVIES, P.; BAJAJ, A.K.. **Identification of nonlinear and viscoelastic properties of flexible polyurethane foam**. Nonlinear Dynamics, 34(3):319–346, 2003.

[6] RICHARDS, C.M.; SINGH, R.. **Characterization of rubber isolator nonlinearities in the context of single- and multi-degree-of-freedom experimental systems**. Journal of Sound and Vibration, 247(5):807–834, 2001.

[7] CAUGHEY, T.K.; VIJAYARAGHAVAN, A.. **Free and forced oscillations of a dynamic system with "linear hysteretic damping" (non-linear theory)**. International Journal of Non-Linear Mechanics, 5(3):533–555, 1970.

[8] TOMLINSON, G.R.; HIBBERT, J.H.. **Identification of the dynamic characteristics of a structure with coulomb friction**. Journal of Sound and Vibration, 64(2):233–242, 1979.

[9] SHERIF, H.A.; ABU OMAR, T.M.. **Mechanism of energy dissipation in mechanical system with dry friction**. Tribology International, 37(3):235–244, 2004.

[10] AL-BENDER, F.; SYMENS, W.; SWEVERS, J.; VAN BRUSSEL, H.. **Theoretical analysis of the dynamic behavior of hysteresis elements in mechanical systems**. International Journal of Non-Linear Mechanics, 39(10):1721–1735, 2004.

[11] BABITSKY, V.I.; VEPRIK, A.; KRUPENIN, V.L.. **Vibration of Strongly Nonlinear Discontinuous Systems**. Foundations of Engineering Mechanics. Springer Berlin Heidelberg, 2012.

[12] WEHNER, J.H.; JEKEL, D.; SAMPAIO, R.; HAGEDORN P.. **Damping Optimization in Simplified and Realistic Disc Brakes**. SpringerBriefs in Applied Sciences and Technology. Springer International Publishing, 2012.

[13] KERSCHEN, G.; WORDEN, K.; VAKAKIS, A.F.; GOLINVAL, J-C.. **Past, present and future of nonlinear system identification in structural dynamics**. Mechanical Systems and Signal Processing, 20:505–592, 2006.

[14] NOËL, J.P.; RENSON, L.; KERSCHEN, G.. **Complex dynamics of a nonlinear aerospace structure: Experimental identification and modal interactions**. Journal of Sound and Vibration, 333(12):2588–2607, 2014.

[15] DETROUX, T.; RENSON, L.; MASSET, L.; KERSCHEN, G. **The harmonic balance method for bifurcation analysis of large-scale nonlinear mechanical systems**. Computer Methods in Applies Mechanics and Engineering, 296:18–38, 2015.

[16] MOORE, G.. **Floquet theory as a computational tool**. SIAM Journal on Numerical Analysis, 42(6):2522–2568, 2006.

[17] LAZARUS, A.; THOMAS, O.. **A harmonic-based method for computing the stability of periodic solutions of dynamical systems**. Comptes Rendus Mécanique, 338(9):510–517, 2010.

[18] TRAVERSA, F. L.; BONANI, F.; GUERRIERI, S.D.. **A frequency-domain approach to the analysis of stability and bifurcations in nonlinear systems described by differential-algebraic equations**.

International Journal of Circuit Theory and Applications, 36(4):421–439, 2008.

[19] TRAVERSA, F. L.; BONANI, F.. **Improved harmonic balance implementation of floquet analysis for nonlinear circuit simulation**. AEU - International Journal of Electronics and Communications, 66(5):357–363, 2012.

[20] KUETHER, R.J.; RENSON, L.; DETROUX, T.; GRAPPASONNI, C.; KERSCHEN, G.. **Nonlinear normal modes, modal interactions and isolated resonance curves**. Journal of Sound and Vibration, 351:299–310, 2015.

[21] ROSENBERG, R.M.. **Normal modes of nonlinear dual-mode systems**. Journal of Applied Mechanics, 27(2):263–268, 1960.

[21] ROSENBERG, R.M.. **The normal modes of nonlinear n-degree-of-freedom systems**. Journal of Applied Mechanics, 29(1):7–14, 1962.

[22] ROSENBERG, R.M.. **On nonlinear vibration of systems with many degrees of freedom**. Advances in Applied Mechanics, 9:155–242, 1966.

[23] SHAW, S.W.; PIERRE, C.. **Non-linear normal modes and invariant manifolds**. Journal of Sound and Vibration, 150(1):170–173, 1991.

[24] SHAW, S.W.; PIERRE, C.. **Normal modes for non-linear vibratory systems**. Journal of Sound and Vibration, 164(1):85–124, 1993.

[25] SHAW, S.W.; PIERRE, C.. **Normal modes of vibration for non-linear continuous systems**. Journal of Sound and Vibration, 169(3):319–347, 1994.

[26] SIMO, J.C.; VU-QUOC, L.. **On the dynamics of flexible beams under large overall motions—the plane case: Part i**. Journal of Applied Mechanics, 53(4):849–854, 1986.

[27] SIMO, J.C.; VU-QUOC, L.. **On the dynamics of flexible beams under large overall motions—the plane case: Part ii**. Journal of Applied Mechanics, 53(4):855–863, 1986.

[28] WAGNER, G.; LIMA, R.; SAMPAIO, R.. **Benefits of OKID in system realization with low amount of samples (in preparation)**.

[29] FOINY, D.; WAGNER, G.; LIMA, R.; SAMPAIO, R.. **Dynamical systems identification with smooth decomposition**. In: PROCEEDINGS OF

THE XVII INTERNATIONAL SYMPOSIUM ON DYNAMIC PROBLEMS OF MECHANICS, 2017.

[30] WAGNER, G.; FOINY, D.; LIMA, R.; SAMPAIO, R.. **A new formulation of the SVMD with noise control and uncertainty quantification**. In: PROCEEDINGS OF THE ICVRAM-ISUMA UNCERTAINTIES CONFERENCE, 2018.

[31] WAGNER, G.; FOINY, D.; LIMA, R.; SAMPAIO; R.. **The robust smooth orthogonal decomposition method for operational modal analysis**. In: PROCEEDINGS OF THE 17TH INTERNATIONAL OPERATIONAL MODAL ANALYSIS CONFERENCE, 2017.

[32] WAGNER, G.; LIMA, R.; SAMPAIO, R.. **Modal identification of a light and flexible wind turbine blade under wind excitation (in preparation)**. 2022.

[33] WAGNER, G.; FOINY, D.; LIMA, R.; SAMPAIO, R.. **Operational modal analysis under wind load using stochastic subspace identification**. In: PROCEEDINGS OF THE XVII INTERNATIONAL SYMPOSIUM ON DYNAMIC PROBLEMS OF MECHANICS, 2017.

[34] WORDEN, K.; TOMLINSON, G.R.. **Nonlinearity in structural dynamics**. IOP Publishing, London, 1st edition, 2001.

[35] WAGNER, G.; LIMA, R.; SAMPAIO, R.. **Nonlinear normal modes of flexible beams using a co-rotational finite element formulation**. Journal of Enfineering Mathematics (accepted).

[36] EVANS, T.. **Nonlinear Dynamics**. IntechOpen, Croatia, 2010.

[37] RITTO, T.G.. **Numerical analysis of the nonlinear dynamics of a drill-string with uncertainty modeling**. Phd thesis, Mechanical Engineering Department, Pontifical Catholic University of Rio de Janeiro, Rio de Janeiro, 2010.

[38] CUNHA, A.; SOIZE, C.; SAMPAIO, R.. **Computational modeling of the nonlinear stochastic dynamics of horizontal drillstrings**. Computational Mechanics, 56:849–878, 2015.

[39] RITTO, T.G.; ESCALANTE, M.R.; SAMPAIO, R.; ROSALES, M.B.. **Drill-string horizontal dynamics with uncertainty on the frictional force**. Journal of Sound and Vibration, 332(1):145–153, 2013.

[40] SAMPAIO, R.; FERREIRA, E.L.C.; BRANDÃO, A.S.. **Análise e processamento de sinais**, volume 22 de **Notas em Matemática Aplicada**. Sociedade Brasileira de Matemática Aplicada e Computacional, 2012.

[41] BRANDT, A.. **Noise and vibration analysis:signal analysis and experimental procedures**. John Wiley and Sons, West Sussex, UK, 1st edition, 2011.

[42] NAYFEH, A.H.; MOOK, D.T.. **Nonlinear oscillations**. Wiley Classics Library, 1995.

[43] CAMERON, T.M.; GRIFFIN, J.H.. **An alternating frequency/time domain method for calculating the steady-state response of nonlinear dynamic systems**. Journal of Applied Mechanics, 56(1):149–154, 03 1989.

[44] GUILLEN, J.; PIERRE, C.. **An efficient, hybrid, frequency-time domain method for the dynamics of large-scale dry-friction damped structural systems.** In: PFEIFFER, F.; GLOCKER, C., editor, IUTAM SYMPOSIUM ON UNILATERAL MULTIBODY CONTACTS, p. 169–178, Dordrecht, 1999. Springer Netherlands.

[45] NACIVET, S.; PIERRE, C.; THOUVEREZ, F.; JEZEQUEL, L.. **A dynamic lagrangian frequency–time method for the vibration of dry-friction-damped systems**. Journal of Sound and Vibration, 265(1):201–219, 2003.

[46] KRACK, M.. **Nonlinear modal analysis of nonconservative systems: Extension of the periodic motion concept**. Computers and Structures, 154:59–71, 2015.

[47] MATTOS, H.S.C.. **Uma Contribuição à Formulaćão Termodinâmica da Elastoplasticidade e Elastoviscoplasticidade**. Phd thesis, Mechanical Engineering Department, Pontifical Catholic University of Rio de Janeiro, Rio de Janeiro, 1988.

[48] ROCHINHA, F.A.. **Modelagem e Simulação Numérica de Estruturas Unidimensionais**. Phd thesis, Mechanical Engineering Department, Pontifical Catholic University of Rio de Janeiro, Rio de Janeiro, 1990.

[49] NEWMARK, N.M.. **A method of computation for structural dynamics**. Journal of the Engineering Mechanics Division, 85(3):67–94, 1959.

[50] HILBER, H.M.; HUGHES, T.J.R.; TAYLOR, R.L.. **Improved numerical dissipation for time integration algorithms in structural dynamics**. Earthquake Engineering & Structural Dynamics, 5(3):283–292, 1977.

[51] BELYTSCHKO, T.; HUGHES, T.J.R.. **Computational Methods for Transient Analysis**. 1. North-Holland, 1983.

[52] CHUNG, J.; HULBERT, G.M.. **A time integration algorithm for structural dynamics with improved numerical dissipation: The generalized-α method**. Journal of Applied Mechanics, 60(2):371–375, 06 1993.

[53] KERSCHEN, G.. **Modal analysis of nonlinear mechanical systems**. Springer, Udine, Italy, 1st edition, 2014.

[54] SEYDEL, R.. **Practical bifurcation and stability analysis**. Springer, New York, 3rd edition, 2010.

[55] MAMIYA, E.N.. **Aplicacao do Metodo de Continuação A Problemas de Elasticidade Finita de Materiais Incompressiveis**. Phd thesis, Mechanical Engineering Department, Pontifical Catholic University of Rio de Janeiro, Rio de Janeiro, 1988.

[56] KRACK, M.; GROSS, J.. **Harmonic Balance for Nonlinear Vibration Problems**. Springer Nature Switzerland AG, Switzerland, 1st edition, 2019.

[57] PEETERS, M.. **Theoretical and Experimental Modal Analysis of Nonlinear Vibrating Structures using Nonlinear Normal Modes**. Phd thesis, Aerospace and Mechanical Engineering Department, University of Liège, Liège, 2010.

[58] HE, J.; FU, Z.F.. **Modal analysis**. Butterworth-Heinemann, Oxfort, UK, 1st edition, 2001.

[59] MAIA, N.M.M; SILVA, J.M.M.. **Theoretical and experimental modal analysis**. Research studies press, Somerset, England, 1st edition, 1997.

[60] BRINCKER, R.; VENTURA, C.. **Introduction to operational modal analysis**. John Wiley and Sons, West Sussex, UK, 1st edition, 2015.

[61] EWINS, D.J.. **Modal Testing: theory and practice**. Wiley, 1st edition, 1984.

[62] FRISWELL, M.; MOTTERSHEAD, J.E.. **Finite Element Model Updating in Structural Dynamics**. Kluwer academic publishers, 1995.

[63] AVITABILE, P.. **Modal Testing: A Practitioner's Guide**. Wiley, West Sussex, UK, 1st edition, 2017.

[64] PEETERS, M.; VIGUIÉ, R.; SÉRANDOUR, G.; KERSCHEN, G.; GOLINVAL, J-C.. **Nonlinear normal modes, part ii: Toward a pratical computation using numerical continuation techniques**. Mechanical Systems and Signal Processing, 23:195–216, 2009.

[65] KERSCHEN, G.; PEETERS, M.; GOLINVAL, J-C.. **Nonlinear modal analysis ofa full-scale aircraft**. Journal of Aircraft, 50(5):1409–1419, 2013.

[66] LAXALDE, D.; THOUVEREZ, F.. **Complex non-linear modal analysis for mechanical systems: Application to turbomachinery bladings with friction interfaces**. Journal of sound and vibration, 322:1009–1025, 2009.

[67] RENSON, L.. **Nonlinear Modal Analysis of Conservative and Nonconservative Aerospace Structures**. Doctor in engineering sciences thesis, Aerospace and Mechanical Engineering Department, University of Liège, Liège, 2014.

[68] RENSON, L.; DELIÉGE, G.; KERSCHEN, G.. **An effective finite-element-based method for the computation of nonlinear normal modes of nonconservative systems**. Meccanica, 49:1901–1916, 2014.

[69] HABIB, G.; CIRILLO, G.I.; KERSCHEN, G.. **Isolated resonances and nonlinear damping**. Nonlinear Dynamics, 93:979–994, 2018.

[70] TOUZÉ, C.; AMABILI, M.. **Nonlinear normal modes for damped geometrically nonlinear systems: Application to reduced-order modelling of harmonically forced structures**. Journal of Sound and Vibration, 298(4):958–981, 2006.

[71] BLANC, F.; TOUZÉ, C.; MERCIER, J.-F.; EGE, K.; BONNET BEN-DHIA, A.-S.. **On the numerical computation of nonlinear normal modes for reduced-order modelling of conservative vibratory systems**. Mechanical Systems and Signal Processing, 36(2):520–539, 2013.

[72] THOUVEREZ, F.. **Presentation of the ecl benchmark**. Mechanical System and Signal Processing, 17(1):195–202, 2003.

[73] NÖEL, J-P.; RENSON, L.; GRAPPASONNI, C.; KERSCHEN, G.. **Identification of nonlinear normal modes of engineering structures under broadband forcing**. Mechanical Systems and Signal Processing, 74:95–110, 2016.

[74] RENSON, L.; GONZALEZ-BUELGA, A.; BARTON, D.A.W.; NEILD, S.A.. **Robust identification of backbone curves using control-based continuation**. Journal of Sound and Vibration, 367:145–158, 2016.

[75] RENSON, L.; HILL, T.L.; EHRHARDT, D.A.; BARTON, D.A.W.; NEILD, S.A.. **Force appropriation of nonlinear structures**. Proc. R. Soc. A, 474, 2018.

[76] ANASTASIO, D.; MARCHESIELLO, S.; KERSCHEN, G.; NOËL, J-P.. **Experimental identification of distributed nonlinearities in the modal domain**. Journal of Sound and Vibration, 458:426–444, 2019.

[77] NÖEL, J-P.; KERSCHEN, G.. **Nonlinear system identification in structural dynamics: 10 more years of progress**. Mechanical Systems and Signal Processing, 83:2–35, 2017.

[78] RENSON, L.; KERSCHEN, G.; COCHELIN, B.. **Numerical computation of nonlinear normal modes in mechanical engineering**. Journal of Sound and Vibration, 364:177–206, 2016.

[79] ALBU-SCHÄFFER, A.; DELLA SANTINA,C.. **A review on nonlinear modes in conservative mechanical systems**. Annual Reviews in Control, 50:49–71, 2020.

[80] KERSCHEN, G.; PEETERS, M.; GOLINVAL, J.C.; VAKAKIS, A.F.. **Nonlinear normal modes, part i: A useful framework for the structural dynamicist**. Mechanical System and Signal Processing, 23:170–194, 2009.

[81] OUEINI, S.S.; CHIN, C.M.; NAYFEH, A.H.. **Dynamics of a cubic nonlinear vibration absorber**. Nonlinear Dynamics, 20:283–295, 1997.

[82] HSIAO, K.M.; JANG, J.Y.. **Dynamic analysis of planar flexible mechanisms by co-rotational formulation**. Computer Methods in Applied Mechanics and Engineering, 87(1):1–14, 1991.

[83] IURA, M.; IWAKUMA, T.. **Dynamic analysis of the planar timoshenko beam with finite displacement**. Computers & Structures, 45(1):173–179, 1992.

[84] IURA, M.; ATLURI, S.N.. **Dynamic analysis of planar flexible beams with finite rotations by using inertial and rotating frames**. Computers & Structures, 55(3):453–462, 1995.

[85] BEHDINAN, K.; STYLIANOU, M.C.; TABARROK, B.. **Co-rotational dynamic analysis of flexible beams**. Computer Methods in Applied Mechanics and Engineering, 154(3):151–161, 1998.

[86] REDDY, J.N.. **On locking-free shear deformable beam finite elements**. Computer Methods in Applied Mechanics and Engineering, 149(1):113–132, 1997.

[87] GALVANETTO, U.; CRISFIELD, M.A.. **An energy-conserving co-rotational procedure for the dynamics of planar beam structures**. International Journal for Numerical Methods in Engineering, 39(13):2265–2282, 1996.

[88] CRISFIELD, M.A.; GALVANETTO, U.; JELENIC, G.. **Dynamics of 3-d co-rotational beams**. Computational Mechanics, 20:507–519, 1997.

[89] LE, T.N.; BATTINI, J.M.; HJIAJ, E.. **Efficient formulation for dynamics of corotational 2d beams**. Computational Mechanics, 48:153–161, 2011.

[90] BATTINI, J.M.. **Analysis of dampers for stay cables using non linear beam elements**. Structures, 16:45–49, 2018.

[91] YANG, J.; XIA, P.. **Corotational nonlinear dynamic analysis of thin-shell structures with finite rotations**. AIAA Journal, 53(3):663–677, 2015.

[92] VAKAKIS, A.F.; MANEVITCH, L.I.; MIKHLIN, Y.V.; PILIPCHUK, V.N.; ZEVIN, A.A.. **Normal Modes and Localization in Nonlinear Systems**. Wiley Series in Nonlinear Science. Wiley, Germany, 2008.

[93] PESHECK, E.. **Reduced order modeling of nonlinear structural systems using nonlinear normal modes and invariant manifolds**. Phd thesis, University of Michigan, Michigan, 2000.

[94] PESHECK, E.; PIERRE, C.; SHAW, S.W.. **A new galerkin-based approach for accurate non-linear normal modes through invariant manifolds**. Journal of Sound and Vibration, 249(5):971–993, 2002.

[95] BELLIZZI, S.; BOUC, R.. **A new formulation for the existence and calculation of nonlinear normal modes**. Journal of Sound and Vibration, 287(3):545–569, 2005.

[96] BELLIZZI, B.; BOUC, R.. **An amplitude-phase formulation for nonlinear modes and limit cycles through invariant manifolds**. Journal of Sound and Vibration, 300(3):896–915, 2007.

[97] WRIGHT, J.R.; COOPER, J.E.; DESFORGES, M.J.. **Normal-mode force appropriation—theory and application**. Mechanical Systems and Signal Processing, 13(2):217–240, 1999.

[98] ATKINS, P.A.; WRIGHT, J.R.; WORDEN, K.. **An extension of force appropriation to the identification of non-linear multi-degree of freedom systems**. Journal of Sound and Vibration, 237(1):23–43, 2000.

[99] PEETERS, M.; KERSCHEN, G.; GOLINVAL, J.C.. **Dynamic testing of nonlinear vibrating structures using nonlinear normal modes**. Journal of Sound and Vibration, 330(3):486–509, 2011.

[100] PEETERS, M.; KERSCHEN, G.; GOLINVAL, J.C.. **Modal testing of nonlinear vibrating structures based on nonlinear normal modes: Experimental demonstration**. Mechanical Systems and Signal Processing, 25(4):1227–1247, 2011.

[101] EHRHARDT, D.A.; HARRIS, R.B.; ALLEN, M.S.. **Numerical and experimental determination of nonlinear normal modes of a circular perforated plate**. In: J. DE CLERCK, editor, TOPICS IN MODAL ANALYSIS I, VOLUME 7, p. 239–251, Cham, 2014. Springer International Publishing.

[102] ZAPICO-VALLE, J.L.; GARCÍA-DIÉGUEZ, M.; ALONSO-CAMBLOR, R.. **Nonlinear modal identification of a steel frame**. Engineering Structures, 56:246–259, 2013.

[103] GERADIN, M.; RIXEN, D.J.. **Mechanical Vibrations: Theory and Application to Structural Dynamics**. Wiley, 2015.

[104] MEIROVITCH, L.. **Principles and Techniques of Vibrations**. Prentice Hall, 1997.

[105] CUNHA JR, A.B.. **Modeling and Uncertainty Quantification in the Nonlinear Stochastic Dynamics of Horizontal Drillstrings**. Phd

thesis, Mechanical Engineering Department, Pontifical Catholic University of Rio de Janeiro, Rio de Janeiro, 2015.

[106] FONSECA, C.; LIMA, R.; WAGNER, G.; SAMPAIO, R.. **Design of a nonlinear dynamical absorber for an uncertain system**. In: PROCEEDINGS OF THE UNCERTAINTIES 2014, 2014.

A
Linear modes

This appendix presents a review on vibration modes of linear mechanical systems. It is the starting point for the main topic of this thesis and helps in the extension of the theory of vibration modes to nonlinear systems. The nomenclature of this appendix A is self-contained and differs from the rest of the thesis, although some effort has been made to keep it as close as possible. This appendix is organized in a crescent order of complexity. It starts with conservative normal systems, then deals with gyroscopic conservative system and finishes with nonconservative systems. The theory presented here follows [104] closely.

A.1
Conservative natural systems

The first and simplest linear mechanical system considered here is the conservative natural case. It represents a linear system in the absence of gyroscopic, viscous damping, circulatory and externally forces. It is represented by the following equation of motion:

$$\mathbf{M}\ddot{\mathbf{q}}(t) + \mathbf{K}_s\mathbf{q}(t) = \mathbf{0}, \tag{A-1}$$

where $\mathbf{M}$ and $\mathbf{K}_s \in \mathbb{R}^{n\times n}$ are two symmetric matrices representing the mass and stiffness matrices of the system, respectively. Additionally, $\mathbf{M}$ is assumed here to be positive definite. The vector $\mathbf{q} \in \mathbb{R}^n$ represents the displacements of the system, and $\dot{\mathbf{q}}$ and $\ddot{\mathbf{q}}$ are the first and second time derivatives, respectively. n represents the number of degrees of freedom (DOF) of the system.

We start the study of linear modes by searching a synchronous motion of $\mathbf{q}$, i.e., a motion in which all the DOF follow the same time function. It is characterized for having all DOF reaching their extreme values and cross zero simultaneously. To evaluate the possibility of synchronous motion, an initial *Ansatz* for $\mathbf{q}(t)$ is given in the following form:

$$\mathbf{q}(t) = \tilde{\mathbf{q}}e^{st}, \tag{A-2}$$

where s is a constant scalar and $\tilde{\mathbf{q}} \in \mathbb{R}^n$ is a constant vector. Substituting Eq. (A-2) into Eq. (A-1), it is possible to write

$$\mathbf{K}_s\tilde{\mathbf{q}} = \lambda\mathbf{M}\tilde{\mathbf{q}}, \tag{A-3}$$

where $\lambda = -s^2$. Equation (A-3) represents an algebraic eigenvalue problem, also known as the characteristic-value problem. Here, it is written in terms of two real and symmetric matrices. Its solution and the respective properties are better discussed if the eigenvalue problem is first rewrite in a more convenient format, i.e., in terms of only a single matrix. This could be easily obtained by pre-multiplying both sides of Eq. (A-3) by $\mathbf{M}^{-1}$, but important properties would be obscured because the symmetry of $\mathbf{M}^{-1}\mathbf{K}_s$ can no longer be guarantee. Instead, we start by first decomposing the mass matrix as

$$\mathbf{M} = \mathbf{P}^T\mathbf{P}, \tag{A-4}$$

where $\mathbf{P} \in \mathbb{R}^{n\times n}$ is a nonsingular matrix. Inserting Eq. (A-4) into (A-3), we obtain

$$\mathbf{K}_s\tilde{\mathbf{q}} = \lambda\mathbf{P}^T\mathbf{P}\tilde{\mathbf{q}}. \tag{A-5}$$

Next, let's define a linear transformation as

$$\mathbf{P}\tilde{\mathbf{q}} = \boldsymbol{\phi} \tag{A-6}$$

and the respective inverse transformation as

$$\tilde{\mathbf{q}} = \mathbf{P}^{-1}\boldsymbol{\phi}, \tag{A-7}$$

where $\mathbf{P}^{-1}$ is guaranteed because $\mathbf{P}$ is nonsingular. Inserting Eq. (A-6) and Eq.(A-7) into Eq. (A-5) and pre-multiplying both side by $\left(\mathbf{P}^T\right)^{-1}$, we reduce the eigenvalue problem to

$$\mathbf{A}\boldsymbol{\phi} = \lambda\boldsymbol{\phi} \tag{A-8}$$

where

$$\mathbf{A} = \left(\mathbf{P}^T\right)^{-1}\mathbf{K}_s\mathbf{P}^{-1} = \left(\mathbf{P}^{-1}\right)^T\mathbf{K}_s^T\mathbf{P}^{-1} = \mathbf{A}^T. \tag{A-9}$$

$\mathbf{A}$ is a real symmetric matrix only because $\mathbf{K}_s$ is symmetric and the relation $\left(\mathbf{P}^T\right)^{-1} = \left(\mathbf{P}^{-1}\right)^T$ exists. Equation (A-8) represents the same eigenvalue defined in Eq. (A-3), but in the so called standard form. Before discussing the nature of the eigensolution, let's first rewrite Eq. (A-8) as

$$\left(\mathbf{A} - \lambda\mathbf{I}\right)\boldsymbol{\phi} = \mathbf{0} \tag{A-10}$$

where $\mathbf{I} \in \mathbb{R}^{n\times n}$ is the identity matrix. From linear algebra, it is known that a system of n linear homogeneous algebraic equation with n unknowns possesses a nontrivial solution if and only if the matrix of coefficients is singular, which leads to

$$\det\left[\mathbf{A} - \lambda\mathbf{I}\right] = \mathbf{0} \tag{A-11}$$

Equation (A-11) represents a polynomial equation of degree n in terms of λ. It is known as characteristic equation. It possesses n solutions $\lambda_r (r = 1, 2, \ldots, n)$,

the roots of the polynomial, and represents the eigenvalues of matrix $\mathbf{A}$. For each eigenvalue λ_r there is a vector $\boldsymbol{\phi}_r$ that satisfies

$$(\mathbf{A} - \lambda_r \mathbf{I})\,\boldsymbol{\phi}_r = \mathbf{0} \quad \text{for } r = 1, \ldots, n. \tag{A-12}$$

This vector is known as an eigenvector of $\mathbf{A}$. Since Eq. (A-12) is homogeneous, any multiple of $\boldsymbol{\phi}_r$ is also a solution, which means that the eigenvector is uniquely defined, except for the magnitude. A normalization is then required and the magnitude of the eigenvector can be chosen arbitrary. A convenient normalization widely used corresponds in restrict all the eigenvectors to have unit norm. This is represented by the following normalization equation:

$$\boldsymbol{\phi}_r^T \boldsymbol{\phi}_r = 1, \quad \text{for } r = 1 \ldots n. \tag{A-13}$$

Considering this normalization scheme and pre-multiplying Eq. (A-12) by $\boldsymbol{\phi}_r^T$, it follows that

$$\boldsymbol{\phi}_r^T \mathbf{A} \boldsymbol{\phi}_r = \lambda_r, \quad \text{for } r = 1 \ldots n. \tag{A-14}$$

The adopted normalization is convenient and will be used in the following when presenting important properties of the eigensolutions. Most of those properties are a consequence of the symmetry of $\mathbf{A}$.

Real eigensolutions: Let's consider that one pair of eigensolution $(\lambda_r, \boldsymbol{\phi}_r)$ is complex. Since $\mathbf{A}$ is real, the complex conjugate of this pair, $(\lambda_r^*, \boldsymbol{\phi}_r^*)$, must also be a solution. Therefore, both pairs satisfy the eigenvalue problem:

$$\mathbf{A}\boldsymbol{\phi}_r = \lambda_r \boldsymbol{\phi}_r \tag{A-15}$$

$$\mathbf{A}\boldsymbol{\phi}_r^* = \lambda_r^* \boldsymbol{\phi}_r^*. \tag{A-16}$$

Now, let's pre-multiply Eq. (A-15) by $(\boldsymbol{\phi}_r^*)^T$ and Eq. (A-16) by $\boldsymbol{\phi}_r^T$, and subtract the second from the first. Using the fact that $\mathbf{A}$ is symmetric, we obtain

$$(\boldsymbol{\phi}_r^*)^T \mathbf{A}\boldsymbol{\phi}_r - \boldsymbol{\phi}_r^T \mathbf{A}\boldsymbol{\phi}_r^* = 0 = \lambda_r (\boldsymbol{\phi}_r^*)^T \boldsymbol{\phi}_r - \lambda_r \boldsymbol{\phi}_r^T \boldsymbol{\phi}_r^* = (\lambda_r - \lambda_r^*) \|\boldsymbol{\phi}_r\|, \tag{A-17}$$

where $\|\boldsymbol{\phi}_r\|$ is the L^2-norm of $\boldsymbol{\phi}_r$. Such norm must be positive for any nonzero vector. Then, it follows that

$$\lambda_r - \lambda_r^* = 0. \tag{A-18}$$

In order to satisfy Eq. (A-18), the eigenvalues must be real. Additionally, since matrix $\mathbf{A}$ and the respective eigenvalues are real, so are the eigenvectors.

Orthogonality of the eigenvectors: First, Let's now consider two distinct eigenvalues, λ_r and λ_j, and the respective eigenvectors $\boldsymbol{\phi}_r$ and $\boldsymbol{\phi}_j$. Those pairs

of eigensolutions must satisfy

$$\mathbf{A}\boldsymbol{\phi}_r = \lambda_r \boldsymbol{\phi}_r \tag{A-19}$$

$$\mathbf{A}\boldsymbol{\phi}_j = \lambda_j \boldsymbol{\phi}_j. \tag{A-20}$$

Similarly as before, if we pre-multiply Eq. (A-19) by $\left(\boldsymbol{\phi}_j\right)^T$ and Eq. (A-20) by $\boldsymbol{\phi}_r^T$, take the transpose of the second equation and subtract it from the first, we obtain:

$$\boldsymbol{\phi}_j^T \mathbf{A}\boldsymbol{\phi}_r - \left(\boldsymbol{\phi}_r^T \mathbf{A}\boldsymbol{\phi}_j\right)^T = 0 = \lambda_r \boldsymbol{\phi}_j^T \boldsymbol{\phi}_r - \lambda_j \boldsymbol{\phi}_r^T \boldsymbol{\phi}_j = \left(\lambda_r - \lambda_j\right) \boldsymbol{\phi}_j^T \boldsymbol{\phi}_r \tag{A-21}$$

Since the eigenvalues are distinct, Eq. (A-21) is satisfied if and only if

$$\boldsymbol{\phi}_j^T \boldsymbol{\phi}_r = 0, \quad \text{for} \quad r, j = 1 \ldots, n \quad \text{and} \quad r \neq j. \tag{A-22}$$

Equation (A-22) shows that two eigenvectors of a real symmetric matrix belonging to two distinct eigenvalues are mutually orthogonal. Additionally, if we consider this result and pre-multiply Eq. (A-19) by $\boldsymbol{\phi}_j^T$, it follows that

$$\boldsymbol{\phi}_j^T \mathbf{A}\boldsymbol{\phi}_k = 0, \quad \text{for} \quad k, j = 1 \ldots, n \quad \text{and} \quad k \neq j. \tag{A-23}$$

Equation (A-23) shows that, besides being mutually orthogonal, the eigenvectors associated with two distinct eigenvalues of a real symmetric matrix $\mathbf{A}$ are also orthogonal with respect to $\mathbf{A}$.

For the case where the eigenvalues have multiplicity, it is possible to show that the eigenvectors associated with this eigenvalue are also mutually orthogonal. Interested readers can look for the proof in [103]. However, the eigenvectors associated with repeated eigenvalues are not unique since any linear combination of them is also an eigenvector. In summary, it is possible to affirm that all the eigenvectors of a real symmetric matrix are orthogonal regardless of whether the associated eigenvalue have multiplicity or not.

Combining the adopted normalization scheme and the orthogonality of the eigenvectors, we can write

$$\boldsymbol{\phi}_j^T \boldsymbol{\phi}_r = \delta_{rj} \qquad \text{for } r, j = 1, \ldots, n \tag{A-24}$$

$$\boldsymbol{\phi}_j^T \mathbf{A}\boldsymbol{\phi}_r = \lambda_r \delta_{rj} \qquad \text{for } r, j = 1, \ldots, n, \tag{A-25}$$

where δ_{rj} represents the Kronecker delta.

Next, let's analyze how the orthogonality of the eigenvectors $\boldsymbol{\phi}_r$ can be extended to the eigenvectors $\tilde{\mathbf{q}}_r$ of the original eigenvalue problem defined in Eq. (A-3). To this end, let's recall the relationship between those eigenvector, which was defined by the linear transformation in Eq. (A-6) and by the inverse

transformation in Eq. (A-7). It results in

$$\boldsymbol{\phi}_r = \mathbf{P}\tilde{\mathbf{q}}_r, \quad \tilde{\mathbf{q}}_r = \mathbf{P}^{-1}\boldsymbol{\phi}_r, \quad \text{for } r = 1, \ldots, n. \tag{A-26}$$

Substituting those relationship in Eq. (A-24), it follows that

$$\boldsymbol{\phi}_j^T \boldsymbol{\phi}_r = \tilde{\mathbf{q}}_j^T \mathbf{P}^T \mathbf{P} \tilde{\mathbf{q}}_r = \tilde{\mathbf{q}}_j^T \mathbf{M} \tilde{\mathbf{q}}_r = \delta_{rj}, \quad \text{for} \quad r, j = 1 \ldots, n \tag{A-27}$$

which shows that the eigenvectors $\tilde{\mathbf{q}}_r$ are orthogonal with respect to the mass matrix $\mathbf{M}$, instead of being mutually orthogonal as $\boldsymbol{\phi}_r$. It should be highlighted that Eq. (A-27) takes into account the magnitude normalization defined by Eq. (A-13), so that $\tilde{\mathbf{q}}_j^T \mathbf{M} \tilde{\mathbf{q}}_r$ becomes one when $r = j$. Another value could be obtain if another normalization was adopted, but the orthogonality with respect to $\mathbf{M}$ would remain true.

Similarly, if we now substitute the relationship defined by the transformation in Eq. (A-26) into Eq. (A-25) and take Eq. (A-9) into consideration, it follows that

$$\boldsymbol{\phi}_j^T \mathbf{A} \boldsymbol{\phi}_r = \boldsymbol{\phi}_j^T \left(\mathbf{P}^T\right)^{-1} \mathbf{K}_s \mathbf{P}^{-1} \boldsymbol{\phi}_r = \tilde{\mathbf{q}}_j^T \mathbf{K}_s \tilde{\mathbf{q}}_r = \lambda_r \delta_{rj} \quad \text{for } r, j = 1, \ldots, n \tag{A-28}$$

Equation (A-28) shows that the eigenvectors $\tilde{\mathbf{q}}_r$ are also orthogonal with respect to the stiffness matrix $\mathbf{K}_s$. Once again, the adopted normalization scheme was considered in Eq. (A-28) but it does not affect in the orthogonality property.

Sign of the eigenvalues: So far, it was established that the eigenvalues are real, but nothing was said about their signs. When the conservative natural system was defined in Eq.(A-1), it was assumed that the mass matrix $\mathbf{M}$ was positive definite. This term plays then no effect on the signs of the eigenvalues. The sign properties of stiffness matrix $\mathbf{K}_s$ on the other hand will contribute exclusive in the signs of the eigenvalues.

If the stiffness matrix $\mathbf{K}_s$ is positive definite, the analyzed system becomes positive definite and all the eigenvalues λ_r are positive. In this case, it is possible to introduce a convenient notation defined as

$$\lambda_r = \omega_r^2 \quad \text{for } r = 1, \ldots, n. \tag{A-29}$$

Recalling that $\lambda = -s^2$, we can conclude that, for each eigenvalue λ_r, there is a corresponding pair of pure imaginary complex conjugate exponents

$$s_r, s_r^* = \pm \mathbf{i} \omega_r \quad \text{for } r = 1, \ldots, n. \tag{A-30}$$

Substituting those exponents in the *Ansatz* defined in Eq. (A-2), it is possible to conclude that the conservative natural systems with positive definite stiffness

matrix admit n synchronous motion in the form of

$$\mathbf{q}_r(t) = \left(a_r e^{\mathbf{i}\omega_r t} + a_r^* e^{-\mathbf{i}\omega_r t}\right) \tilde{\mathbf{q}}_r = A_r \cos\left(\omega_r t - \theta_r\right) \tilde{\mathbf{q}}_r \quad \text{for } r = 1, \ldots, n, \tag{A-31}$$

where A_r and θ_r represent the amplitude and phase of the periodic motion. Also, the coefficient a_r^* of $e^{-\mathbf{i}\omega_r t}$ was taken as complex conjugate of a_r because $\mathbf{q}_r(t)$ must be real. Equation (A-31) show that the synchronous motion of a positive definite system corresponds to a monoharmonic function with oscillatory frequency ω_r, known as the natural frequency of the system. The associated eigenvector $\tilde{\mathbf{q}}_r$ is then called natural mode, or normal mode, and it defines a constant ratio between the displacements of all DOF during the synchronous motion.

Now, if the stiffness matrix $\mathbf{K}_s$ is only positive semidefinite, the system becomes positive semidefinite. This is the case when the system is unrestrained. In this case, the eigenvalues become nonnegative, implying that the system can have some zero eigenvalues and the rest being positive. The synchronous motion associated with a zero eigenvalues, say λ_i, becomes then

$$\mathbf{q}_i(t) = (a_i + t b_i)\tilde{\mathbf{q}}_i, \tag{A-32}$$

which is a divergent motion and therefore unstable. It is also nonoscillatory. The eigenvector $\tilde{\mathbf{q}}_i$ are then identified as rigid-body modes of the system.

If we now consider the case where the stiffness matrix $\mathbf{K}_s$ is sign-variable, the eigenvalues can be either positive, zero or negative. For the negative eigenvalues, say λ_p, the exponents s becomes two real values defined by

$$s_{2p-1}, s_{2p} = \pm\sqrt{\| - \lambda_p \|}. \tag{A-33}$$

The negative exponent $s_{2p} = -\sqrt{\| - \lambda_p \|}$ represents a solution that decays exponentially, whereas the positive exponent $s_{2p-1} = +\sqrt{\| - \lambda_p \|}$ expressed a motion that diverges with time. Therefore, if the system presents at least one real negative eigenvalue, it becomes an unstable system.

A.2
Gyroscopic conservative systems

In this section, we consider the existence of gyroscopic forces in the conservative system analyzed in the previous section. Such forces are conservative, although being written proportionally to the velocity as the viscous damping forces. The equation of motion of a linear gyroscopic conservative system can be written as

$$\mathbf{M}\ddot{\mathbf{q}}(t) + \mathbf{C}_w\dot{\mathbf{q}}(t) + \mathbf{K}_s\mathbf{q}(t) = \mathbf{0} \tag{A-34}$$

where $\mathbf{C}_w \in \mathbb{R}^{n\times n}$ corresponds to a constant skew symmetric gyroscopic matrix. The mass matrix $\mathbf{M} \in \mathbb{R}^{n\times n}$ is once again considered as symmetric positive definite and $\mathbf{K}_s \in \mathbb{R}^{n\times n}$ is said, for now, only symmetric. Following a similar procedure performed in the previous section, an *Ansatz* of a synchronous motion can be given as

$$\mathbf{q}(t) = \tilde{\mathbf{q}}e^{st}, \tag{A-35}$$

where s is a constant scalar and $\tilde{\mathbf{q}} \in \mathbb{C}^n$ is now assumed to be a complex vector. Substituting this *Ansatz* in Eq. (A-34), performing the following derivatives, and dividing by e^{st}, the following eigenvalue problem is obtained:

$$s^2\mathbf{M}\tilde{\mathbf{q}} + s\mathbf{C}_w\tilde{\mathbf{q}} + \mathbf{K}_s\tilde{\mathbf{q}} = \mathbf{0} \tag{A-36}$$

Pre-multiplying the entire equation by $(\tilde{\mathbf{q}}^*)^T$, the transpose of the complex conjugate of $\tilde{\mathbf{q}}$, it becomes

$$ms^s + \mathbf{i}gs + k = 0 \tag{A-37}$$

where

$$m = (\tilde{\mathbf{q}}^*)^T \mathbf{M}\tilde{\mathbf{q}} > 0 \tag{A-38}$$

$$\mathbf{i}g = (\tilde{\mathbf{q}}^*)^T \mathbf{C}_w\tilde{\mathbf{q}} \tag{A-39}$$

$$k = (\tilde{\mathbf{q}}^*)^T \mathbf{K}_s\tilde{\mathbf{q}}. \tag{A-40}$$

Equation (A-37) corresponds to a scalar quadratic equation with its two roots being

$$s_1, s_2 = \mathbf{i}\left(-\frac{g}{2m} \pm \frac{1}{2m}\sqrt{g^2 + 4mk}\right). \tag{A-41}$$

The nature of the roots depends only on the value of k, and therefore on $\mathbf{K}_s$. Next, three possibilities for the nature of the roots are analyzed

- If k is positive, then $g^2 + 4mk$ is also positive. Therefore the roots are pure imaginary, which implies a pure oscillatory motion (stable).
- If k is zero for some $\tilde{\mathbf{q}} \neq \mathbf{0}$, then the associated root becomes zero, which implies a divergent motion. Such unstable motion represents a rigid body mode, as explained in the previous section.
- If k is negative, then two possibilities exists. If g^2+4mk remains positive, the root are pure imaginary and the motion is stable. In the absence of the gyroscopic force, the motion would be unstable. Hence, we can conclude that gyroscopic forces can sometimes stabilize an unstable conservative system. Now, if $g^2 + 4mk$ is negative, at least one root has positive real part, which implies an unstable motion.

In the following of this section, we will assume that k is always positive, which means that the stiffness matrix $\mathbf{K}_s$ is positive definitive. This is

motivated by the fact that this is the typical situation found in structural dynamics. Then, considering that the roots are pure imaginary, we can write $s = \mathbf{i}\omega$, and substituting it in Eq. (A-36). The following eigenvalue problem is then obtained:

$$-\omega^2\mathbf{M}\tilde{\mathbf{q}} + \mathbf{i}\omega\mathbf{C}_w\tilde{\mathbf{q}} + \mathbf{K}_s\tilde{\mathbf{q}} = \mathbf{0}. \tag{A-42}$$

This eigenvalue problem differs significantly from the one defined in Eq. (A-3) for the natural conservative systems. It is complex and contains ω and ω^2. To analyze the properties of the eigenvalues and eigenvector of this problem, some additional algebraic manipulations are necessary.

Complex conjugate eigenvalues: So far, we have shown that the eigenvalues of a gyroscopic conservative system with symmetric and positive definite mass and stiffness matrices are pure imaginary. Now, the goal is to show that they also occurs in pairs of pure imaginary complex conjugates. We start showing that ω must satisfy the characteristic equation

$$\det\left[-\omega^2\mathbf{M} + \mathbf{i}\omega\mathbf{C}_w + \mathbf{K}_s\right] = 0. \tag{A-43}$$

Since the determinant of a matrix is equal to the determinant of the same matrix transposed, we can write

$$\det\left[-\omega^2\mathbf{M} + \mathbf{i}\omega\mathbf{C}_w + \mathbf{K}_s\right]^T = \det\left[-\omega^2\mathbf{M} - \mathbf{i}\omega\mathbf{C}_w + \mathbf{K}_s\right] = 0. \tag{A-44}$$

Equation (A-44) shows that, if $\mathbf{i}\omega$ is a root of the characteristic equation, so it is $-\mathbf{i}\omega$. It then follows that the eigenvalues of a gyroscopic conservative system occurs in pairs of pure imaginary complex conjugate: $s_r, s_r^* = \pm\mathbf{i}\omega_r$ for $r = 1, \ldots, n$, where ω_r correspond to the natural frequency of the system.

State space form The eigenvalue problem defined in Eq. (A-42) is written in terms of ω and ω^2. Such difficulty can be overcome if the problem is recast in state space form. Defining the the state of the system as $\mathbf{y} = \left[\mathbf{q}^T(t) \quad \dot{\mathbf{q}}^T(t)\right]^T$, the equation of motion Eq. (A-34) can be rewritten as

$$\bar{\mathbf{M}}\dot{\mathbf{y}}(t) = -\bar{\mathbf{G}}\mathbf{y}(t), \tag{A-45}$$

where,

$$\bar{\mathbf{M}} = \begin{bmatrix} \mathbf{K}_s & \mathbf{0} \\ \mathbf{0} & \mathbf{M} \end{bmatrix} = \bar{\mathbf{M}}^T \tag{A-46}$$

$$\bar{\mathbf{G}} = \begin{bmatrix} \mathbf{0} & -\mathbf{K}_s \\ \mathbf{K}_s & \mathbf{C}_w \end{bmatrix} = -\bar{\mathbf{G}}^T \tag{A-47}$$

are two $2n \times 2n$ matrices. Notice that $\bar{\mathbf{M}}$ is a symmetric positive definite matrix, while $\bar{\mathbf{G}}$ is skew symmetric. Considering the fact that the eigenvalues of Eq. (A-42) are pure imaginary, an *Ansatz* of the periodic solution of Eq. (A-45) can be given as

$$\mathbf{y}(t) = \tilde{\mathbf{y}} e^{\mathbf{i}\omega t} \tag{A-48}$$

where $\tilde{\mathbf{y}} \in \mathbb{C}^{2n}$. Replacing Eq. (A-48) into Eq. (A-45), we obtain

$$\mathbf{i}\omega\bar{\mathbf{M}}\tilde{\mathbf{y}} = -\bar{\mathbf{G}}\tilde{\mathbf{y}}. \tag{A-49}$$

Equation (A-49) corresponds to an eigenvalue problem having ω in the first power only, which is beneficial. The cost, on the other hand, is that the dimension of the problem became $2n$. Additionally, it is still complex, which adds some difficulties. To overcome it, we can first define the real and imaginary part of the eigenvector explicit as $\tilde{\mathbf{y}}^{(R)}$ and $\tilde{\mathbf{y}}^{(I)}$, respectively, so that $\tilde{\mathbf{y}} = \tilde{\mathbf{y}}^{(R)} + \mathbf{i}\tilde{\mathbf{y}}^{(I)}$. Substituting this notation in Eq. (A-49) and equating the real and imaginary parts on both sides of the resulting equation, it follows that

$$\omega\bar{\mathbf{M}}\tilde{\mathbf{y}}^{(R)} = -\bar{\mathbf{G}}\tilde{\mathbf{y}}^{(I)} \tag{A-50}$$

$$\omega\bar{\mathbf{M}}\tilde{\mathbf{y}}^{(I)} = \bar{\mathbf{G}}\tilde{\mathbf{y}}^{(R)} \tag{A-51}$$

Solving Eq. (A-51) for $\tilde{\mathbf{y}}^{(I)}$ and replacing it in Eq. (A-50), and solving Eq. (A-50) for $\tilde{\mathbf{y}}^{(R)}$ and replacing it in Eq. (A-51), we obtain

$$\bar{\mathbf{K}}\tilde{\mathbf{y}}^{(R)} = \lambda\bar{\mathbf{M}}\tilde{\mathbf{y}}^{(R)} \tag{A-52}$$

$$\bar{\mathbf{K}}\tilde{\mathbf{y}}^{(I)} = \lambda\bar{\mathbf{M}}\tilde{\mathbf{y}}^{(I)} \tag{A-53}$$

where $\lambda = \omega^2$ and

$$\bar{\mathbf{K}} = \bar{\mathbf{G}}^T\bar{\mathbf{M}}^{-1}\bar{\mathbf{G}} = \begin{bmatrix} \mathbf{K}_s\mathbf{M}^{-1}\mathbf{K}_s & \mathbf{K}_s\mathbf{M}^{-1}\mathbf{C}_w \\ \mathbf{C}_w^T\mathbf{M}^{-1}\mathbf{K}_s & \mathbf{K}_s + \mathbf{C}_w^T\mathbf{M}^{-1}\mathbf{C}_w \end{bmatrix} = \bar{\mathbf{K}}^T \tag{A-54}$$

corresponds to a symmetric positive definite matrix. The eigenvalue problems defined in Eq. (A-52) and Eq. (A-53) shares the same structure of the eigenvalue of the conservative natural system defined in Eq. (A-3). Therefore, the same procedure used in the previous section can be applied again to transform the eigenvalue problem to its standard form as in Eq. (A-10). Also, the properties discussed in the previous section can be used here. However, some differences exist. The dimension of the eigenvalue problem is now $2n$ instead of n. In addition, Eq. (A-52) and Eq. (A-53) show that the real and the imaginary parts of $\tilde{\mathbf{y}}$ satisfy the same eigenvalue problem. This means that each eigenvalue has multiplicity two, i.e., for each $\lambda_r = \omega_r^2$ there is two eigenvectors $\tilde{\mathbf{y}}_r^{(R)}$ and $\tilde{\mathbf{y}}_r^{(I)}$ associated with it. Since the system is positive definite, those two

eigenvectors are independent and can be rendered as orthogonal. The solution of the two real eigenvalues defined in Eq. (A-52) and (A-53) can be used to form the solution of the complex eigenvalue problem defined in Eq. (A-49). The eigensolutions are given as

$$s_r, s_r^* = \pm \mathbf{i}\omega_r \tag{A-55}$$

$$\tilde{\mathbf{y}}_r, \tilde{\mathbf{y}}_r^* = \tilde{\mathbf{y}}_r^{(R)} \pm \tilde{\mathbf{y}}_r^{(I)} \tag{A-56}$$

for $r, 1 \ldots, n$. Substituting those eigensolutions in the *Ansatz* defined in Eq. (A-48), it is possible to conclude that a gyroscopic conservative system admits n synchronous motions in the form of

$$\mathbf{y}_r(t) = a_r e^{\mathbf{i}\omega_r t}\tilde{\mathbf{y}}_r + a_r^* e^{-\mathbf{i}\omega_r t}\tilde{\mathbf{y}}_r^* \tag{A-57}$$

$$= A_r \left[\cos(\omega_r t - \theta_r)\tilde{\mathbf{y}}_r^{(R)} - \sin(\omega_r t - \theta_r)\tilde{\mathbf{y}}_r^{(I)}\right] \tag{A-58}$$

for $r, 1 \ldots, n$. Once again the amplitude A_r and phase θ_r of the motion must be defined.

A.3
Natural systems with proportional damping

Before jumping into a general nonconservative system, let's first analyze a system with viscous damping matrix that is proportional to the mass and stiffness matrices. The equation of motion can be written as

$$\mathbf{M}\ddot{\mathbf{q}}(t) + \mathbf{C}_p\dot{\mathbf{q}}(t) + \mathbf{K}_s\mathbf{q}(t) = \mathbf{0} \tag{A-59}$$

where,

$$\mathbf{C}_p = \alpha\mathbf{M} + \beta\mathbf{K}_s. \tag{A-60}$$

Most of the results obtained for the conservative natural system will be used hereafter to analyze the natural systems with proportional damping. From the eigensolution of Eq. (A-3), we know that the eigenvectors are orthogonal with respect to $\mathbf{M}$ and $\mathbf{K}_s$, as showed in Eq. (A-27) and in Eq. (A-28). A set of *Ansatz* for the solution of Eq. (A-59) can be choice in a form of synchronous motion defined by

$$\mathbf{q}(t) = \tilde{\mathbf{q}}_r e^{s_r t} \quad \text{for } r = 1, \ldots, n, \tag{A-61}$$

where $\tilde{\mathbf{q}}_r$ comes from the eigensolution of the underlying conservative natural system and it was defined in Eq. (A-26). The constant s_r is assumed to be complex-valued and it is yet to be defined. Substituting this *Ansatz* into the equation of motion and pre-multiplying the result by $\tilde{\mathbf{q}}_r^T$, one obtains

$$\left[s_r^2 + (\alpha + \beta\lambda_r) + \lambda_r\right] e^{s_r t} = 0 \quad \text{for } r = 1, \ldots, n, \tag{A-62}$$

where λ_r comes from the eigensolution of the underlying conservative natural system and represents the square of the natural frequency of the system, as defined in Eq. (A-29). Defining a damping ratio of the natural system with proportional damping as

$$\zeta_r = \frac{\alpha}{2\omega_r} + \frac{\beta\omega_r}{2} \quad \text{for } r = 1, \ldots, n, \tag{A-63}$$

equation (A-62) becomes

$$\left[s^2 + 2\zeta_r\omega_r s + \omega_r^2\right] e^{s_r t} = 0 \quad \text{for } r = 1, \ldots, n \tag{A-64}$$

Since the above equation must be satisfied for all values of t, the following characteristic equation is obtained:

$$s^2 + 2\zeta_r\omega_r s + \omega_r^2 = 0 \quad \text{for } r = 1, \ldots, n. \tag{A-65}$$

The roots of this quadratic equation can be expressed as

$$s_r = -\zeta_r\omega_r \pm \underbrace{\omega_r\sqrt{(\zeta_r^2 - 1)}}_{\omega_{dr}} \quad \text{for } r = 1, \ldots, n \tag{A-66}$$

Here we assume that α and β are positive, so that the system dissipates energy. There are three possibilities for the nature of the roots, depending on the values of ζ_r:

– If $\zeta_r < 1$, the roots come as a pair of complex conjugates, which means that the motion is oscillatory with a frequency equal to ω_{dr}. Since the real part is always negative, the motion is also stable. The system is called underdamped. The synchronous motion becomes

$$\begin{aligned} \mathbf{q}_r(t) &= \left(a_r e^{\mathbf{i}\omega_{dr}t} + a_r^* e^{-\mathbf{i}\omega_{dr}t}\right) e^{-\zeta_r\omega_r t}\tilde{\mathbf{q}}_r \\ &= A_r \cos\left(\omega_{dr}t - \theta_r\right) e^{-\zeta_r\omega_r t}\tilde{\mathbf{q}}_r \end{aligned} \tag{A-67}$$

where A_r represents the initial amplitude of the motion and θ_r the respective phase.

– If $\zeta_r = 1$, the root becomes a negative real value. The system is called critically damped and the motion is non-oscillatory (relaxation motion) and stable. The synchronous motion becomes

$$\mathbf{q}_r(t) = (a_r + b_r t)\, e^{-\omega_r t}, \tag{A-68}$$

where a_r and b_r are constant defined by initial conditions.

– If $\zeta_r > 1$, the roots come as a pair of negative real values. The system is called overdamped and the motion is non-oscillatory. It also returns to the static equilibrium, but in a slower rate compared to the critically

damped system. The synchronous motion becomes

$$\mathbf{q}_r(t) = \left(a_{r,1}e^{s_{r,1}t} + a_{r,2}e^{s_{r,2}t}\right)\tilde{\mathbf{q}}_r, \tag{A-69}$$

where $a_{r,1}$ and $a_{r,2}$ are defined from initial conditions.

A.4
Nonconservative systems

The last type of system analyzed in this appendix corresponds to a general nonconservative linear system. It includes systems with viscous damping and circulatory forces, simultaneously. Since the system is no longer conservative, the free response is no longer pure oscillatory. The equation of motion is given by

$$\mathbf{M}\ddot{\mathbf{q}}(t) + (\mathbf{C}_s + \mathbf{C}_w)\,\dot{\mathbf{q}}(t) + (\mathbf{K}_s + \mathbf{K}_w)\,\mathbf{q}(t) = \mathbf{0} \tag{A-70}$$

where $\mathbf{M} \in \mathbb{R}^{n\times n}$ is the symmetric positive definite mass matrix, $\mathbf{C}_s$ and $\mathbf{C}_w \in \mathbb{R}^{n\times n}$ represent the viscous damping and the gyroscopic matrices, respectively, and $\mathbf{K}_s$ and $\mathbf{K}_w$ represent the stiffness and circulatory forces matrices. To analyze the characteristics of the free response and the vibration modes, the equation of motion is first reduced to a first order differential equation in state space form:

$$\dot{\mathbf{y}}(t) = \mathbf{H}\mathbf{y}(t) \tag{A-71}$$

where $\mathbf{y}(t) = \begin{bmatrix}\mathbf{q}^T(t) & \dot{\mathbf{q}}^T(t)\end{bmatrix}$ corresponds to the system's state and

$$\mathbf{H} = \begin{bmatrix} \mathbf{0} & \mathbf{I} \\ -\mathbf{M}^{-1}(\mathbf{K}_s + \mathbf{K}_w) & -\mathbf{M}^{-1}(\mathbf{C}_s + \mathbf{C}_w) \end{bmatrix} \tag{A-72}$$

corresponds to a $2n \times 2n$ real nonsymmetric matrix. An *Ansatz* for the solution of Eq. (A-71) is given in the exponential form as

$$\mathbf{y}(t) = \tilde{\mathbf{y}}e^{\lambda t} \tag{A-73}$$

where λ is a complex scalar and $\tilde{\mathbf{y}} \in \mathbb{C}^{2n}$. Substituting this *Ansatz* in Eq. (A-71), and dividing the entire equation by $e^{\lambda t}$, a general algebraic eigenvalue problem is created:

$$\mathbf{H}\tilde{\mathbf{y}} = \lambda\tilde{\mathbf{y}} \tag{A-74}$$

The eigensolution of this problem corresponds to $2n$ eigenvalues, λ_r, and $2n$ eigenvectors, $\tilde{\mathbf{y}}_r$, that satisfy

$$\mathbf{H}\tilde{\mathbf{y}}_r = \lambda_r\tilde{\mathbf{y}}_r \quad \text{for } r = 1, \ldots, 2n. \tag{A-75}$$

In this thesis, we will restrict the analysis to systems having distinct eigenvalues. Because the matrix $\mathbf{H}$ is nonsymmetric, the mutual orthogonality of the eigenvectors can be not longer guaranteed, only their independence. Also, the

eigenvectors are not orthogonal with respect to the matrix $\mathbf{H}$. Nevertheless, some type of orthogonality is present. To demonstrate it, let's first remember that the determinant of a matrix is equal to the determinant of its transpose. Hence, it is possible to write

$$\det\left[\mathbf{H}-\lambda\mathbf{I}\right]=\det\left[\mathbf{H}-\lambda\mathbf{I}\right]^{T}=\det\left[\mathbf{H}^{T}-\lambda\mathbf{I}\right]. \tag{A-76}$$

Equation (A-76) shows that the matrices $\mathbf{H}$ and $\mathbf{H}^T$ have the same eigenvalues. Therefore, an eigenvalue problem associated with $\mathbf{H}^T$ can be constructed as

$$\mathbf{H}^{T}\check{\mathbf{y}}=\lambda\check{\mathbf{y}} \tag{A-77}$$

Such problem is referred in the literature as the adjoint eigenvalue problem associated to the eigenvalue problem for $\mathbf{A}$, Eq. (A-74). As before, it admits the same $2n$ eigenvalues λ_r, but with a new set of $2n$ new eigenvectors $\check{\mathbf{y}}_r$ associated to it. They are called the adjoint eigenvector of $\tilde{\mathbf{y}}_r$. The eigenvalues and the adjoint eigenvectors satisfy the equation

$$\mathbf{H}^{T}\check{\mathbf{y}}_{r}=\lambda_{r}\check{\mathbf{y}}_{r}\quad\text{ for }r=1,\ldots,2n, \tag{A-78}$$

which it is equivalent to

$$\check{\mathbf{y}}_{r}^{T}\mathbf{H}=\lambda_{r}\check{\mathbf{y}}_{r}\quad\text{ for }r=1,\ldots,2n. \tag{A-79}$$

Equation (A-79) shows why the adjoint eigenvectors are also known as left eigenvectors of $\mathbf{H}$. Following the same logic, the eigenvectors $\tilde{\mathbf{y}}_r$ are also called right eigenvectors. Notice that for the case of $\mathbf{H}$ being symmetric, there is no distinction between Eq. (A-74) and Eq. (A-77). The left and right eigenvectors of $\mathbf{H}$ are therefore identical, and the eigenvalue problem is said to be self-adjoint.

Biorthogonality of the right and left eigenvectors: For the case of distinct eigenvalues, it is possible to show that the left and right eigenvectors are orthogonal. Multiplying Eq. (A-75) on the left by $\check{\mathbf{y}}_j^T$ and Eq. (A-79) on the right by $\tilde{\mathbf{y}}_j$, and subtracting the second from the first, we obtain

$$\left(\lambda_{r}-\lambda_{j}\right)\check{\mathbf{y}}_{j}^{T}\tilde{\mathbf{y}}_{r}=0. \tag{A-80}$$

With the assumption of distinct eigenvalues, it is possible to conclude that

$$\check{\mathbf{y}}_{j}^{T}\tilde{\mathbf{y}}_{r}=0\quad\text{for}\quad j,r=1\ldots,2n\quad\text{and}\quad j\neq r. \tag{A-81}$$

Equation (A-81) shows that the left and right eigenvectors of a real nonsymmetric matrix with distinct eigenvalues are orthogonal. The sets of left and right eigenvectors are then said to be biorthogonal. Next, it is also possible to

show that they are also orthogonal with respect to the matrix **H**. Premultiplying Eq. (A-75) by $\check{\mathbf{y}}_j^T$ and using the result of Eq. (A-81), we conclude that

$$\check{\mathbf{y}}_j^T \mathbf{H} \tilde{\mathbf{y}}_r = 0 \quad \text{for} \quad j, r = 1 \ldots, 2n \quad \text{and} \quad j \neq r. \tag{A-82}$$

The biorthogonality presented in Eq. (A-81) and Eq. (A-82) can not be extend to the right and left eigenvectors belonging to the same eigenvalue. A normalization can be defined so that $\check{\mathbf{y}}_r^T \tilde{\mathbf{y}}_r = 1$ for $r = 1, \ldots, 2n$. It transforms the sets of biorthogonal eigenvectors into sets of biorthonormal eigenvectors. With such normalization, it is possible to show that the eigenvectors satisfy the biorthonormality relation

$$\check{\mathbf{y}}_j^T \tilde{\mathbf{y}}_r = \delta_{j,r} \quad \text{for} \quad j, r = 1 \ldots, 2n \tag{A-83}$$

Then, it also follows that

$$\check{\mathbf{y}}_j^T \mathbf{H} \tilde{\mathbf{y}}_r = \lambda_r \delta_{j,r} \quad \text{for} \quad j, r = 1 \ldots, 2n. \tag{A-84}$$

Considering Eq. (A-73) and the properties of the eigenvectors, it is possible to write the free response of a nonconservative systems as

$$\mathbf{y}(t) = \sum_{r=1}^{2n} \tilde{\mathbf{y}}_r e^{\lambda_r t} a_r \tag{A-85}$$

where a_r depends on the initial conditions of the system. Setting $t = 0$ in Eq. (A-85), we obtain

$$\mathbf{y}(0) = \sum_{r=1}^{2n} \tilde{\mathbf{y}}_r a_r. \tag{A-86}$$

Considering now the biorthogonality properties between the sets of left and right eigenvectors, we can premultiply both sides of Eq. (A-86) by $\check{\mathbf{y}}_r^T$ to obtain

$$a_r = \check{\mathbf{y}}_r^T \mathbf{y}(0) \quad \text{for } r = 1, \ldots, 2n. \tag{A-87}$$

The free response can then be written is terms of the initial conditions as

$$\mathbf{y}(t) = \sum_{r=1}^{2n} \tilde{\mathbf{y}}_r e^{\lambda_r t} \check{\mathbf{y}}_r^T \mathbf{y}(0) \tag{A-88}$$

B
Nonlinear normal modes: Invariant manifold definition

A NNM defined as invariant manifolds is a generalization of the Rosenberg's definition and was first proposed by Shaw and Pierre [23, 24, 25]. They defined a NNM as a two-dimensional invariant manifold in phase space, which allows the extension of the NNM concept to non-conservative and non-self-adjoint systems. It was developed based on geometric arguments and using the center manifold technique. The invariant manifolds are parameterized using a pair of state variables, referred as master coordinates, and the remaining state variables are then written as functions of them. Such formulation can be constructed using a physical or a modal coordinate system. When the initial condition is set to be a point in the invariant manifold, it remains on it for all time. This extends the invariance property of LNM to nonlinear systems.

As presented in [92], the NNMs of the underlying conservative system (from Rosenberg's definition) often have the same topological structure of the actual non-conservative system, but not always. Sometimes it can deviates significantly as showed in [78] for the same 2 DOF system presented in section 4.2.1. This motivates the development of methods that can compute NNM based on the invariance manifold definition [93, 94, 71, 68, 95, 96].

Before presenting the NNM as invariant manifold, some basic definitions are required. We start by defining the equation of motion for the mechanical system under analysis. It is equal to Eq. (3-23) without the external forces and the nonlinear forces are assumed to be time-invariant, which makes the system autonomous. Its mathematical model is given by

$$\dot{\mathbf{y}}(t) = \mathbf{g}\left(\mathbf{y}(t)\right) \tag{B-1}$$

where $\mathbf{y}(t) = \begin{bmatrix}\mathbf{q}^T(t) & \dot{\mathbf{q}}^T(t)\end{bmatrix}^T \in \mathbb{R}^{2n}$ and

$$\mathbf{g}\left(\mathbf{y}\right) = \begin{bmatrix}\mathbf{q} \\ \mathbf{M}^{-1}\left[-\mathbf{C}\dot{\mathbf{q}} - \mathbf{K}\mathbf{q} - \mathbf{f}_{nl}\left(\mathbf{q}, \dot{\mathbf{q}}\right)\right]\end{bmatrix}. \tag{B-2}$$

The time dependency of $\mathbf{y}$ and $\mathbf{q}$ was omitted for simplicity. Equation (B-1) is the state space representation of the second order equation of motion usually obtained using Lagrange's method or Hamilton's principle.

A fixed point of this autonomous system is given by any point $\mathbf{y}_e$ that

satisfies $\mathbf{g}(\mathbf{y}_e) = 0$. As suggested by its name, if the system starts at $\mathbf{y}_e$, it remains on that point for all time. Similar to the stability analysis of periodic solutions in section 3.3, the fixed point can also be stable or unstable. A fixed point is asymptotically stable if all solutions started near $\mathbf{y}_e$ approximate to $\mathbf{y}_e$ as $t \to \infty$. In Eq. (B-1), the model was constructed so that $\mathbf{y} = \mathbf{0}$ is a fixed point. This particularity is always achievable using a translation of coordinates.

A linearization of Eq. (B-1) is given by the linear time-invariant system $\dot{\mathbf{y}} = \mathbf{A}\mathbf{y}$, where $\mathbf{A} = \frac{\partial \mathbf{g}}{\partial \mathbf{y}}\Big|_{\mathbf{y}=\mathbf{0}}$ is the Jacobian of $\mathbf{g}(\mathbf{y})$ evaluated at the fixed point $\mathbf{y}_e = \mathbf{0}$. The eigenspaces of this fixed point is given by the subspaces spanned by the eigenvectors of $\mathbf{A}$. They can be classified as stable, unstable or center eigenspace depending on the real part of the associated eigenvalues. The eigenvectors associated to eigenvalues having negative real part span the stable eigenspace E^s. Similarly, the eigenvectors associated to eigenvalues having positive real part span the unstable eigenspace E^u. The center eigenspace E^c is spanned by eigenvectors associated to eigenvalues having zero real part. For complex-valued eigenvectors, the real and imaginary parts are used to span the respective eigenspaces. An important properties of those eigenspaces is that the sum of all three eigenspace's dimensions must be equal to $2n$, the dimension of the state space model. Also, the eigenspaces are invariant under the flow.

An invariant manifold associated to the autonomous system $\dot{\mathbf{y}} = \mathbf{g}(\mathbf{y})$ is a set of points S in the state space in which all solutions starting at an initial condition $\mathbf{y}(0) \in S$ stays in S for all time. Similarly to the eigenspaces, they can also be classified as stable, unstable or center. Invariant manifolds about a fixed point can be seen as a generalization of eigenspaces when moving away from that fixed point. Therefore, the eigenspaces of the linearized model are tangent to the invariant manifolds at $\bar{\mathbf{y}}$ and have the same dimensions.

A NNM can then be defined as *a parameterized family of responses that lie on a two-dimension invariant manifold that is tangent to a linear mode eigenspace* [53]. Visually, it corresponds to a generally curved surface that constrains the motion of all DOF to a pair of masters coordinates. When assuming invariance of an individual mode, it is possible to assume the existence of initial conditions in which the entire system behaves like a single DOF. When dealing with linear system, the subordination is given through linear combinations of the displacement and velocity of the master coordinates. For example, if the state of a particular DOF in the physical coordinate system (q_r and $\dot{q}_r$) is chosen as master coordinates, the state of the remaining DOF

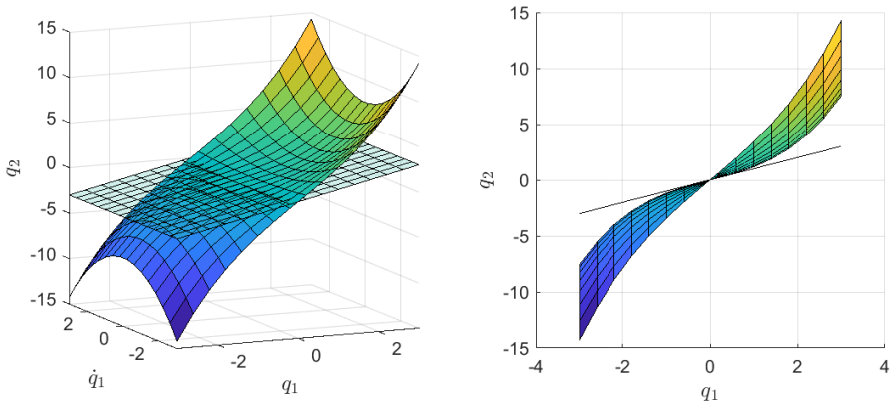

Figure B.1: Example of a manifold for the 2DOF system

can be expressed as

$$\begin{aligned} q_i(t) &= a_{ir}q_r + b_{ir}\dot{q}_r(t) \\ \dot{q}_i(t) &= c_{ir}q_r + d_{ir}\dot{q}_r(t), \quad i = 1, \ldots, n, \end{aligned} \tag{B-3}$$

where a_{ir}, b_{ir}, c_{ir} and d_{ir} are real coefficient that defines each linear mode and therefore the eigenspaces. When dealing with nonlinear systems, the subordination is changed by generic functions of the master coordinates pair, transforming Eq. (B-3) into

$$\begin{aligned} q_i &= B_i\left(q_r, \dot{q}_r\right) \\ \dot{q}_i &= D_i\left(q_r, \dot{q}_r\right), \quad i = 1, \ldots, n. \end{aligned} \tag{B-4}$$

The functions B_i and D_i are responsible for the definition of the manifold.

Figure B.1 shows one of the invariant manifolds of the 2 DOF oscillator described by Eq. (5-10). The curved surface corresponds to the in-phase NNM while the flat surface represent the eigenspace of the respective underlying linear system. As expected, the plane representing the eigenspace crosses the manifold at the equilibrium position and it is also tangent to it. This shows that at low energy levels the eigenspace can be used to represent the dynamics of the system. This means that a linear model would be acceptable under those conditions.

C
Computation of isolas using NNMs

In general, the vibration of nonlinear mechanical systems is rich and complex. The energy dependency, bifurcation and instability of the oscillatory motion are some of the features already presented in the previous chapters when computing the NFRCs and the NNMs. Another important phenomena present in nonlinear vibration is the possibility of having isolas, i.e., branches of periodic force responses that are isolated from the primary branch. Such phenomena is exemplified in Fig. C.1. It is crucial to consider the existence of isolas in the analysis, since they can be dangerous to the integrity of the system. If only the primary response branch is considered, the vibration level can be underestimated at some conditions. In the example of Fig. C.1, the amplitude (RMS) of the periodic response at 3.7Hz in the primary branch is approximately 0.007m, but it can reaches up to 0.15m if the system is vibrating at its isolated force response curve. In another words, the system can drastically change its response amplitude if the motion is changed from the basin of attraction related to the primary branch to the one related to the isola. It is worth mention that isolas can also be placed below the primary response branch, but in this case, the outcome is usually less problematic than the former.

To emphasize the importance of computing isolas, let's consider once

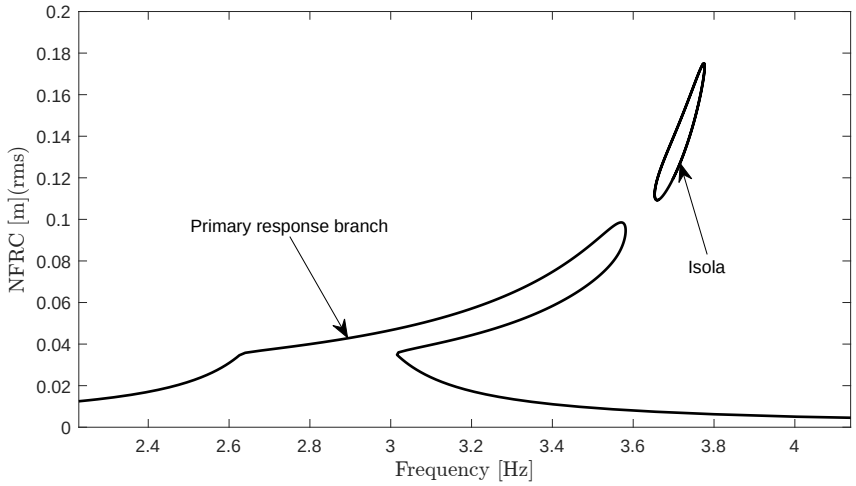

Figure C.1: Representation of an isolated force response curve (isolas) and the primary force response branch.

again the example of the cantilever beam with the unilateral spring described in section 5.4.3. There is an external force applied at the middle of the beam and the response is measure at its free end. The excitation signal corresponds to a sine sweep that varies its frequency linearly from 2 to 4.5Hz with a rate of 0.02Hz/s. The force amplitude is first defined as 1.7N. The response of the system is then simulated using the Newmark method described in section 3.1 with sampling interval $v = 0.002$s. The resulting displacement is presented in the left hand-side plot of Fig. C.2 with a yellow line. The motion grows symmetrically until the excitation frequency reaches approximately 2.6Hz. At this time, the amplitude of the response at the free end of the beam is high enough to overcame the gap of the unilateral spring, activating it. Then, the amplitude of the response continues to grow (not symmetrically because of the unilateral spring) until approximately 3.6Hz, where a jump in the amplitude occurs, reducing it significantly. Finally, the amplitude continues at a low level all the way to 4.5Hz. Around 3.1Hz, it is also possible to see a quasiperiodic regime of the response, i.e., a loss of stability in the motion. The RMS of the response is also presented in the middle plot of Fig. C.2. The curve shape is similar to the NFRCs computed in the example of section 5.4.3 and repeated here for convenience in the right hand-side plot of Fig. C.2. If the same simulation is repeated with a small increment in the force amplitude, the response is practically not effected, as showed by the red curves in Fig. C.2. Only a small increment in the amplitude is noted and the behavior continues the same. However, if a second increment in the force amplitude is applied, the simulated response becomes quite different than the two previous ones, as illustrated by the blue curves. A much higher vibration level is observed in the interval between 3.6Hz and 4Hz. This sudden amplitude increment is a consequence of the merging between the primary solution branch and an isola. The isola was actually already present for the lower excitation levels (1.7N and 2.1N), but it was not reached by the sweep excitation.

To illustrate a possible problem when neglecting isolas, lets consider now the case where the beam is excited at the middle point with a sine wave. The amplitude corresponds to 2.1N and the frequency is equal to 3.7Hz. The response of the beam is observed once again at its free end and the system is initially at rest. After around 20s the transient part of motion was already dissipated and the system vibrates at a steady state condition, as showed in Fig. C.3. The amplitude of the response is around 0.02m, which means that the beam is not even touching the unidirectional spring. After 60s of simulation, a perturbation was applied in the system in a form of an impact at the free end of the beam. The perturbation created a transient response that was once again

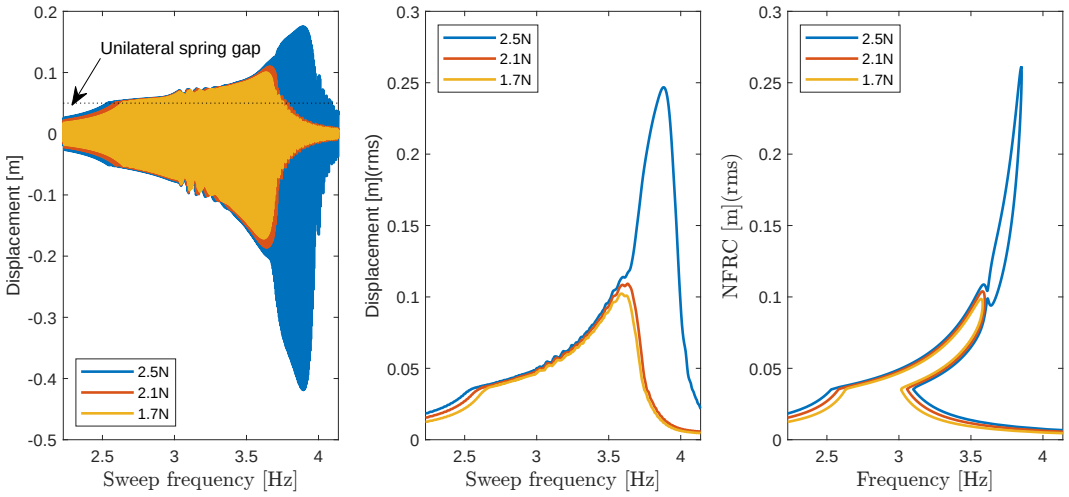

Figure C.2: Sine sweep response of the cantilever beam with unilateral spring.

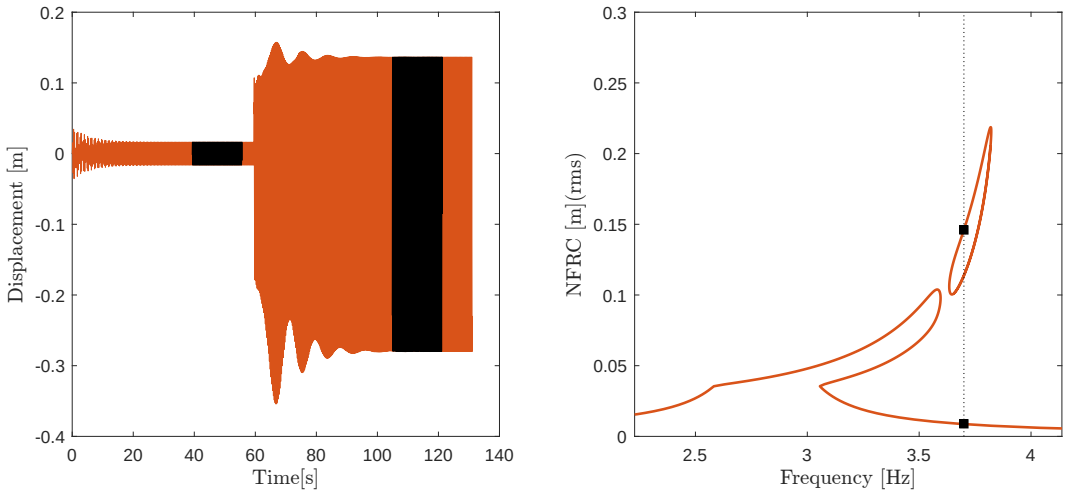

Figure C.3: Response to a sine wave with amplitude of 2.1N and frequency of 3.7Hz. Illustration of change of basin of attraction after a perturbation.

dissipated by the structural damping of the beam. The difference is that, at this time, the steady state response has a much higher amplitude (more then 10 times the previous one). The perturbation was responsible in changing the system state to another basin of attraction, being this latter one related to the isola. Such motion can be dangerous to the integrity of the structure if not predicted, which shows the importance of computing isolas.

C.1
Relationship between NFRCs and NNMs

Before defining a procedure to compute isolas using a NNM, it is important to establish some relationships between the NFRCs and the NNMs. In particular two concepts are analyzed: the force appropriation and the energy balance. Both concepts were extended from linear systems to nonlinear system

and were already applied in the computation of isolas by Kuether et al. in [20].

C.1.1 Force appropriation

Force appropriation, also known as normal-mode tuning, is a method of physically exciting the normal-modes of a strucutre at their corresponding undamped natural frequency. The main idea is to apply forces at different locations in the structure so that they can cancel out the dissipation forces of the system, leaving a pure normal mode motion. For linear system, this requires mono-harmonic forces applied at different locations with different amplitudes. A perfect force appropriation is obtained when the response across the structure is vibrating in a monophase way (synchronously) and in quadrature to the excitation (phase lag of 90^{o}). The authors in [97] provides a reviewing article on the force appropriation methods used in modal identification of linear system.

The extension of force appropriation from linear to nonlinear systems was first proposed in [98] through a method known as force appropriation of nonlinear systems (FANS). It consists in exciting the system at several locations using higher harmonics that are able to counteract the nonlinear coupling terms, forcing the system to vibrate in one of its linear normal mode. Peeters et al. [99] proposed a different force appropriation methodology that induces the NNM motion of a nonlinear system using a multi-point, multi-harmonic excitation. The applied forces cancel out only the dissipation forces and imposes the NNM motion to the system. A generalization of the phase lag quadrature is necessary to locate the single-NNM response and validate the force appropriation. It defines that a nonlinear system is vibrating as a single NNM if all the harmonics of the periodic response is in quadrature with the respective harmonics of the excitation. Such method is discussed in more detail in the following.

Let assume that a NNM is defined by the periodic motion $\mathbf{q}_N(t)$. This motion can then be substituted into the equation of motion of the system, which yields in

$$\mathbf{M}\ddot{\mathbf{q}}_N(t) + \mathbf{C}\dot{\mathbf{q}}_N(t) + \mathbf{K}\mathbf{q}_N(t) + \mathbf{f}_{nl}\left(\mathbf{q}_N(t)\right) = \mathbf{f}_{ap}(t), \tag{C-1}$$

where $\mathbf{f}_{ap}(t)$ is a specific external force that must be applied to satisfy the equation of motion. It allows the system to vibrate in one of its NNMs, i.e., perform a perfect force appropriation. To compute such special force, one can use the Rosemberg's definition of NNM, which means that $\mathbf{q}_N(t)$ must satisfy the following differential equation:

$$\mathbf{M}\ddot{\mathbf{q}}_N(t) + \mathbf{K}\mathbf{q}_N(t) + \mathbf{f}_{nl}\left(\mathbf{q}_N(t)\right) = \mathbf{0}. \tag{C-2}$$

Subtracting Eq. (C-2) from Eq. (C-1), it results in

$$\mathbf{f}_{ap}(t) = \mathbf{C}\dot{\mathbf{q}}_N(t), \tag{C-3}$$

which shows that the force required to perfectly impose a NNM motion in the system is proportional to the velocity and must be applied at all DOF of the structure, which is practically impossible. Nevertheless, let's now write the NNM motion $\mathbf{q}_N(t)$ as a Fourier series:

$$\mathbf{q}_N(t) = \sum_{k=-\infty}^{k=\infty} \tilde{\mathbf{q}}_{N,k}^{(e)} e^{\mathbf{i}k\Omega t}. \tag{C-4}$$

$\tilde{\mathbf{q}}_{N,k}^{(e)}$ represents the k-th Fourier coefficient of $\mathbf{q}_N(t)$ in the exponential representation and Ω is the fundamental frequency of NNM. Substituting Eq. (C-4) into Eq. (C-3), one has

$$\begin{aligned} \mathbf{f}_{ap}(t) &= \mathbf{C}\frac{d}{dt}\left(\sum_{k=-\infty}^{k=\infty} \tilde{\mathbf{q}}_{N,k}^{(e)} e^{\mathbf{i}k\Omega t}\right) \\ &= \sum_{k=-\infty}^{k=\infty} \underbrace{\mathbf{i}k\Omega\mathbf{C}\tilde{\mathbf{q}}_{N,k}^{(e)}}_{\tilde{f}_{ap,k}^{(e)}} e^{\mathbf{i}k\Omega t}, \end{aligned} \tag{C-5}$$

where $\tilde{f}_{ap,k}^{(e)}$ is the k-th Fourier coefficient of the applied force. In this chapter, we assume that the NNMs correspond to a monophase motion. This means that the displacements of all DOFs reach their extreme values simultaneously. Therefore, each Fourier coefficient of $\mathbf{q}_N(t)$ can be written in terms of a unique phase:

$$\tilde{\mathbf{q}}_{N,k}^{(e)} = \left|\tilde{\mathbf{q}}_{N,k}^{(e)}\right| e^{\mathbf{i}\upsilon_k}, \tag{C-6}$$

where υ_k is the respective phase of $\tilde{\mathbf{q}}_{N,k}^{(e)}$. Substituting Eq. (C-6) into Eq. (C-5), it is possible to write each Fourier coefficient of the applied force as

$$\begin{aligned} \tilde{f}_{ap,k}^{(e)} &= \mathbf{i}k\Omega\mathbf{C}\tilde{\mathbf{q}}_{N,k}^{(e)} \\ &= \mathbf{i}k\Omega\mathbf{C}\left|\tilde{\mathbf{q}}_{N,k}^{(e)}\right| e^{\mathbf{i}\upsilon_k} \\ &= \underbrace{k\Omega\mathbf{C}\left|\tilde{\mathbf{q}}_{N,k}^{(e)}\right|}_{\left|\tilde{f}_{ap,k}^{(e)}\right|} e^{\mathbf{i}\left(\upsilon_k+\frac{\pi}{2}\right)} \end{aligned} \tag{C-7}$$

The above equation shows that, for a perfect force appropriation, each Fourier coefficient of the excitation must be 90° ahead from the the corresponding Fourier coefficient of the NNM motion. This represents the phase lag quadrature criterion mentioned earlier.

A perfect force appropriation is unlike to be obtained experimentally since it requires different inputs at all DOF of the structure. Nevertheless, a few researches [99, 100, 101, 102] have shown that simpler forms of excitation can lead to accurate approximation of the NNM motion. Peeters et al. [99, 100] used a single point, monoharmonic excitation in lightly damped structures. Good numerical and experimental results were obtained, showing a first connection between the NFRCs and the NNMs. Such connection will be explored latter when computing isolas.

C.1.2 Energy balance

In this section a relationship between the NNMs and a periodically forced response of a non-conservative system is established based on the energy balance technique. Such relationship allows one to estimate the force amplitude required for the non-conservative system to vibrate according to one of its NNM.

It is assumed in this chapter that the energy added to the system by the external force is equal, over one oscillation, to the energy dissipated by the damping forces. For the mechanical system considered in this chapter, the energy added in the system along one oscillation can be defined as

$$E_{\text{in}} = \int_0^T \dot{\mathbf{q}}(t)^{\text{T}} \mathbf{f}_{ex}(t) dt \tag{C-8}$$

Similarly, the energy dissipated by the damping forces along one cycle is given by

$$E_{\text{out}} = \int_0^T \dot{\mathbf{q}}(t)^{\text{T}} \mathbf{C} \dot{\mathbf{q}}(t) dt. \tag{C-9}$$

If we assume now that a perfect force appropriation is given so that $\mathbf{f}_{ex}(t) = \mathbf{f}_{ap}(t)$ and $\mathbf{q}(t) = \mathbf{q}_N(t)$, one can write the energy balance equation as

$$E_{\text{in}} = \int_0^T \dot{\mathbf{q}}_N(t)^{\text{T}} \mathbf{f}_{ap}(t) dt = \int_0^T \dot{\mathbf{q}}_N(t)^{\text{T}} \mathbf{C} \dot{\mathbf{q}}_N(t) dt = E_{\text{out}}. \tag{C-10}$$

As mentioned earlier, a perfect force appropriation is not feasible because it requires excitation at all DOFs. Instead, if we assume now that a single point, monoharmonic excitation is applied in the system, we can write the input energy as

$$E_{\text{in}} = \int_0^T \dot{\mathbf{q}}(t)^{\text{T}} \left[\Gamma \mathbf{e}_i \cos(\omega t)\right] dt, \tag{C-11}$$

where $\Gamma \in \mathbb{R}$ is the force amplitude and $\mathbf{e}_i \in \mathbb{R}^n$ is a vector of zeros, except i-th entry, which equal to one. This vector is responsible for identifying the DOF where the single point, monoharmonic force is applied. If we assume that the excitation frequency is the fundamental frequency of one of the NNMs ($\omega = \Omega$), and that the resulting motion is close enough to the respective NNM

motion, an estimation the force amplitude required to excite the NNM is given using the energy balance equation, i.e.:

$$\Gamma \approx \frac{\int_0^T \dot{\mathbf{q}}_N(t)^{\mathrm{T}} \mathbf{e}_i \cos(\Omega t) dt}{\int_0^T \dot{\mathbf{q}}_N(t)^{\mathrm{T}} \mathbf{C} \dot{\mathbf{q}}_N(t) dt} \tag{C-12}$$

Equation (C-12) is only an approximation because a single point, monoharmonic excitation is unlikely to produce a perfect NNM motion in the system. But, as long as resulting motion is close to the NNM, the estimation can be used to relate the NFRCs and the NNM. This is shown in more detail in the following section.

C.2
Computation of isolas using a numerical example

A numerical example will be used now to illustrate how the force appropriation and the energy balance equation can be used to compute isolas using the NNMs. The chosen system corresponds to the cantilever beam with unilateral spring used in the beginning of this chapter. It corresponds to a weakly damped system with a strong nonlinearity caused by the unilateral spring (causes discontinuity in the dynamic model).

The procedure used to identify and compute isolas starts with the computation of the NNMs as described in chapter 5. Let's assume that the first NNM of the was computed using the HBM and the prediction-correction scheme. The truncation order was defined as $H = 5$, so that only one mode interaction was computed (see Fig. 5.12). The mode shape and the fundamental frequency of the respective NNM was computed for several discrete values of energy. For each of those energy level, the periodic solution that characterizes the NNM can be used to estimate the amplitude Γ of single point, monoharmonic force using Eq. (C-12). This leads to a mapping between the NNM and the required force amplitude to approximately excite this mode. The result for the cantilever beam example is presented in Fig. C.4.

For each point in the frequency-energy plot (FEP), there is a corresponding one in the frequency-force plot. The frequency-force plot allows one to predict the force amplitude, in which some of dynamic characteristics are changed. For example, it is possible to predict the force amplitude (≈ 0.1N) required for the beam to touch the unilateral spring (leave the linear model). It is also possible to observe that, from certain force amplitude (≈ 1.45N), there are three (resonance) frequencies associated to each value of Γ. This multiplicity in the number of frequencies emerged from the 5:1 mode interaction. This later characteristic is used in the detection of isolas. When there is no isola, the system presents only one resonance frequency. It corresponds to the frequency of

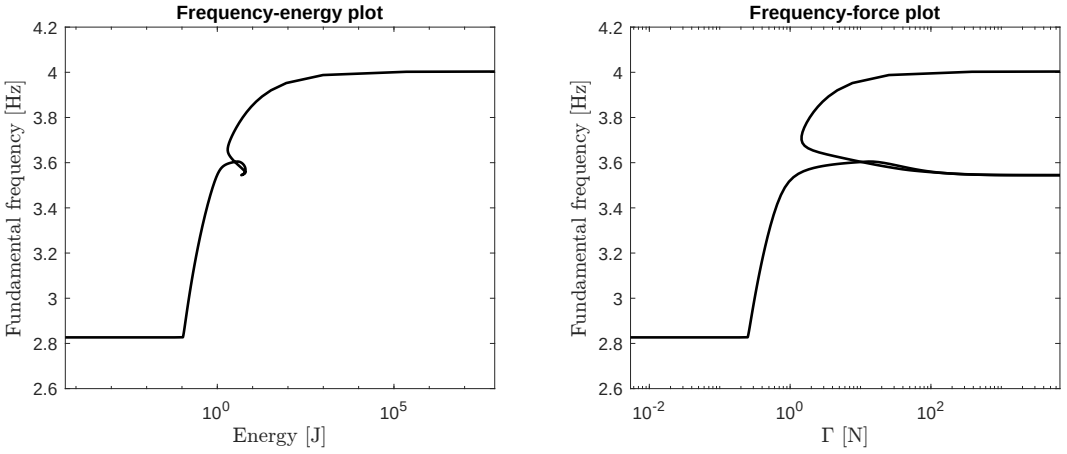

Figure C.4: Energy balance of the NNM.

the peak in the NFRCs. But, when an isola exists, the edges of corresponding isolated curve are also considered as resonance frequencies since those edges also cross the backbone curve of the NFRC. For the example considered here, we can then say that there is a potential isola when the system is excited with an amplitude above 1.45N.

The left plot in Fig. C.5 shows the same frequency-force plot, but now highlighting the three resonance frequencies associated with the force amplitude of 1.7N. On the right hand-side plot, the NFRC (primary branch and the isola) associated to this specific force amplitude is presented. The NNM is also showed as dashed black line and it represents the backbone of the NFRC. The three resonance frequencies are highlighted along the backbone curve (NNM). Those three points are indeed close to the peak of the primary branch and the edges of the isola. The result only approximates to those edges because the single point, monoharmonic excitation did not actually excited the NNM. There is not an exact relationship between the NFRCs and the NNM. Nevertheless, when it is close enough (sufficiently to converge), the periodic motion of the NNM can be used as initial guess for the first solution point of the isolated force response curve. If this first solution point is indeed found, the entire isola can be computed using the standard continuation method. To satisfy the phase lag quadrature criteria the initial guess using the NNM motion must have a 90° phase lag to the single point, monoharmonic excitation.

This was the procedure adopted here to compute isolas for different excitation levels. Some of the results are presented in Fig. C.6. It shows only the primary branch for $\Gamma = 1.2$N, since only one resonance frequency is found for this force amplitude. For $1.5N \leq \Gamma \leq 2.4$N, isolas were also computed since three resonance frequencies were obtained in this interval. For $\Gamma \geq 2.7$N, the isola was already merged with the primary branch. In all of the cases, the

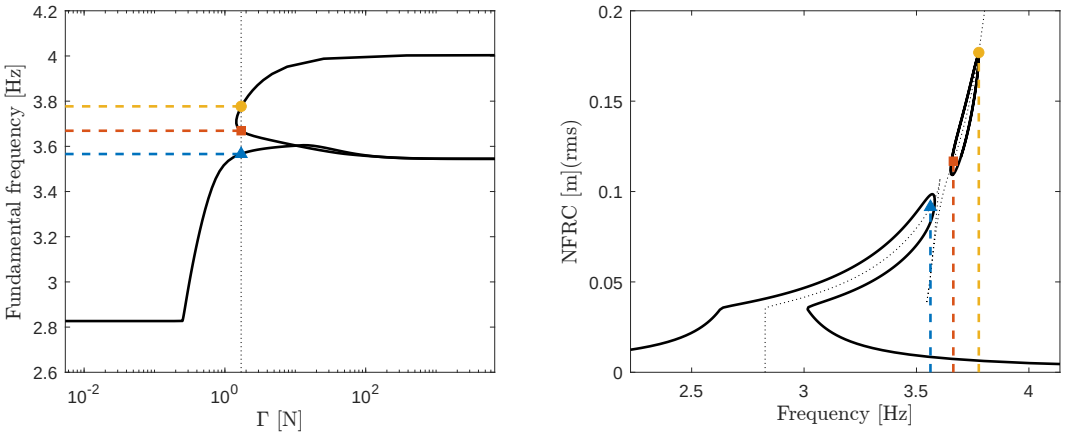

Figure C.5: Identification of isolas points.

NNM were used as initial guess for the first solution point of the isolas and no convergence problem was found. This indicates that the NNM motion was actually close to the resonance motions.

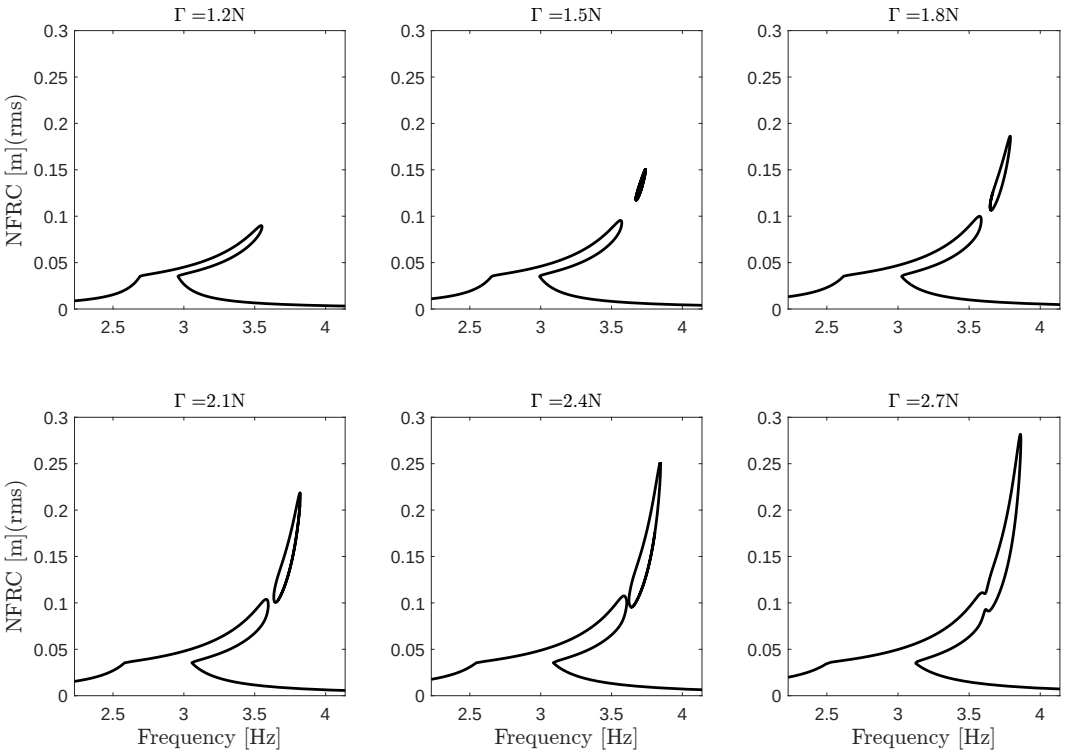

Figure C.6: NFRCs of the cantilever beam with unilateral spring considering isolas.